Dynamic Strain Measurement Based Damage Identification for Structural Health Monitoring

Mohamed Elbadawy

Dissertation submitted to the Faculty of the Virginia Polytechnic Institute and State University in partial fulfillment of the requirements for the degree of

Doctor of Philosophy

In

Engineering Mechanics

Mahendra P. Singh, Chair

Saad A Ragab

Surot Thangjitham

Matthew R. Eatherton

Pablo A. Tarazaga

Saurabh Bisht

October 11, 2018

Blacksburg, Virginia

Keywords: structural health monitoring, structural frames, strain response, damage identification, stiffness identification, modal approach, strain mode shapes, damage localization, flexibility-based damage identification, optimal sensor placement.

Dynamic Strain Measurement Based Damage Identification for Structural Health Monitoring

Mohamed Elbadawy

ABSTRACT

Structural Health Monitoring (SHM) is a non-destructive evaluation tool that assesses the functionality of structural systems that are used in the civil, mechanical and aerospace engineering practices. A much desirable objective of a SHM system is to provide a continuous monitoring service at a minimal cost with ability to identify problems even in inaccessible structural components. In this dissertation, several such approaches that utilize the measured dynamic response of structural systems are presented to detect, locate, and quantify the damages that are likely to occur in structures. In this study, the structural damage is identified as a reduction in the stiffness characteristics of the structural elements. The primary focus of this study is on the utilization of measured dynamic strains for damage identification in the framed structures which are composed of interconnected beam elements. Although linear accelerations, being more convenient to measure, are commonly used in most SHM practices, herein the strains being more sensitive to elemental damage are considered. Two different approaches are investigated and proposed to identify the structural element stiffness properties. Both approaches are mode-based, requiring first the identification of system modes from the measured strain responses followed by the identification of the element stiffness coefficients. The first approach utilizes the Eigen equation of the finite element model of the structure, while the second approach utilizes the changes caused by the damage in the structural curvature flexibilities. To reduce size of the system which is primarily determined by the number of sensors deployed for the dynamic data collection, measurement sensitivity-based sensor selection criterion is observed to be effective and thus used. The mean square values of the measurements with respect to the stiffness coefficients of the structural elements are used as the effective measures of the measurement sensitivities at different sensor locations. Numerical simulations are used to evaluate the proposed identification approaches as well as to validate the sensitivity-based optimal sensor deployment approach.

Dynamic Strain Measurement Based Damage Identification for Structural Health Monitoring

Mohamed Elbadawy

General Audience Abstract

All modern societies depend heavily on civil infrastructure systems such as transportation systems, power generation and transmission systems, and data communication systems for their day-to-day activities and survival. It has become extremely important that these systems are constantly watched and maintained to ensure their functionality. All these infrastructure systems utilize structural systems of different forms such as buildings, bridges, airplanes, data communication towers, etc. that carry the service and environmental loads that are imposed on them. These structural systems deteriorate over time because of natural material degradation. They can also get damaged due to excessive load demands and unknown construction deficiencies. It is necessary that condition of these structural systems is known at all times to maintain their functionality and to avoid sudden breakdowns and associated ensuing problems. This condition assessment of structural systems, now commonly known as structural health monitoring, is commonly done by visual onsite inspections manually performed at pre-decided time intervals such as on monthly and yearly basis. The length of this inspection time interval usually depends on the relative importance of the structure towards the functionality of the larger infrastructure system. This manual inspection can be highly time and resource consuming, and often ineffective in catching structural defects that are inaccessible and those that occur in between the scheduled inspection times and dates. However, the development of new sensors, new instrumentation techniques, and large data transfer and processing methods now make it possible to do this structural health monitoring on a continuous basis. The primary objective of this study is to utilize the measured dynamic or time varying strains on structural components such as beams, columns and other structural members to detect the location and level of a damage in one or more structural elements before they become serious. This detection can be done on a continuous basis by analyzing the available strain response data. This approach is expected to be especially helpful in alerting the owner of a structure by identifying the

occurrence of a damage, if any, immediately after an unanticipated occurrence of a natural event such as a strong earthquake or a damaging wind storm.

Acknowledgement

This research is partially supported by the National Science Foundation through grant number CMMI-1333965. This financial support is gratefully acknowledged. The opinions, findings and conclusions or recommendations expressed in this work are those of the writers and do not necessarily represent the views of the National Science Foundation.

Contents

List of Figures

List of Tables

Chapter 1: Introduction

Engineering systems such as the infrastructure systems, that modern societies need to function and survive, require a continuous assessment of their health to avoid untimely breakdowns. Such incidents disrupt their performance and can cause undue hardships to their user communities. These infrastructure systems are also getting more complex to meet the ever-growing societal demands. Thus, increasing attention is being paid to develop health assessment strategies for these systems through–constantly evolving "internet of things" to maintain their efficient performance that a modern society expects and demands.

One of the most noticeable applications of health monitoring is the condition assessment of civil infrastructure components such as buildings, bridges and other structural systems. This is being commonly referred to as structural health monitoring (SHM). This topic is currently in much need of advanced research, primarily to maintain the performance and safety of the civil infrastructure for all users. It has gained popularity as one of the major topics of research which includes a variety of non-destructive evaluation tools. The importance of an infrastructure component maintenance is not limited to just the assessment and performance of the mechanical behavior of its structural members; it is rather broad enough that it includes the performance of all other systems such as the electrical system, HVAC system, etc. As these health monitoring systems are getting more complex, a new sub discipline of "Sensors Health Monitoring (SHM)" is emerging to oversee the monitoring systems.

For health monitoring of a component of a civil infrastructure system such as a bridge structure, a periodic visual inspections of accessible critical areas of the component has been a well-established traditional approach. The critical invisible areas, if suspected for damage, have also been examined through more sophisticated approaches such as wave propagation based acoustic or ultrasonic methods, eddy current interrogation, magnetic field measurement approaches, X-ray and gamma ray imaging, measuring state of stress, etc. However, to do these investigations the damage location need to be narrowed down as much as possible to avoid missed detection and the identified damage location should also be accessible for testing. This intermittent inspection approach, of course, has many limitations

and deficiencies and has been observed to be quite ineffective in ensuring a system's performance. Therefore, more effective and continuous approaches that can identify a damage as it occurs are being constantly sought and developed.

A comprehensive structural health monitoring consists of two main phases, (a) damage identification followed by (b) evaluating the effect of the detected damage on the serviceability, safety, repair needs, and remaining service life of the structure (Ostachowicz and Güemes 2013). The first step of damage identification is at the core of any structural health monitoring. This step involves three tasks of (i) *damage detection* (that is, is there a damage?), (ii) *damage localization (*that is, where it is.) and (iii) *damage quantification* (that is, how big it is). The first task of damage detection is the easiest, and in the context of monitoring a structural system it can be inferred from an observed change in the basic properties such as the natural frequencies of the system. The second task focuses on damage localization where the location of damage, either at single or multiple positions, is identified. The third step is the damage quantification, which defines the severity and the extent of the damage is the primary focus of this study and, in essence, it also includes the first two tasks. The second phase of structural health monitoring is also known as the prognosis which analyzes the impact of the condition change, if any, on the performance of the entire system in terms of its remaining service life as well as on the user services. This is, of course, the ultimate objective of a health monitoring system. The objective of this study is to focus on the third task to develop workable approach or approaches to identify the location, severity and extent at all possible damages that can happen in a structural system.

Continuous health monitoring of a structural systems can be achieved by tracking changes in its structure properties. This is usually done by tracking the change in the parameters of a mathematical model that describes the structure. This requires a continuous collection of data, usually the vibration response data caused by various operating and extreme environmental loads that a system is likely to experience over the period of its useful service life. This data is collected over enough locations on the system to define its condition over its physical space, especially its critical structural components, that are represented by the mathematical model. There is a high demand for such model-based non-destructive approaches to identify the occurrence, location and extent of structural damages as soon as

they occur to maintain the performance expected from a building structure or a structural system in civil infrastructure.

Monitoring a structure is an operation that demands a collaboration between various teams. The SHM operation is initiated by the data acquisition and sensor technology team which selects the appropriate sensors considering the physical and environmental parameters like sensor mass and inertia, type of adhesion, ambient temperature in the site of operation, humidity, solar radiation, etc. The desired data is collected through–wired or wireless transmission to a data collection and processing station. If necessary and possible, the arrangements are made to collect data on the excitation signal such as wind and earthquake loadings, or intentionally applied forces at certain locations or members if they are part of the structural health monitoring strategy.

The phase of data acquisition and transmission is followed by information condensation and feature extraction. It involves processing of the recorded dynamic measurements to extract the structural model parameters. Some of these parameters that are of common interest are the modal parameters like natural frequencies, damping, and mode shapes. These parameters provide very important information about the system but alone they may not be adequate. They need further analysis to extract information about the structure's mechanical properties like element bending stiffness. This study will focus on development of the modal parameter based damage identification approaches. These approaches will extensively utilize the modal parameters which will be extracted through feature extraction step to be discussed soon a little later.

In usual structural health monitoring practice, some relevant signatures of structural responses are initially recorded to define the initial undamaged state. These initial state response signatures are then compared to the signatures recorded later to detect the damage. However, in many situations where no past response history is available and only the data on the current state can be gathered, then more complicated mathematical models may be needed for the condition assessment. These assessments, however, are likely to be less reliable. In this study, we will primarily focus only on the change in the structural condition assessment from a previously known state.

Statistical analysis may be applied for further model reduction using Machine Learning algorithms for pattern recognition. Two classes of machine learning are used; supervised and unsupervised learning. In general, machine learning is concerned with problems in which there is little or no knowledge about the system to be monitored. Consider, for example, a structure so complicated to build a mathematical model, or a structure with missing essential parameters. In such cases, that mathematical model is worthless. Machine Learning does not build a transfer function, which requires a set of known system parameters, but rather builds simpler models; linear or nonlinear regression models for example.

1.1. Strain Response Measurements for Structural Health Monitoring

The main objective of a health monitoring of a structural system is to provide information about any variation or changes in its mechanical properties which affects the performance of the structural system. The mechanical properties of primary interest to characterize a structural system are the stiffness characteristics of its structural components or structural members such as beams, columns, plates, etc. A reduction in the stiffness characteristics of these basic elements mostly implies a presence of structural damage in the elements. The changes in the stiffness of the structural components cause a change in the structural response, such as the deformation and acceleration responses, when the structure is subjected to any natural or planned external excitation. Since it may be difficult to apply external excitation manually on large civil structures to cause a meaningfully measurable response, the response measurements are often made when the structure under investigation is subjected to earthquake induced ground excitation, wind loading, or other ambient random excitation. For the health monitoring of bridge structures, the response measurements under traffic induced external loading have also been considered. Since the measurements to define external excitations for health monitoring can be difficult, and sometimes even impossible for loadings such as wind loading on sprawling and distributed civil structures, different methods have been proposed to modify the measured responses to include the unmeasured loading effects in the structural health monitoring. For example, it is most common to assume the external excitation to be a Gaussian white noise random

process. This modeling assumption has been utilized in Subspace System Identification-based approaches by Ljung (1999), Van Overchee and De Moor (1996), and Peeters (1999). In the approaches such as the Natural Excitation technique developed by James et al (1993) which utilize the Eigensystem Realization Algorithm (ERA) developed by Juang and Pappa (1985), the measured response quantities are converted to the input-free response quantities for modal parameter extraction. Further discussions on this will be presented later.

In structural health monitoring, it has been a common practice to utilize the linear acceleration measurements in the damage identification process. It is primarily because the linear accelerations are easier to measure than other response quantities such as deformation related rotations and linear displacements and related velocities. In addition to the linear acceleration, displacement response can also be used for damage identification. However, a fixed reference is needed for accurate displacement measurement, this is very difficult especially for large structures to observe such displacement with respect to such fixed points. Laser or other optical devices can achieve such a purpose, however, so costly. New technologies are currently arising such as the GPS measurements. LiDAR has also been used to detect post-earthquake damage in structures (Li et al. 2008). But the accuracy of such methods is questionable. The Lidar accuracy for example ranges between 15 to 30 cm (Campbell and Wynne 2011).

The linear acceleration can be very conveniently measured by small accelerometers. Because of the ease of their measurement and data collection, they have been effectively used in extracting the system eigen frequencies. The frequencies can be helpful in detecting the occurrence of damage - based on the frequency shift measured from the DFT of the time response - but have difficulty in localizing or quantify the damage severity. In some specific situations, natural frequencies alone may provide information to detect, locate and quantify damage. Liang et al. (1992) used three natural frequencies to localize and quantify damage of a single beam under different sets of boundary conditions. This is, however, impractical for complex structures such as 2D- and 3D frames. Consequently, the acceleration measurement although done most frequently have only been of limited use in structural damage identification.

As the structural damage is often associated with flexural deformations caused by bending of structural components, the measured linear acceleration, though include the effect of bending related deformations, do not provide adequate information to identify the damage associated with bending. To identify these common form of structural damage, the measurements of rotational accelerations associated with curvatures of the structural elements have been considered. However, the measurement of rotational and displacement related deformations on a vibrating or moving civil or aero structure can be a difficult and expensive proposition, even if it is possible. The rotational acceleration measurements tend to be more expensive (a linear accelerometer is about 10 times more expensive than a strain gauge, and the accelerometers that record angular accelerations are known to be several times more expensive) as well as they are strongly affected by measurement errors.

Moreover, although indirectly related to strain measurements, interest in the modal strain energy has grown for damage localization (Yao, et al, 1992; Stubbs, et al., 1996; Shi, et al, 1998, 2000; Cornwell et al, 1999; Yang, et al, 2004; Park, et al., 2007; Guan and Karbhari (2008); and Li, 2010) as well as for damage quantification (Shi, et al 2002; Li, et al, 2006; Hu et al, 2006; Hsu and Loh, 2008; Wang 2013). Guan and Karbhari (2008), for instance, have developed an improved technique for damage detection utilizing the modal strain energy that overcame some numerical weaknesses in the modal curvature-based damage detection. On the other hand, Wang (2013) proposed an iterative modal strain energy approach that is capable only of quantifying damage that is localized by other damage localization methods. The modal strain energy have been updated by (Li et. al, 2007) who used the cross-modal strain energy (CMSE), which requires less constraints than the conventional MSE approaches. They applied it to three dimensional frame structures as well. Moreover, experimental verification for the modal strain energy utilization in damage identification, in plate like structures, has shown its effectiveness in damage detection, however, at high levels of damage (Samali et. al, 2010).

However, such studies have been utilizing the displacement mode shapes. Other studies (Yao et. al, 1992, Sanayei and Saletnik 1996, Abdel Wahab and De Roeck 1999, Rynders et. al, 2007, and Park et. al, 2007) that have examined the direct utilization of the static and dynamic strain measurements as well as the consideration of strain and curvature mode

shapes and flexibilities (Zonta et. al, 2006, Unger et. al, 2007, and Bernal et. al, 2014) for damage detection and health monitoring.

Another response which is directly affected by flexural deformation and local curvature is the local flexural strain. The strains are also most commonly measured in structural testing for material and structural component characterizations in labs. They can be easily measured in static and dynamic testing. Thus their utilization for structural health monitoring is quite natural. Some earlier as well as more recent studies in health monitoring (Li et al , 1989; Bernasconi and Ewins , 1989; Tsang, 1990; Pandey and Biswas, 1994; Abdel Wahab and De Roeck ,1999; Zonta et al, 2006; Unger et al., 2005; Reynders et al. 2007; Park et al., 2007; Qiao and Fan 2011; and recently by Bernal 2014) did, indeed, suggest their application mostly for beam like structures such as bridge girders. An experimental study by Yao et al. in 1992 on a steel frame also showed the effectiveness of strain measurement in damage localization, especially if the strain measurements are close to the damage location. In general, a strain measurement on a structural component is likely to be affected more by nearby structural damage than the other structural motion characteristics such as the acceleration or displacement response. That is, the strain measurement made on a structural component is likely to be more sensitive to the damage which affects the component stiffness than a nearby acceleration measurement. In an experimental study, Hu and Wu (2009) used the modal strain energy, in damage identification, due to its high sensitivity to the little changes in structural response than the frequencies and mode shapes. As it is as convenient to measure the strains as the accelerations, focus of this study will be on the use of strains measured at several locations for efficient structural damage identification.

1.2. Current Study

The primary objective of this study is to develop an efficient and accurate structural health monitoring approach to identify the damage utilizing the measured dynamic response. The focus will be on the identification of damage in building and other structural systems that consist of interconnected beam elements. The identification will consists of damage localization as well as its quantification. The level of damage will be quantified as a reduction

in an appropriately selected stiffness characteristic such as the flexural rigidity (*EI*) of a beam element. Both 2-d and 3-D frame structures are considered, in Chapter 2 and Chapter 3 respectively, as demonstration example problems for damage identification.

Moreover, since the higher modes tend to be more polluted than the lower modes. The utilization of such polluted modes should, thus, be avoided in any identification process. In Chapter 4, this study examines the development of a new strain mode shape-based curvature flexibility approach for element stiffness coefficient identification using the flexibility gradients approach initiated by Singh and Bisht (2007). Only a first few strain mode shapes will be utilized in this approach.

Since the structural strains can be measured as conveniently as the acceleration response on a structure, and since they also provide a more complete and damage sensitive dynamic data, this study will focus on the efficient utilization of such measurements for damage identification. Therefore, in Chapter 5, this research focuses on the development of response sensitivity-based methodologies for optimal placement of strain sensors to meet the critical damage identification objectives. The objective of this part of the work is to identify the minimum number and locations of the strain sensors needed for different damage identification scenarios considering the strain response sensitivities.

2. Chapter 2: Damage Identification of Two Dimensional Frame Structures

2.1. Introduction

The health of a structural system such as a building or a bridge is determined by the health of its structural components such as beams and columns that make the structure. These structural elements can get damaged by overstressing, cracking, corrosion or other forms of material degradation. The damage in structural elements tends to reduce their stiffness values. Thus, the primary objectives of the SHM schemes has been to identify the stiffness characteristics.

To identify the stiffness characteristics of a structure, the most effective approach is to measure the structural deformations under some controlled forcing environment; that is, measure the structural response as well as the forcing function. However, since a complete measurement of the external force may not be feasible on most structural systems especially the civil, aircraft and ship structures it has been common to utilize only the measured structural response with no information about the input for structural health monitoring.

Different methods that have been proposed to do this can be broadly classified in to two categories: (a) the methods that work with the measured dynamic responses in time and/or frequency domains and (b) the method that work in the modal domain. This study is concerned with the modal approach which utilize the measurements of flexural strains with and without the measured linear acceleration responses. The measured responses are first utilized to calculate the structural frequencies and response mode shapes which are then processed to calculate the structural stiffness characteristics to detect the magnitude and location of the damage. In the following, to highlight the impact of strain measurements on the modal information being sought we first provide a brief description of how the measured responses relate to the system's modal characteristics, followed by the processing of these responses for stiffness identification.

2.2. Problem Formulation

For a structure consisting of interconnected finite elements the equation of motion can be written in the following form,

$$M\ddot{X}(t) + C\dot{X}(t) + KX(t) = F(t) \tag{1}$$

where M, C and K are n by n mass, damping and stiffness matrices, respectively; and $X(t), \dot{X}(t),$

and $\ddot{X}(t)$, respectively, are the n by 1 displacement, velocity and acceleration response vectors associated with the structural degrees of freedom, and $F(t)$ is the n by 1 forcing vectors. Since this study's numerical examples are focused on the buildings excited by earthquake induced ground motions, the forcing function vector in this situation is expressed as $F(t) = -Mr\ddot{X}_g(t)$ where $\ddot{X}_g(t)$ is the base acceleration, and r is the ground motion influence vector.

In the analysis of a framed structure, it is common to assume that the linear displacement degrees of freedom are associated with major structural mass whereas the rotational degrees of freedom are usually considered to be massless, although in a consistent finite element formulation even the rotational degrees of freedom will have some inertial mass but usually with relatively smaller values. Assuming that the rotational degrees of freedom are associated with little mass, usually they can be condensed out in the calculation of dynamic response. Focusing mainly on the systems excited by earthquake induced ground motion, the equations of motion associated with the kept degrees of freedom can be written as:

$$M_k^*\ddot{X}_k(t) + C_k^*\dot{X}_k(t) + K_k^*X_k(t) = F_k(t) = -M_k r\ddot{x}_g(t) \tag{2}$$

where M^*, C_k^* and K_k^* are n_k x n_k condensed mass, damping and stiffness matrices associated with kept dynamic degrees of freedom where n_k is number of these kept degrees of freedom; X_k and $F_k(t)$ are the response and forcing function vectors, respectively,

associated with the kept degrees of freedom. The mass matrix M^* is the non-zero part of the total mass matrix M and the condensed stiffness matrix K_k^* is defined as:

$$K_c^* = (K_{kk} - K_{kr}K_{rr}^{-1}K_{rk}) \tag{3}$$

where the submatrices in Eq. (3) associated with the kept and reduced degrees of freedom are the parts of the system stiffness matrix which is defined as follows:

$$K = \begin{bmatrix} K_{kk} & K_{kr} \\ K_{rk} & K_{rr} \end{bmatrix} \tag{4}$$

The eigenvalue problem associated with the condensed equation of motion can be expressed as:

$$K_k^* \varphi_{kj} = \omega_j^{\,2} M^* \varphi_{kj} \qquad ; j = 1,...n_k \tag{5}$$

wherein φ_{kj} is the j^{th} mode shape vector associated with the kept dynamic degrees of freedom and ω_j natural frequency. The eigenvalue problem associated with complete system can also be defined as:

$$K\varphi_j = \omega_j^{\,2} M \varphi_j \qquad ; \qquad j = 1,...n_k \tag{6}$$

wherein the complete mode shapes φ_j can be defined in terms of the mode shapes φ_{kj} of the condensed equation as,

$$\varphi_j = \begin{Bmatrix} \varphi_{kj} \\ \varphi_{rj} \end{Bmatrix} = \begin{Bmatrix} \varphi_{kj} \\ -K_{rr}^{-1}K_{rk}\varphi_{kj} \end{Bmatrix} = \begin{Bmatrix} 1 \\ -K_{rr}^{-1}K_{rk} \end{Bmatrix} \varphi_{kj}; \quad j = 1,...n_k \tag{7}$$

For structural health monitoring purposes, one measures some dynamic responses by using appropriate sensors. As mentioned earlier, the most commonly measured response is the linear absolute acceleration response, which for a system considered above will be the linear accelerations of the mass. This measured acceleration for the example system excited by ground motion is the absolute acceleration associated with the kept degrees of freedom and can be written as follows:

$$\ddot{X}_A(t) = \ddot{X}_k(t) + r\ddot{x}_g(t) = -\sum_{j=1}^{n_k}\left(\omega_j^2 q_j + 2\beta_j\omega_j\dot{q}_j\right)\varphi_{kj} \tag{8}$$

where $q_j(t)$ is the time variation of the principal coordinate response which is the solution of the following un-coupled modal equation:

$$\ddot{q}_j + 2\beta_j\omega_j\dot{q}_j + \omega_j^2 q_j = f_j(t) = -\varphi_j^T M^* r\ddot{x}_g(t) \tag{9}$$

Here it is assumed that the system is classically damped such that the $2\beta_j\omega_j = \varphi_{kj}^T C_k^* \varphi_{kj}$ which defines the modal damping ratio β_j. This further assumes that the mode shape vectors are mass normalized as $\varphi_{kj}^T M^* \varphi_{kl} = \delta_{jl}$. $f_j(t)$ is the generalized forcing function = $\varphi_{kj}^T F_k(t)$ which for a structure excited by earthquake induced ground motion is $= -\varphi_{kj}^T M^* r\ddot{x}_g(t)$ as indicated in Eq. (9).

The last part of the Eq. (8) is shown to emphasize that the acceleration response is related to only the eigenvectors associated with the kept coordinates and not those of the reduced coordinates. Thus the processing of the measured linear acceleration for health monitoring will not provide information about the mode shape values of the reduced coordinates which usually contain the rotational degrees of freedom of a vibrating structure. To provide a more complete information, it is necessary that the measured response quantity used for health monitoring be such that it is also affected by the reduced coordinates such as the rotational degrees of freedom. Since the flexural strains measured on the structural elements are affected by the rotational degrees of freedom, the processing of these will thus provide a more complete information for structural health monitoring.

For a linear structural system, the mode shape ρ_j of any response quantity that is linearly related to the response vector $X(t)$, such as a strain, stress or bending moment at a point p on the member can be simply defined in terms of mode shape vector φ_j. For example for the strain at point p, this mode shape can be written as follows:

$$\rho_j(p) = \mathrm{T}_p \varphi_j \; ; j = 1, n_k \tag{10}$$

where T_p is the transformation vector for the strain response at the point. The elements of this transformation matrix are simply the functions of the mechanical properties of the structural element such as its dimensions.

In terms of the modal quantities, the time variation of the response quantity such as the strain can be expressed as:

$$\varepsilon_p(t) = \sum_{j=1}^{n_k} \rho_j(p)\, q_j(t) \tag{11}$$

This response clearly depends on the mode shapes of all element degrees of freedom including the reduced coordinates associated with the rotational degrees of freedom. Thus the processing of this response will provide a more complete information than the measured acceleration response, especially if we are interested in evaluating the stiffness properties of the elements to assess the health of the system as is indicated later in this study.

Mode Shapes and Frequencies

In this section we briefly describe the methods that are commonly used to calculate the systems modal characteristics form the measured response. The most prevalent methods that are used to extract modal frequencies and mode shapes from measured response are either Eigen realization algorithm (ERA) (Juang 1994) or stochastic subspace identification approaches (Ljung 1987 and Van Overschee 1996). The objective of both of these methods is to identify the state matrix A and output matrix C of the following discrete state space model representation of the dynamic system described by Eq. (1) using the measured

response values y_k:

$$x_{k+1} = Ax_k + Bu_k + w_k$$
$$y_k = Cx_k + Du_k + v_k \tag{12}$$

where x_k is the state vector at time step k consisting of the both the system displacement and velocity vectors; y_k is the measured output response vector such as strains and accelerations at time k; u_k the input vector; and w_k and v_k are the unmeasurable process noise (due to disturbance and modelling) and measurement noise, assumed to be zero-mean white noise. The system matrices are: A = the state matrix; B = input matrix; C = output matrix; and D = direct transmission matrix.

ERA requires that the measurements of the free vibration responses such as those caused by some impulsive forces be available as y_k ; that is, there be no u_k . However, for the purposes of health monitoring it would be almost impossible to generate such impulse responses experimentally for large civil structures. For such structures, it is possible to take measurement under externally applied loads caused by wind, traffic or earthquake induced ground motion but conversion of his motion to free vibration condition will also require measurement of the forcing input. This might be possible to do it for traffic induced forces or for earthquake induced motion where measurements of the support movements could possibly be recorded, but not for wind induced forces. However, as described by James et al. (James et al, 1995), the cross covariance functions of the response quantities of a system excited by white noise input provides a good representation of the free vibration response. This approach is commonly referred to as the natural excitation technique or NExT. For a response such as the dynamic strain response measured at several locations on different structural elements, it is simple to show that for a white noise excitation such as an earthquake induced ground motion the stationary covariance of two strain response values separated by τ can be written as:

$$R_{rs}(\tau) = \sum_{k=1}^{n} \rho_k(r) e^{-\beta_k \varpi_k \tau} \{A_k \cos \omega_{dk} \tau + B_k \sin \omega_{dk} \tau\} \tag{13}$$

wherein $R_{rs}(\tau)$ is the cross covariance function for the strain responses at location r and s ; ω_k, ω_{dk} and β_k, respectively, are the k^{th} natural frequency, damped frequency and damping ratio; $\rho_k(r)$ is the k^{th} strain mode shape value at location r. The factors A_k and B_k are defined by the following equations:

$$A_k = a_g(\gamma_k/\omega_{dk})\sum_{j=1}^{n}\rho_j(s)(\gamma_j/\omega_{dj})\int_0^{\infty} e^{-(\beta_j\omega_j+\beta_k\omega_k)u}\sin\omega_{dj}\,u\sin\omega_{dj}\,u\,du;$$
$$B_k = a_g(\gamma_k/\omega_{dk})\sum_{j=1}^{n}\rho_j(s)(\gamma_j/\omega_{dj})\int_0^{\infty} e^{-(\beta_j\omega_j+\beta_k\omega_k)u}\sin\omega_{dj}\,u\cos\omega_{dj}\,u\,du \quad (14)$$

in which a_g is the intensity of the white noise base motion. Eq. (13) can be considered to represent the strain response at location r corresponding to the initial conditions described by the two factors A_k and B_k. For other types of white noise forcing functions also it can be shown that the response covariance function are of the same form as Eq. (13). Thus, these response covariance functions calculated for different strain locations for increasing values of τ are similar to free vibration response needed by the ERA algorithms to identify the state and output matrices and for calculating the frequencies and mode shapes of the strain at the measurement locations.

In the stochastic subspace identification methods utilizing the classical covariance-driven approach, the measurement records are not converted to covariance functions before. Rather, the unknown input u_k is incorporated as a part of the stochastic white noise components in both the discrete state space model equation as well as the output equations. That is, in Eq. (12) the terms associated with u_k are dropped. The covariance utilized in these approach is essentially achieving the same objective as the inputs calculated by NExT. In the classical covariance driven approach, however, all measurements are used to obtain the covariance matrices and not just one vector of the covariance functions calculated with respect to a chosen reference measurement in NExT. (Peeters and De Roeck 1995) propose a reference-based SSI approach wherein they suggest to utilize more than one but not all measurements to improve the computational efficiency of the SSI.

These identification approaches calculate the estimates of the state and output matrices. The complex eigenvectors ψ_j of the discrete state space matrix are also the state eigenvectors of its continuous counterpart whereas its eigenvalues divided by the time step increment can be used to define the system frequencies and modal damping ratios. To obtain the mode shapes associated with response quantities measured at the chosen structural locations we use the output matrix C as:

$$\varphi_j = C\psi_j \tag{15}$$

We utilize these calculated mode shapes for damage identification in the following section.

2.2 Damage identification using the Eigen Equation

Many approaches have been proposed to detect the occurrence, estimate the level, and identify the location of damage in structures. The utilization of systems modal properties and attributes related to the modal properties have been proposed. With some limitation, a simple change in the modal properties or an appropriately selected modal characteristics can some time indicate the occurrence of a damage. The identification of the damage severity and location is, however, more difficult as it requires the calculation of the stiffness characteristics of structural elements such as beams and columns that make up the system. Related to what is proposed in this study, (Caicedo et al. 2004) have proposed a workable identification approach utilizing the displacement mode shapes. The displacement mode shapes were obtained using NExT and ERA approach with the acceleration response time histories for the IASC-ASCE benchmark problem. This approach can be effective with building structures that primarily behave in story shearing modes for which the measured linear floor accelerations essentially provide adequate information for damage identification. This approach with the measurements of linear floor accelerations, however, will not work if the supporting frame of the building is a moment resisting frame with significant joint rotational degrees of freedom as on a civil structure the rotational degrees of freedom would be difficult to measure. Esfandiari and group (Esfandiari et al, 2010, Sipple and Sanayei 2010, Esfandiari 2014, and Pedram and Khedmati 2016) utilize the strain

frequency response functions and spectral density functions obtained from the measured strains (which include the contributions of the rotational degrees of freedom) in their structural identification approach. These frequency response function or spectral density function-based approaches, however, need an accurate description of the input for which the strains were measured to define the spectral functions. This situation is quite possible in laboratory conditions, but impractical to acheive for most civil structures. However, as shown below the strain measurements on the structural elements of the frame can capture this much-needed information on the joint rotations. In the following we present an approach to estimate the complete system mode shapes including the rotational and displacement degrees of freedom which can then be used to identify thechanges in stiffness characteristics of the structure with illustrative examples of multi-story and multi-bay steel frame structures subjected to earthquake induced base motion.

The strain mode shapes extracted from the measured strain data using SSI or NExT-ERA can be used to estimate the complete system mode shape φ_j, which also include system's rotational degrees of freedom as follows. Considering Eq. 10, the vector of strain mode shape can be expressed as:

$$\rho_j = T\varphi_j \; ; j = 1, n_k \tag{16}$$

where ρ_j is the j^{th} modal vector of all strains measured at m locations on the structure and T is a $m \times n$ transformation matrix. Eq. 16 can be used to obtain the least square estimate of the mode shape vector $\bar{\varphi}_j$ in terms of the estimated strain mode shapes $\bar{\rho}_j$ as follows:

$$\bar{\varphi}_j = T^{+}\bar{\rho}_j \; ; j = 1, n_k \tag{17}$$

Where T^{+} is the pseudo inverse of the transformation matrix T which can be defined as:

$$T^{+} = (T^{T}T)^{-1}T^{T} \tag{18}$$

For large problems this pseudo inverse operation in Eq. 18 can be more effectively done by QR or singular value decomposition. Knowing the complete mode shapes, the mean square estimation of the element-wise stiffness parameters of the system, such as $k_i = (\mathrm{EI})_i \;\; i = 1, n_e$ (the bending stiffness parameter commonly used to define the stiffness characteristics of prismatic beam element) can now be calculated using the system's i^{th} characteristic equation as follows (Caicedo et al,2004 and Udwadia 2005):

$$K\bar{\varphi}_i = \omega_i^2 M\bar{\varphi}_i \tag{19}$$

The total stiffness matrix of the system in Eq. 19 can be expressed as a sum of the stiffness contributions of individual elements as:

$$K = \sum_{j=1}^{n_e} K_j = \sum_{j=1}^{n_e} k_j U_j \tag{20}$$

where n_e denotes the number of elements, k_j is the stiffness parameter of the j^{th} element, and U_j is a $n \times n$ matrix which when multiplied by k_j defines contribution of the j^{th} element stiffness to the total system stiffness matrix. Utilizing Eq. 20, the characteristic Eq. 19 can be re-written as,

$$K\bar{\varphi}_i = \left(\sum_{j=1}^{n_e} K_j\right)\bar{\varphi}_i = \left(\sum_{j=1}^{n_e} k_j U_j\right)\bar{\varphi}_i = \sum_{j=1}^{n_e} (U_j\bar{\varphi}_i)k_j = \omega_i^2 M\bar{\varphi}_i \tag{21}$$

The last two terms of Eq. 21 can be re-stated as

$$C_i S = \omega_i^2 M\bar{\varphi}_i = \nu_i \tag{22}$$

wherein the $n \times n_e$ matrix C_i, n_e by 1 vector S containing the element stiffness parameters k_j, and $n \times 1$ vector ν_i are defined as,

$$\begin{aligned} C_i &= \left[c_1 c_2 \ldots c_{n_e} \right]; \\ S &= (k_1, k_2, .. k_{n_e})^T ; \\ \nu_i &= \omega_i^2 M \bar{\varphi}_i \end{aligned} \tag{23}$$

The vectors c_j, $j = 1, n_e$ which define the matrix C_i are defined as,

$$c_j = U_j \varphi_i; \quad j = 1, n_e \tag{24}$$

The vector S in Eq. 22 containing the element stiffness parameters values is obtained using the generalized pseudo inverse of C_i as:

$$S = C_i^+ \nu_i \tag{25}$$

In Eq. 25 the pseudo inverse C_i^+ can be defined similar to Eq. 18 as,

$$C_i^+ = (C_i^T C_i)^{-1} C_i^T \tag{26}$$

Eqs. 22 and 25 are applicable for each mode shape or eigenvector that can be extracted from the measured data. Thus, in principle, each eigenvector should be able to provide a mean square estimate of all element stiffness coefficients, k_e. For calculating the mean square estimate, the pseudo inverse is best determined by QR-decomposition. However, if the coefficient matrix C_i is not overdetermined or is not inconsistent then it is best to use the singular value decomposition to calculate the Moore-Penrose generalized pseudo inverse in Eq. 25. This provides the minimum norm mean square estimate to provide the unique value for the vector S. However, the accuracy of this estimate of S depends on the accuracy of the system eigenvector utilized in the characteristic equation, which in turn depends on the

numerical accuracy of the NeXT-ERA or SSI identification approaches and the measurement noise in the data used.

Even if the eigenvectors used in characteristic equation have no errors, the accuracy of the estimated element stiffness values is affected by the two pseudo inversions utilized in their estimations. This process in turn depends on the number of response measurements used, the number of degrees of freedom needed to describe the system and the number of stiffness elements to be estimated to define the system as they clearly affect the size of the transformation matrix *T* and matrix C_i that are used in the pseudo inversions of Eqs. 16 and 22. The size of *T* is determined by the number of strain measurements made and the number of the system degrees of freedom used to describe the structural systems whereas the size of C_i is determined by the number of the system degrees of freedom and the number of structural element that form the structural system. Another factor which seems to affect the accuracy of a calculated k_e value of a particular structural element is the relative importance of the utilized mode to this element's dynamic response.

To demonstrate some of these effects on the accuracy of the calculated stiffness values numerically, three variants of a 2-bay and 4-story moment resistant plane frame structure consisting of 12 columns and 8 beam elements shown in Figure 2.1 are considered. Each structural element in the frame is modeled as a classical 2-D beam elements with one translational and one rotational degrees of freedom at its each end. Assuming that the axial deformations of the beam/column elements can be ignored, this structural system can be represented by a total of 16 degrees of freedom. They include 4 translational degrees of freedom representing the horizontal motions of the frame at each floor level and 12 rotational degrees of freedom representing the rotational motions of the joints. All three variants or models of this frame are assumed to be excited by earthquake induced ground motions at the base.

The first variant or model of this frame has a symmetric layout (with uniform story heights of 3 m and bay spans of 5.5 m) and uniform member stiffness values with $k_e = EI$ = 37.548 $MN.m^2$ for each structural element. Herein this model is called as Model 1 with "uniform G and S", where the letter G referring to geometric symmetry and the letter stiffness S referring

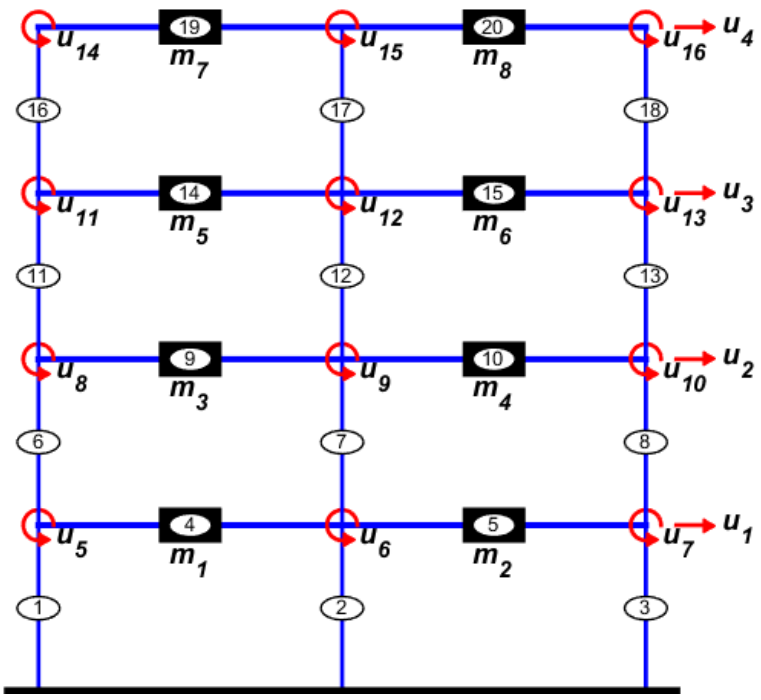

Figure 2.1 Configuration of Models 1, 2 and 3 of the Structural Frames Used in this Study

to stiffness characteristics. The Model 2 of the frame has the same layout as of Model 1, but its 9 arbitrarily selected structural elements have different stiffness values (EI values) than the other members. This model can be assumed to represents a damaged version of Model 1 where the nine structural elements (numbers 2, 4, 6, 8, 12, 13, 17, 18 and 19) are assumed to have sustained damage to reduce their effective element stiffness values, respectively, by 10, 15, 5, 10, 6, 2.5, 10, 2, and 15 percent of their original values. Herein, this "uniform G and non-uniform S" model is called as Model 2. The third variant of this structure, called as Model 3 with "non-uniform G and S", on the other hand has two different story heights (first story = 3.3 m, second and third story heights = 3.0 m and the fourth story height = 2.7m) and bays of two different spans (5.5 m and 4.95m). The stiffness properties of nine elements, again arbitrarily selected as element numbers 1, 3, 4, 9, 11, 15, 18, 19 and 20, in this model are reduced by 10, 15,4.5, 10, 6, 3, 10, 2, 15 percent of their initial values, respectively. This represents a damaged version of a frame where stiffness values of these 9 structural elements have been reduced. These geometric and stiffness variation have been introduced

primarily to alter differently the relative contributions of the systems modes to their structural responses.

The floor and roof slabs masses supported by the frame are assumed to be concentrated at the floor and roof levels. These masses are associated with the horizontal motions of the floors. The rotational degrees of freedom at the nodes are assumed to be associated with little inertial mass. Thus for dynamic analysis, these rotational degrees of freedom are condensed out, leaving only four degrees of freedom associated with the horizontal motions. For these assumed mass and stiffness characteristics, the modal frequencies and participation factors for the base induced ground motion are given in Table 2.1 for these three frame models. For the system expressed by Eq. 2, i^{th} modal participation factor ρ_i is defined as,

$$\rho_i = \varphi_i^T M r / (\varphi_i^T M_k \varphi_i);\ i = 1, .., n_k \tag{27}$$

For linearly behaving structures exposed to earthquake induced ground motion, these factors tend to represent the relative contributions of different modes to a structural response. These factors usually have higher values for the lower modes, indicating the higher levels of their contribution to the system response compared to the contribution of the higher modes. These participation factors are also utilized later in the numerical study.

2.5. Numerical Study

2.5.1. Damage Identification Results Obtained Utilizing the Exact Strain Modes:

To show the effect of the two levels of pseudo inversing on the accuracy of the stiffness identification, first the exact strain mode shapes numerically calculated for the known properties of the structural system were utilized in the calculations of the element stiffness coefficients. The utilization of the exact mode shapes is equivalent to assuming a complete absence of the numerical mode extraction errors as well as the measurement noise. To estimate the element stiffness values, the exact strain response eigenvectors were utilized in Eq. 16 to estimate the system eigenvectors $\bar{\varphi}_j$ associated with the dynamic degrees of

freedom through pseudo-inversing. To assess the impact of this pseudo inversion on the accuracy of the calculated system modes, the difference of the modal MAC values from 1 (that is, 1-MAC value) which is a measure of the error in modal extraction is used. The top part of Table 2.2, shows this value for the four system modes which were calculated from the exact strain modes shapes using pseudo-inversion of Eq. (16). Since values in this part of Table 2 are essentially zero, it clearly indicate that this inversion is not expected to contribute much error in the estimation of the system modes. It is primarily because the linear system of equations represented by Eq. 16 are not rank deficient with overdetermined (with more system equation than unknowns and thus are inconsistent) matrix T. The least square estimates obtained through this pseudo inversion of Eq. 16 are thus the "best" estimates.

Table 2.1 Modal Characteristics of the three models

	Mode Number			
	Mode 1	Mode 2	Mode 3	Mode 4
	Frequencies			
Model 1	1.17912	3.82673	7.083	10.2654
Model 2	1.15753	3.74181	6.9309	10.0542
Model 3	1.13707	3.80496	7.10858	10.1523
	Participation factors			
Model 1	353.7061	128.6007	79.8209	44.5248
Model 2	354.2295	127.1845	79.6077	44.8128
Model 3	360.4363	121.7255	66.0202	30.1653

Table 2.2 (1- ABS(MAC)) Values of the system modes estimated by pseudo inversion of Eq. 16

	Mode Number			
	Mode 1	Mode 2	Mode 3	Mode 4
	For Modes Extracted from Exact Strain Modes as Input			
Model 1	0	0	0	0
Model 2	0	0	0	0
Model 3	0	0	0	0
	For Modes extracted from strain response with 0% measurement noise			
Model 1	1.8569E-06	1.1400E-07	2.3556E-06	2.0054E-07
Model 2	1.3540E-06	2.7193E-07	7.7784E-07	7.0733E-07
Model 3	4.5930E-07	4.9392E-07	1.8448E-07	1.9319E-06
	For Modes extracted from strain response with 10% measurement noise			
Model 1	1.3899E-09	1.0925E-06	4.6165E-04	4.8319E-03
Model 2	5.0023E-10	3.3614E-07	5.1722E-04	2.8386E-03
Model 3	2.6864E-10	1.0995E-05	1.6541E-03	9.0843E-03

Next we examine the impact of the pseudo inversion employed in Eq. 22 on the estimated element stiffness coefficient values k_e. In most cases, the linear set of Eq. 22 is not likely to

be overdetermined if it is used for a single mode. For each mode of the three structural frame models considered in this study, the matrix C_i is 16 by 20. That is, there are only 16 linear equations to estimate 20 structural element stiffness values, resulting into a system of consistent equations with four independent variables giving infinite possible solutions for the element stiffness values. The utilization of the Moore-Penrose pseudo inverse to estimate the vector *S* containing the element stiffness values, in this case, will provide a *least normed mean square estimate* of S. The following set of results show the accuracy of this calculated least normed mean square estimate of S for the three structural models.

Figure 2.2 a, b and c show the percentage errors in the estimated stiffness values of all 20 elements for the three models of this frame using the exact strain mode shapes. This percentage error represents the difference between the calculated and known exact stiffness values for each element. The figure legend also show the root mean square (RMS) values of the percentage errors for each plot. This RMS is simply the square-root-of-the-sum-of-squares of the element errors divided by the number of elements. The results shown in Figure 2.2 a indicate that use of a single strain mode alone in Eqs. 16 and 22 is able provide accurate estimates of the element stiffness values at least for a symmetric system, but the results seem to become less accurate if the non-uniformity or asymmetry in the structural system becomes strong as shown by the results in Figure 2.2 b and c. The RMS error values shown in the figure legends indicate that for models 2 and 3 the RMS error can be as high as 5.6%. Although the exact eigenvector values were used in the estimation of the element stiffness values, the pseudo inversion primarily in Eq. 22 seems to have caused this error in the estimation. That is, for structural systems with strong asymmetry the least normed mean square estimate of vector *S* obtained through pseudo inversion of Eq. 22 may not provide accurate element stiffness values.

The use of a single mode in forming Eq. (22) leads to a set of less number of equations than the number of unknowns. However, if two or more system modes are combined to form Eq.(22), then the number of equation can exceed the number of unknowns. Indeed a collective use of more modes in the stiffness estimation has been suggested earlier (Caicedo et al, 2004, Udwadia 2005, and Mahmood et al, 2014) though not primarily to get more

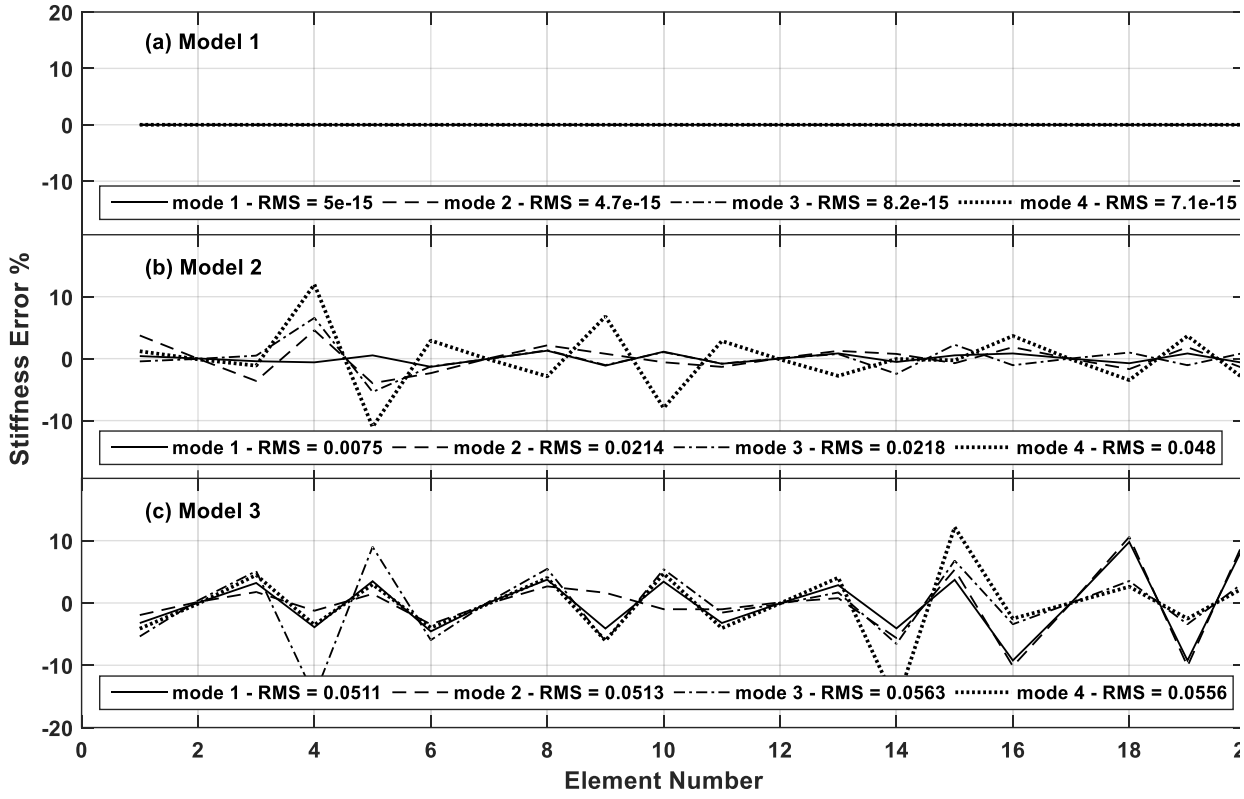

Figure 2.2 Errors in the element stiffness values in Models 1, 2 and 3 when only one mode is used in the stiffness estimation. Utilization of exact modes

equations than the unknowns but under the belief that utilization of more modal data should improve the results. This is achieved by stacking equations like Eq. 22 for each eigenvector and carrying out the inversion of the combined equations to estimate the stiffness coefficient vector S as follows:

$$CS = \begin{bmatrix} \alpha_1 C_1 \\ \alpha_2 C_2 \\ . \\ . \\ \alpha_{n_k} C_{n_k} \end{bmatrix} S = \begin{bmatrix} \alpha_1 \nu_1 \\ \alpha_2 \nu_2 \\ . \\ . \\ \alpha_{n_k} \nu_{n_k} \end{bmatrix} = \nu \tag{28}$$

wherein different values of α_i in Eq. 28 represent the different contributions of different modes in this collective utilization of the modal information. Since, it is not necessary to use a contribution factor when a single mode is used to estimate the vector *S* of element stiffness

coefficient, a simple stacking of the equations without any special weighting factors has been suggested earlier. Herein, however, the effect of using different modal contribution factors on the accuracy of stiffness estimation is also explored through numerical examples.

Initially, two sets of contribution factors are considered. In the first set all α_i are set equal to 1, implying that all modes are equally effective in this estimation. In the second set, these contribution factors are set equal to their modal participation factor defined earlier in Eq. 27. The use of these participation factors as the modal contribution factors α_i in Eq. 28 for the collective utilization of different modes is expected to lessen the negative impact of utilizing the higher modes on the accuracy of the estimated stiffness values. Eq. 28 will now have more equation than the number of variable to be estimated, and if matrix *C* is not rank deficient, then pseudo inversing can be used to obtain the least square estimation of vector S as:

$$S = C^{+}\nu \tag{29}$$

wherein C^{+} is the pseudo inverse of the $(n_k \times n)$ by n_e matrix C.

Figure 2.3 a-c show the errors in the estimated stiffness values calculated with Eq. 29 for mode combinations of 1+2, 1+2+3, and 1+2+3+4 for the three frame models. Also shown in the figure legends are the stiffness RMS values for each modal combination used. Comparison of these results obtained with individual modes, shown in Figure 2.2 a-c, indicates that including other higher modes with mode 1 improves the accuracy of the estimated stiffness values for all three structural models. In fact the errors for all mode combination being very low cannot be differentiated in the figures; the highest error RMS values is now 7.63e-14 -- indeed a very low error value.

2.5.2. Damage Identification Results Obtained with Modes extracted from Noise-Free Strain Responses:

The previous results primarily examined the relative effects of the individual and combined modes on the accuracy of the element stiffness value obtained through pseudo inversion of

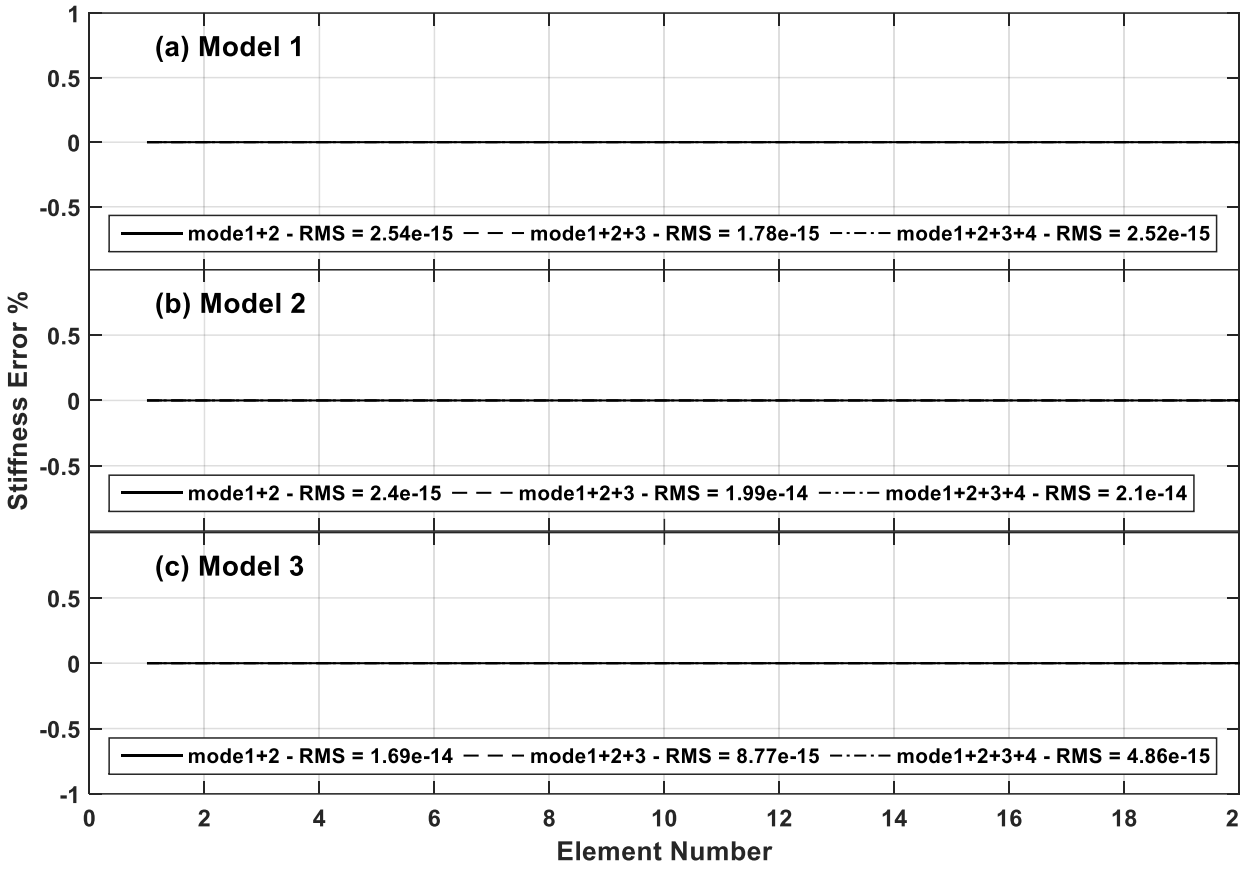

Figure 2.3 Errors in the element stiffness values in Models 1, 2 and 3 with different combinations of modes with equal weights ($\alpha_i = 1$) used in the stiffness estimation. Utilization of exact modes

the coefficient matrices in three structural models. It assumed that the exact modes were available. These modes were not extracted from any measurements but were analytically calculated. The next set of tables and figures show similar results obtained with the extracted strain mode shapes which were obtained by the SSI approach from the noise-free measured strain responses. Comparison of these results with those presented earlier for the analytically calculated exact modes is expected to show the influence of the mode extraction on the accuracy of the proposed stiffness identification approach for structural health monitoring.

The second part of Table 2.2 shows the (1-MAC) values for the system modes which were calculated from Eq. (17) utilizing the strain modes shapes extracted from the measured

noise-free strain response. These values are not as small as those for the exact mode shapes, shown in the part (a) of Table 2.2. Although this difference between the extracted and exact mode shapes appears to be small, it is seen to strongly affect the estimation of the stiffness coefficients which are calculated by pseudo-inversion of Eq. 22. The percentage error in the element stiffness values calculated from these extracted modes are plotted in Figure 2.4 a-c for the three frame models. The RMS error values for different modes used with different structural models now are varying between 0.3% to as high as 12%. Thus a small inaccuracy in the extraction of the system modes can significantly affect the accuracy of the estimated element stiffness values.

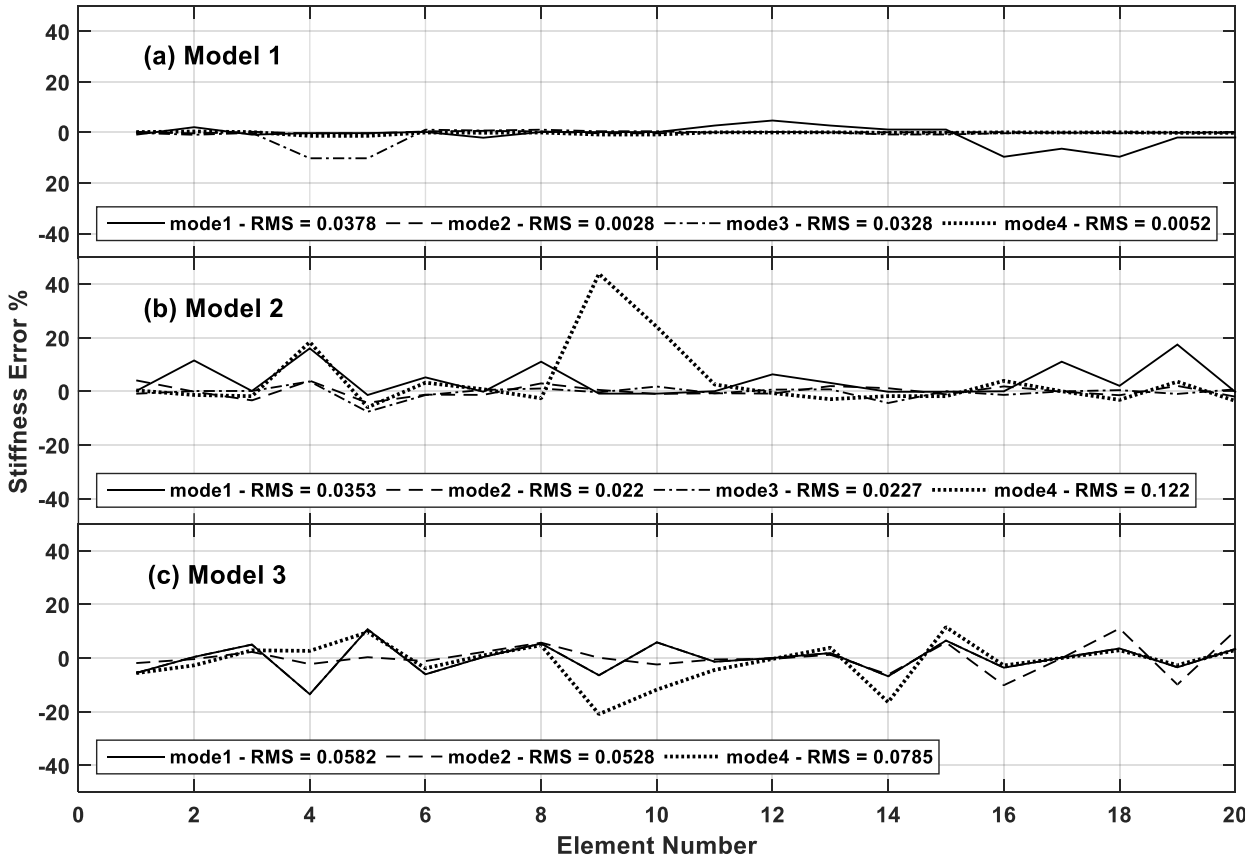

Figure 2.4 Errors in the element stiffness values in Models 1, 2 and 3 when only one mode is used in the stiffness estimation. Modes extracted from noise-free strain responses

Since the utilization of higher exact modes with mode 1 improved the accuracy of the element stiffness estimation as shown through the results in Figure 2.3 a-c, such a combination was also considered with these extracted modes. Figure 2.5 a-c show the effect

of considering more modes on the element stiffness estimation. The simple straight forward combination of more modes with equal weights does not necessarily improve the accuracy of the stiffness estimation in many cases, as it did when the exact modes were used; in fact there is no identifiable trend associated with different combinations of the modes on the RMS values of the element stiffness errors. The RMS values ranged anywhere between a small error of 0.1% when all modes are combined in Model 1 to a relatively larger error of about 15% when modes 1 and 2 are combined in Model 2. In Model 3, even utilizing all the modes in the combination does not improve the accuracy although the modes could be extracted fairly accurately as indicate by the (1-MAC) values in Table 2.2. Similar results (not shown here) were observed when the modes participation factors were used as their modal contribution factors; the error RMS values for different cases differed significantly but with no specific trend. This indicates that the pseudo inversing of Eq. 22 used to calculate element stiffness values is sensitive to changes in the modes and the mode contribution factors α_i. Perhaps an optimal values of α_i exist to improve element stiffness estimation.

The sensitivity of pseudo inversing of C in Eq. 28 can be measured in terms of the condition number of the matrix used C in pseudo inversion. The condition number is also defined as the ratio of the highest to the lowest singular values of the matrix C. For the matrix C to have a stable pseudo inverse and not be ill-conditioned it is desirable to have a small condition number. Since this number is affected by the chosen values of α_i, the values that minimize this condition number are chosen as the optimum set of α_i. Since not all modes can be accurately identified by SSI and NExT-ERA algorithms, it is also desirable to select the system modes that are most accurately extracted as well as to satisfy the modal characteristic Eq. 19 and are orthonormal to other mode used in Eq. 28. The relative accuracy of extracted modes can be assessed if their MAC can be defined. Since the MAC value can only be calculated if the exact modes are known, it becomes difficult to identify the inaccurately extracted modes that need to be excluded from this modal combinations. However, since mode 1 is usually more accurately extracted from the data, the identification of the other modes which are relatively poorly extracted with respect to mode 1 can be effectively done by an examination

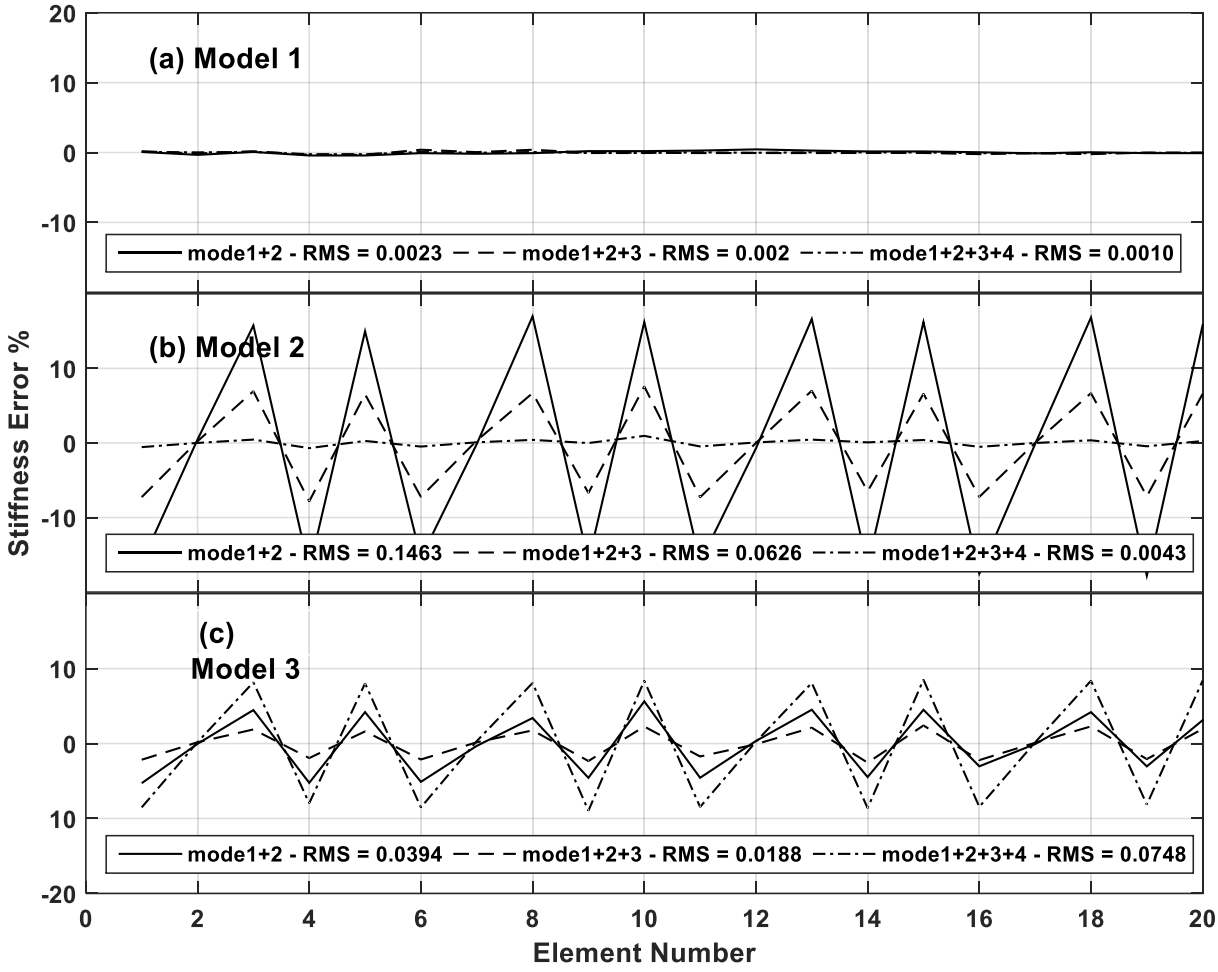

Figure 2.5 Errors in the element stiffness values in Models 1, 2 and 3 when different combinations of modes with equal weights ($\alpha_i = 1$) are used in the stiffness estimation. Modes extracted from noise free strain responses

of the off-diagonal terms of the mode orthogonalization matrix $\varphi^T M \varphi$ that are associated with mode 1. The off-diagonal terms associated with mode 1 and mode k can be defined as,

$$\delta_{1k} = \frac{\varphi_1^T M^* \varphi_k}{\sqrt{(\varphi_1^T M^* \varphi_1)(\varphi_k^T M^* \varphi_k)}} \tag{30}$$

An absolute value of δ_{1k} significantly larger than 0.0 indicates that the orthogonal extraction of these two modes has been affected by the extraction process or the measurement noise. Since the first mode is usually extracted most accurately from the data, it is usually the

accuracy of the k^{th} mode that must be under question. These off diagonal terms associated with mode 1, for the three structural models 1, 2 and 3, respectively, are: Model 1 (1, -0.0006, -0.0004, 0.0012); Model 2 (1, -0.0002, 0.0016, -0.0003) and Model 3 (1, 0.0007, 0.0009, 0.0012). Since all off-diagonal terms for all three models are reasonably small, it is fair to assume that all modes have been extracted as accurately as the first mode. Thus to identify the optimum set of α_i all possible combinations of modes were used in forming Eq. 28 and the set of α_i that gave the smallest condition number defined the optimum set. For each set of mode combination, the α_i values were obtained by using the MATLAB function FMINUNC.

The results shown in Figure 2.6 a and b were obtained with the set of modes and the optimum α_i values that gave the smallest condition number. Figure 2.6 a shows the percentage errors in the element stiffness values for the optimal sets of modes for Models 1, 2 and 3. With element stiffness errors as high as 10% and the RMS error of about 4%, this optimal combination did not improve the results significantly. Since the stiffness values identified for Model 1 and 2 represents the undamaged and damaged versions of the structure, the difference of these element stiffness values is used to calculate the damage in the structural elements defined by Model 2. Figure 2.6 b shows the elements whose stiffness values have changed. The stiffness of elements 2, 4, 6, 8, 12 13, and 19 have been reduced and thus these elements can be considered damaged – indeed a correct identification. But Figure 2.6 b also incorrectly indicates that elements 11 and 14 are damaged and misses to identify element 17 as a damaged element. It also indicates that some elements such as 7, 16 and 18 have negative damage implying that their stiffness values have increased. Smaller levels of such counter intuitive occurrences can usually be ignored. However, it appears that this optimal selection of modes based on the minimization of the condition number of the matrix involved in pseudo inversion is only partially effective in damage identification.

Some of these incorrect damage identification issues can, however, be reduced if minimizing the counter intuitive occurrences of finding higher than the initial element stiffness values is selected as the focus of the optimal search for the modal coefficients, α_i. This can be done if a good estimate of the initial stiffness values of the structural elements that represent the structural model is available. Although the true values of the stiffness coefficients of the

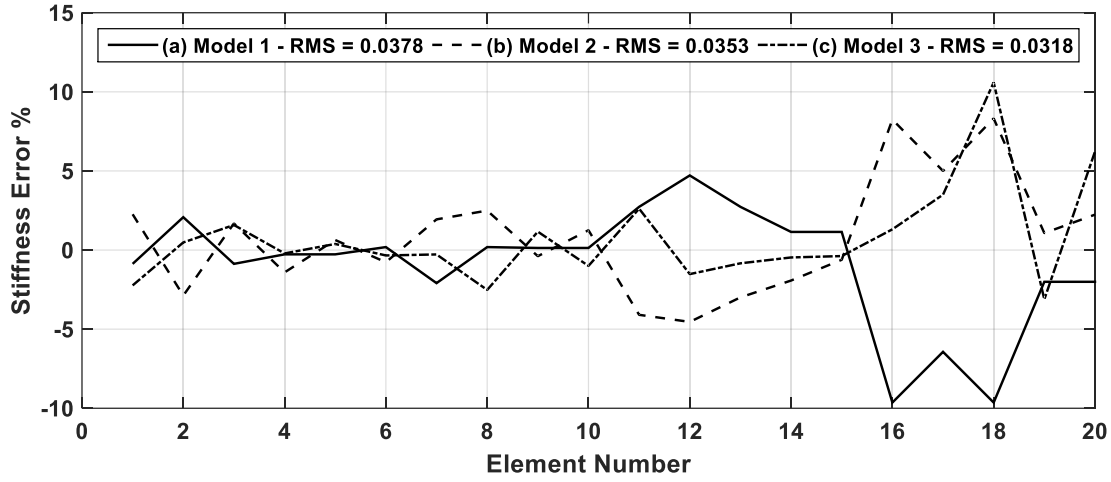

(a) Percent errors in the element stiffness values of Models 1, 2 and 3 when modes in stiffness estimation are combined with optimally selected weights α_i

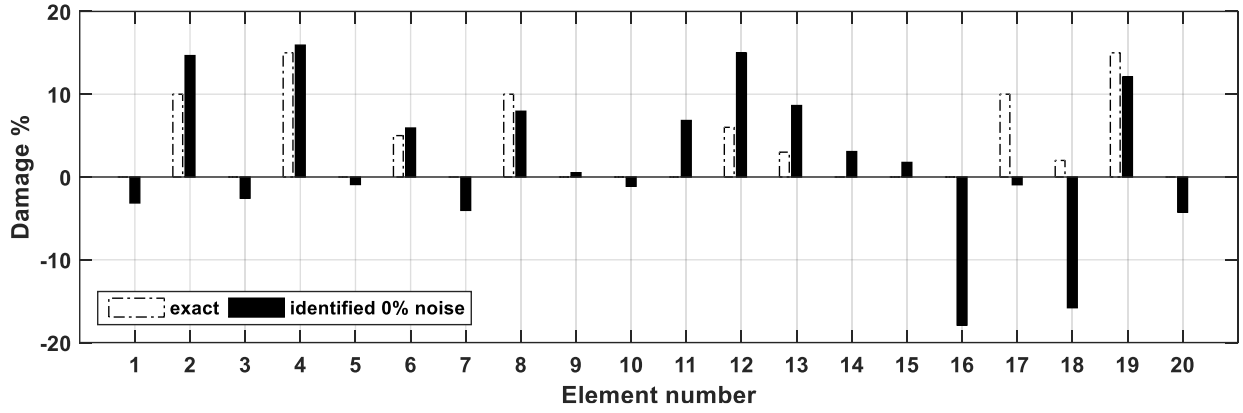

(b) Identified levels of damage in different structural elements of Model 2

Figure 2.6 Percent errors in the element stiffness values of all three models and Identified level of damage in different elements of Model 2 when the modes in stiffness estimation are combined with optimally selected weights α_i. The optimal mode combination weights α_i are selected to minimize the matrix condition number. Modes Extracted from noise free strain responses

structural elements in an as-built structure may be difficult to assess, a good estimate of these initial values can be taken to be the same as the values based on the cross sectional properties of the structural members used in the design and construction of the frame. With this knowledge about the element stiffness coefficients, the search for optimal values of the mode contribution coefficients α_i can be based on minimization of these counter intuitive increases in the element stiffness values. That is minimize the sum of the increases in the stiffness values or so-called the negative damages. From this sum of the increases in the

element stiffness values, the element whose stiffness values have decreased are completely excluded. That is, the optimization criterion to obtain the optimal values of α_i is expressed as follows:

$$\begin{aligned} &Minimize\ the Total\ Negative\ Damage\ \Delta = \sum_{i=1}^{n_e} \Delta k_i(\alpha_i)\ for\ all\ \Delta k_i > 0 \\ &where\ \Delta k_i(\alpha_i) = k_i - k_i^* \end{aligned} \tag{31}$$

Wherein for the i^{th} element, k_i is the stiffness values estimated by the proposed identification algorithm and k_i^* is the initial stiffness coefficient value of the structural model. In the estimation of total negative damage in Eq. 31, the elements with positive damage are not included.

The stiffness identification results discussed below were obtained for such optimally selected modal coefficients α_i utilized in Eq. 28. Figure 2.7 shows the percentage errors in the identified stiffness values of the frame elements for models 1, 2 and 3. These errors are relatively much smaller than those shown in earlier figures obtained with different modal combinations, the largest being less than 1%. Figure 2.8 compares the actual and identified

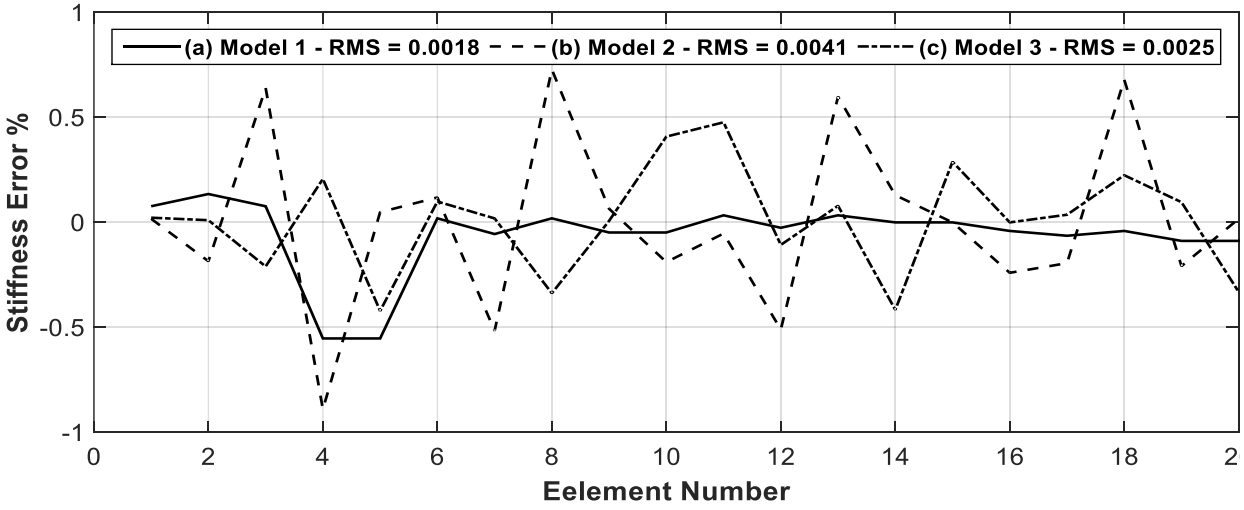

Figure 2.7 Showing % errors in the element stiffness values of all three models when modes used in the stiffness estimation are combined with weights α_i that are optimally selected to minimize the level of total negative damage in the elements. Modes extracted from noise free strain responses

levels of damage in different elements of Model 2 identified for this optimal modal combination. A comparison of Figure 2.8 with Figure 2.6 b clearly indicates a significant improvement in damage identification by this optimal mode combination. The counter intuitive cases of the elements with negative damage have nearly disappeared. Also the identified damage levels in all 9 elements are very close to the actual damage levels.

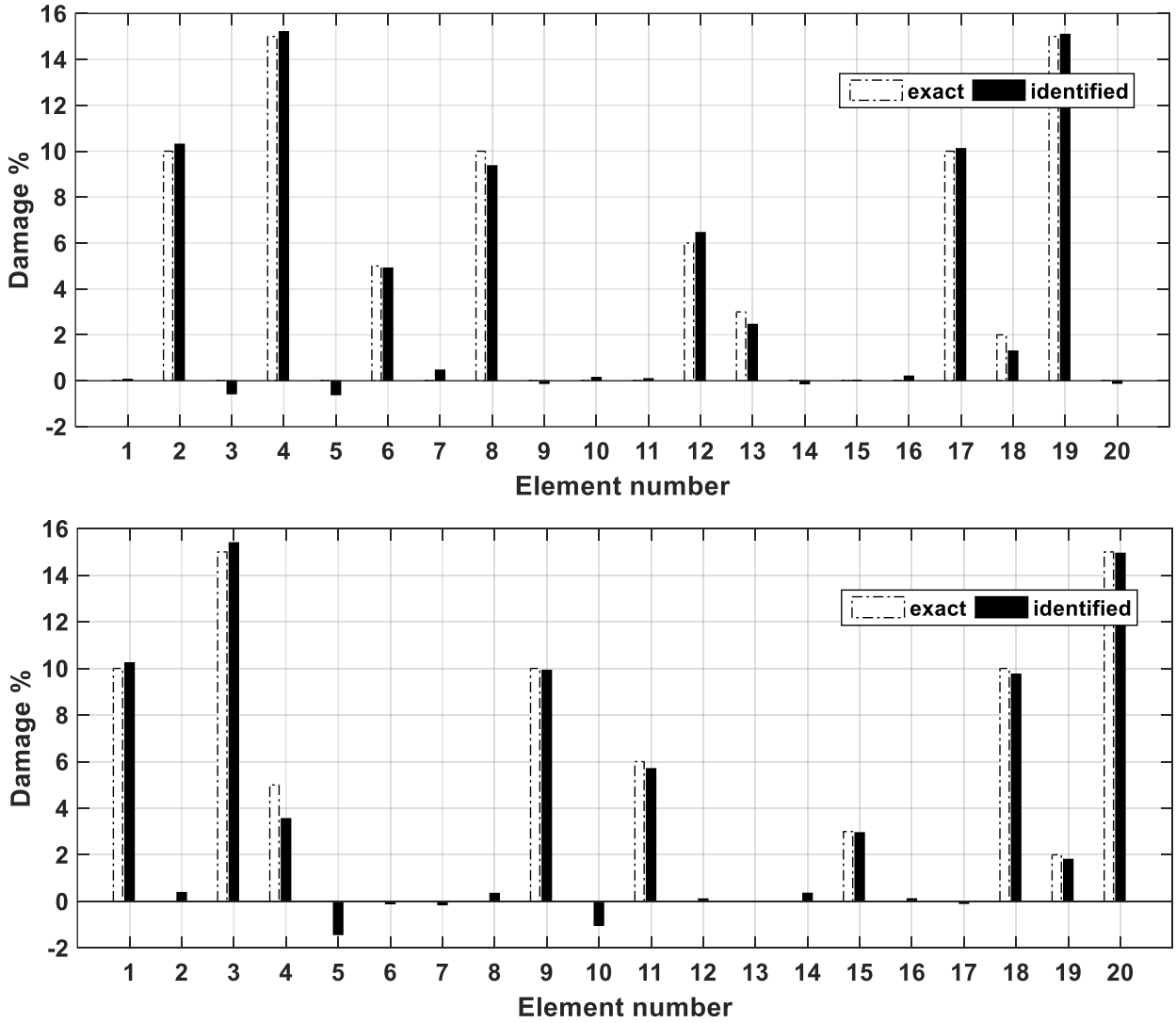

Figure 2.8 Showing the identified levels of damage in different elements of Models 2 and 3 when modes used in the stiffness estimation are combined with optimally elected weights α_i. Weights α_i selected to minimize the level of total negative damage in the elements. Modes extracted from noise free strain responses

2.5.3. Damage Identification with Noisy Strain Responses:

The previous set of results were obtained for the noise-free measured responses. In the following, this stiffness and damage identification approach is now used with strain responses corrupted with a significant level of measurement noise. To define these measured response, the analytically calculated strain response values were changed by adding a zero-mean Gaussian random noise with its standard deviation equal to 10% of the standard deviation of the calculated strain response. These polluted strain responses were then used to calculate the strain mode shapes using SSI algorithm, followed by the calculations of system mode shapes and then element stiffness values as done earlier.

The last part of the Table 2.2 now shows the (1-MAC) values calculated for each of the four system modes for three structural models considered earlier. The (1-MAC) values of the first two modes of all models are reasonably close to zero, almost in the same range as those shown in the second part of this table for the noise-free case. The values for the modes 3 and 4, though still close to zero, indicate that they are less accurately identified with respect to the first two modes. This might be relevant in explaining the impact of including these modes with lower modes on accuracy of the stiffness identification. Also calculated were the off diagonal terms as expressed by Eq. 30 to assess the relative accuracy of the higher modes with respect to the first mode. These were calculated to be: for Model 1 (1, 0.0011, -0.0305, -0.1047), Model 2 (1, -0.0003, 0.0317, -0.0770), and Model 3 (1, -0.0038, 0.0534, -0.0660). These values seem to indicate that mode 4 (and to some lesser extent mode 3) is somewhat less accurately identified than 2. This can also be seen from the (1-MAC) results shown in Table 2.2 which are somewhat higher than those for modes 1 and 2. The impact of using these less accurate modes along with first two modes on the accuracy of the element stiffness identification is thus of interest and is examined.

Figure 2.9 a-c show the % errors in the identified stiffness values for the three structural models using only a single mode. In all three models, the element stiffness errors as well as the RMS errors associated with mode 4 are much higher, thus suggesting that inclusion of mode 4 with other modes may not improve the accuracy of identification. This is, indeed, shown by the results in Figure 2.10 a-c for the three models wherein three simple

combinations (1+2, 1+2+3, and 1+2+3+4) of modes with equal weights are considered where the errors for the case where all four modes are considered are rather large. In model 3, even the inclusion of mode 3 with the first two modes seem to degrade the identification results. In any case, the errors are very high. Figure 2.11 a-c show results similar to those in Figure 2.10, but now the mode participation factor values are taken as the modal combinations factors, α_i. This combinations seems to reduce the impact of mode 4 on the stiffness error since the participation factor for mode is relatively smaller than those of the other three modes, but the stiffness errors are still high.

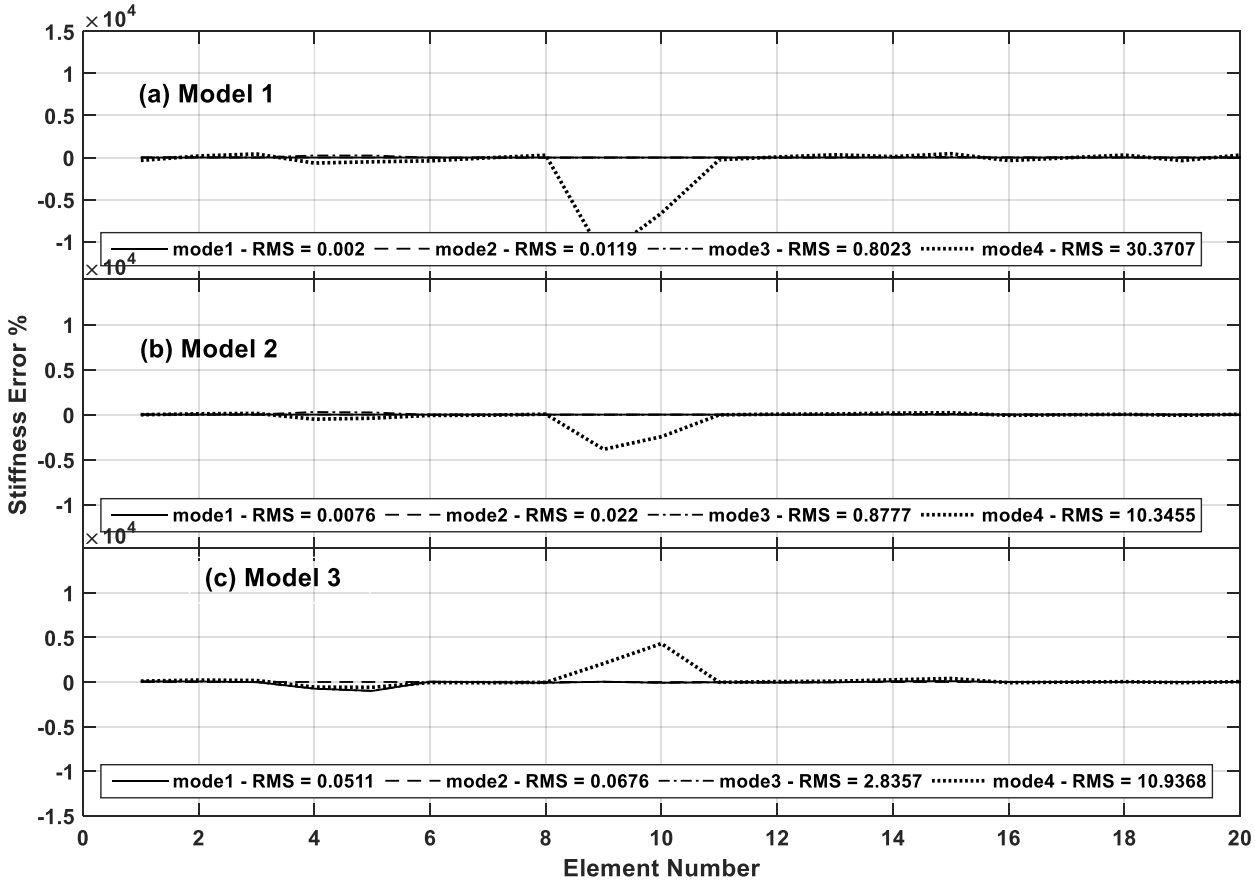

Figure 2.9 Errors in the element stiffness values in Models 1, 2 and 3 with only one mode used in the stiffness estimation. Modes extracted from 10% measurement noise- polluted strain response.

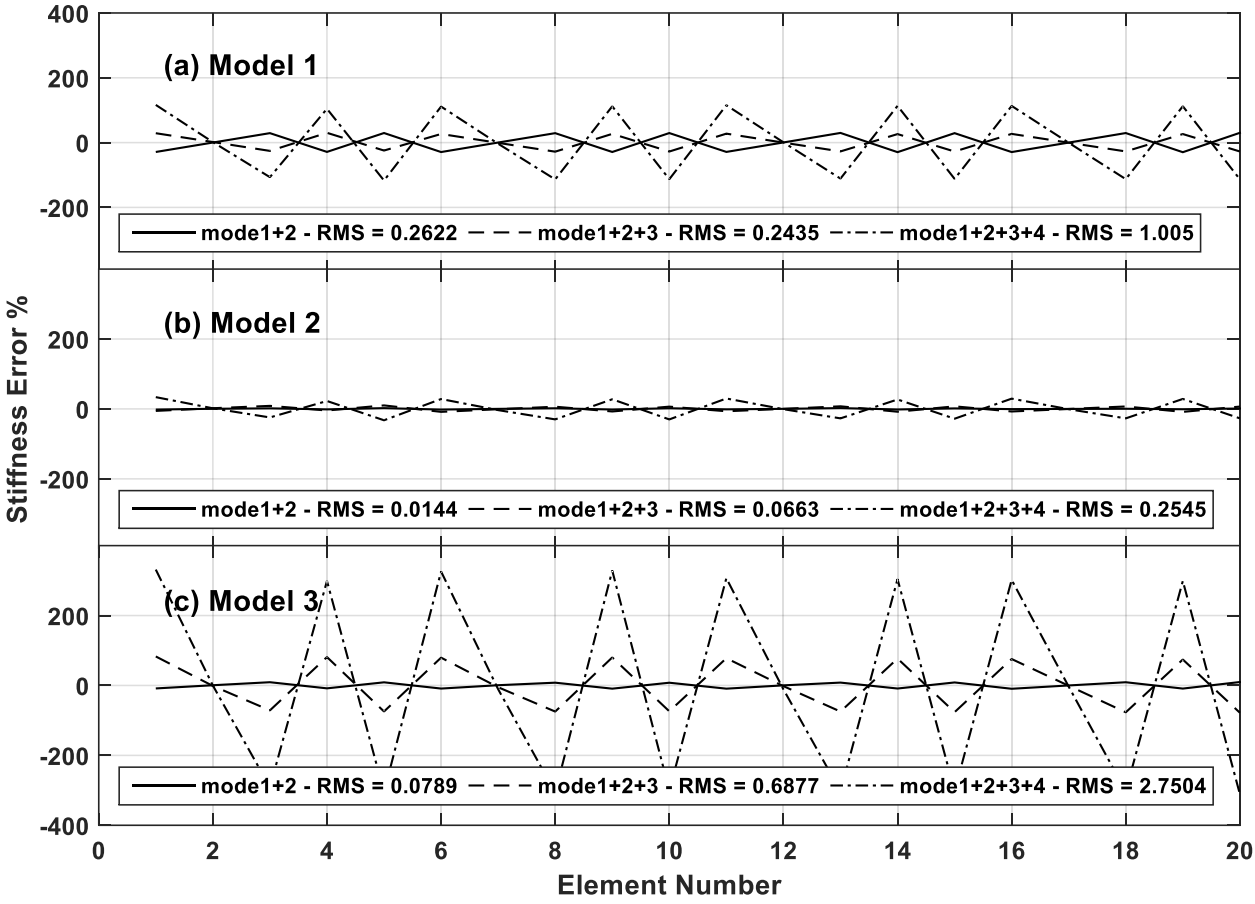

Figure 2.10 Errors in the element stiffness values in Models 1, 2 and 3 when different combinations of modes with equal weights ($\alpha_i = 1$) are used in the stiffness estimation. Modes extracted from strain responses polluted with 10% measurement noise

In Figure 2.12, the element stiffness errors are shown in all three models when the optimal modal weights α_i were used to define Eq. 28. As indicated earlier by Eq. 31, the objective of this optimization is to find the modal coefficients α_i such that the sum of all positive stiffness reductions (or total damage) in structural elements is minimized. Again MATLAB optimization function FMINUNC was used to calculate these optimum weights using only the first three modes; mode 4 was not included primarily because of its being inadequately accurate. The % error is the identified element stiffness values are significantly reduced being less than 1% in most structural elements in all three models. The RMS errors are now less than 0.4%. In Figure 2.13 are compared the actual and identified levels of damage in

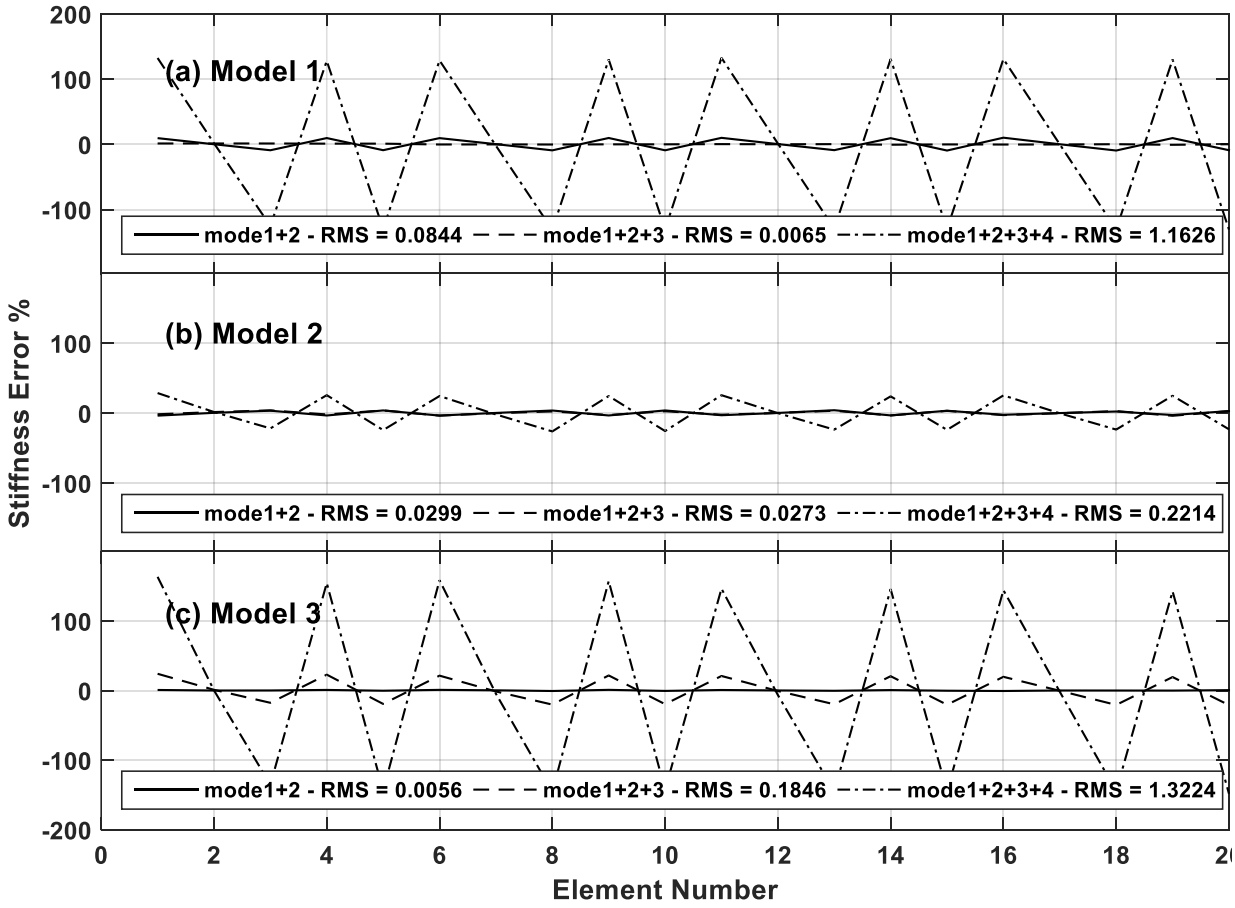

Figure 2.11 Errors in the element stiffness values in (a) Models 1, (b) Model 2 and (c) Model 3 when different combinations of modes with modal participation factors used as the mode contribution factors α_i in the stiffness estimation. Modes extracted from strain responses polluted with 10% measurement noise

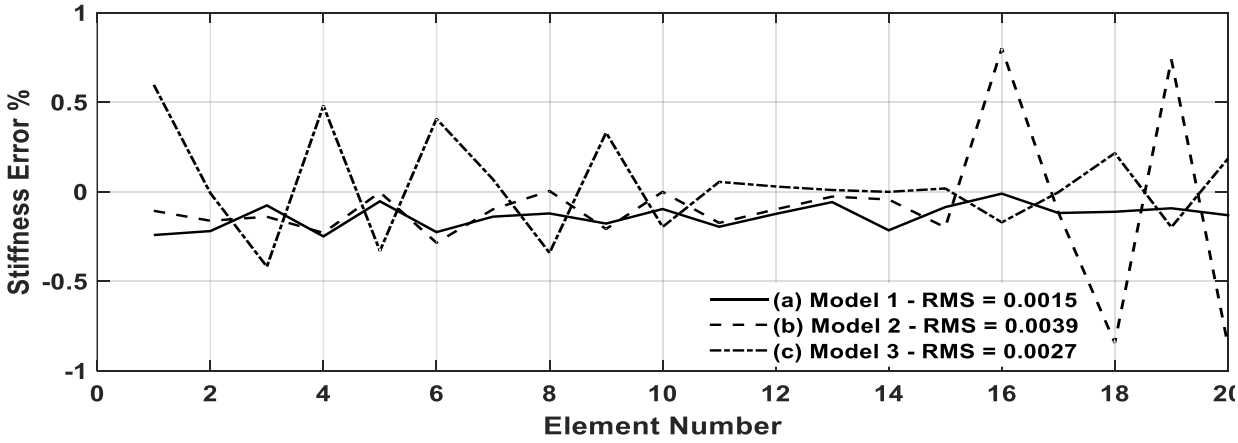

Figure 2.12 Percent errors in the element stiffness values of all three models when modes used in the stiffness estimation are combined with weights α_i that are optimally selected to minimize the level of total negative damage in the elements. Modes extracted from strain responses polluted with 10% measurement noise

various structural elements of the two damaged building models, Model 2 and 3. The identified damage values compare very well with the actual levels of damage assumed to generate the response data used in this damage identification.

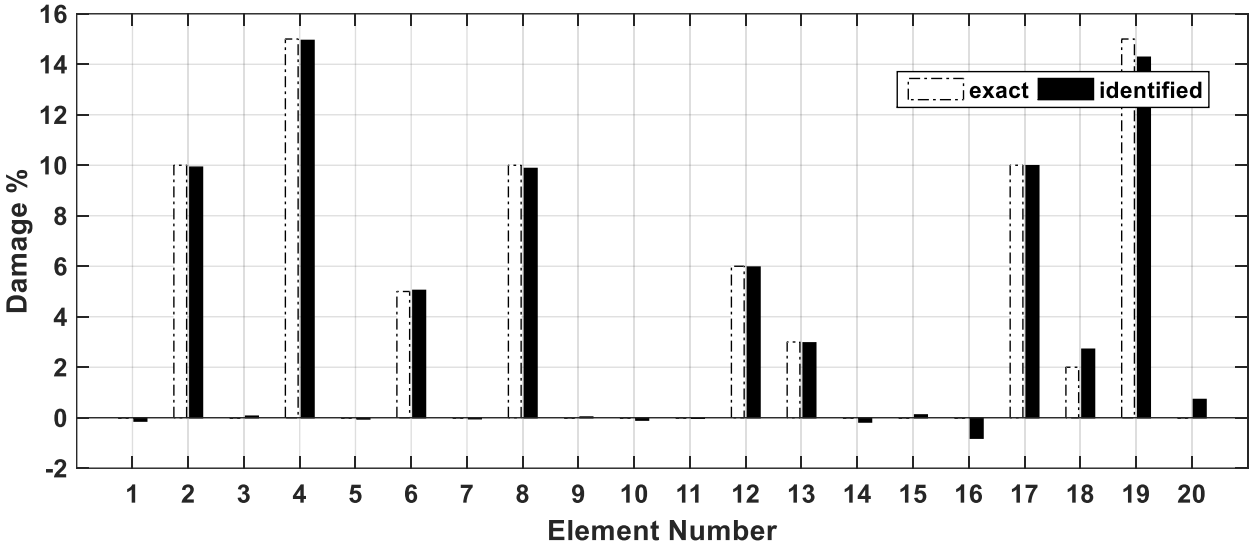

(a) Identified Damage Levels in the element of Model 2

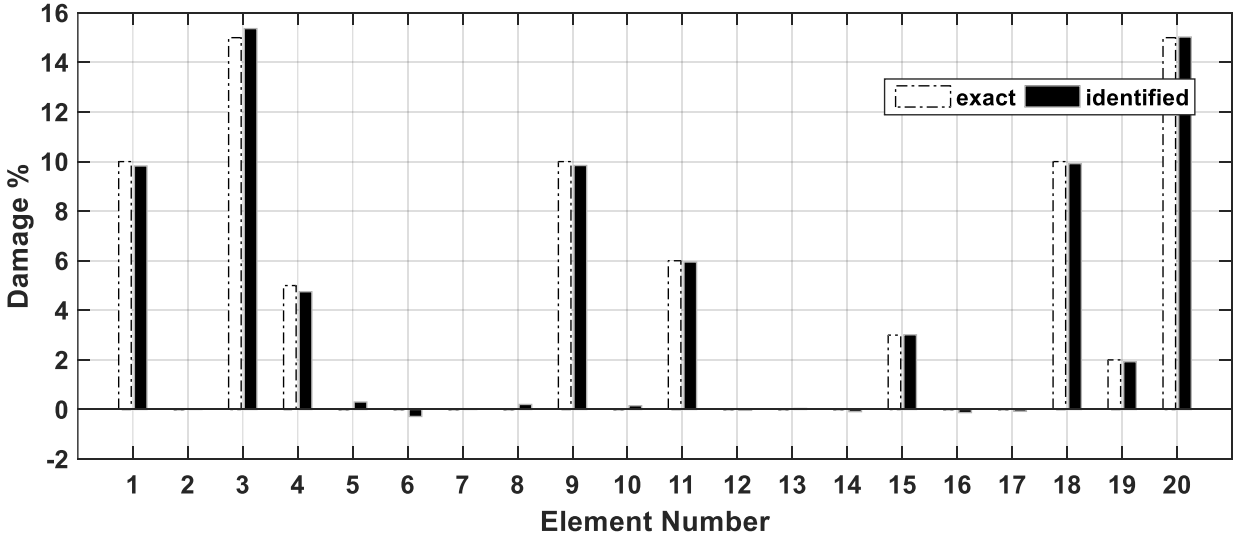

(b) Identified Damage Levels in the element of Model 3

Figure 2.13 Showing the identified levels of damage in different elements of Models 2 and 3 when modes used in the stiffness estimation are combined with optimally elected weights α_i. Weights α_i selected to minimize the level of total negative damage in the elements. Modes extracted from strain responses polluted with 10% measurement noise

2.1. Impact of adding noise to the input

In practice, the collected measurements are polluted with some measurement inaccuracies. The inaccuracies could occur due to several reasons such as measurement digitization and wireless transmission of the signal. Such inaccuracies are famously known as noise. In this research, both input and output signals are analyzed. The input signal is considered as a ground seismic acceleration applied at the base of the building. This signal is taken to be the time history of one of the publicly available earthquake signal records. We considered the Chi-Chi earthquake (Taiwan 1999) for this research. The output signal is the strain signal measured at the ends of each element in the frame structure. In order to obtain this signal, we simulate a numerical model for the structure to generate the measured strain time history. However, this simulated response is noise-free and we needs to apply noise to it. The applied noise is modeled as a random signal with an intensity that is proportional to the intensity of the original signal. We estimate this proportion based on the standard deviations of both of the signals. The noisy random signal is scaled to have a standard deviation σ_n that is proportional to the standard deviation of the collected signal σ_s. For example, for a 10% noise-to-signal ratio, the standard deviation of the added noise signal is determined as $\sigma_n = 0.1\sigma_s$.

In practice, the measurement noise is applied to both the input and the output signals. However, since the input measurement is obtained from an actual earthquake measurement, which is supposed to include an actual measurement noise, we utilize this signal without imposing additional noise. For validation of this assumption, we have run three different cases for three different models where additional noise is imposed on the input excitation signal, and then we compared them to the cases where no additional noise is imposed. The results for six different models are presented below in Table 2.3. The six models present six structure configurations different in their geometry and stiffness distribution as follows:

- Model 1: symmetric undamaged structure
- Model 2: symmetric damaged structure (random damage scenario I)
- Model 3: symmetric damaged structure (random damage scenario II)
- Model 4: Asymmetric undamaged structure
- Model 5: Asymmetric damaged structure (random damage scenario I)
- Model 6: Asymmetric damaged structure (random damage scenario II)

Table 2.3 MAC values for the identified mode shapes using noisy measured output response and two cases for the measured input excitation; (i) an additional noise is imposed, and (ii) no additional noise is imposed. Six different models are tested

Model 1							
(i) MAC values with no additional input noise				(ii) MAC values with additional input noise			
1	0.00114	-0.03054	-0.10469	1	-0.00222	0.02114	0.43803
0.00114	1	0.01593	0.01631	-0.00222	1	-0.01205	0.01332
-0.03054	0.01593	1	0.00373	0.02114	-0.01205	1	0.00728
-0.10469	0.01631	0.00373	1	0.43803	0.01332	0.00728	1
Model 2							
(i) MAC values with no additional input noise				(ii) MAC values with additional input noise			
1	-0.00033	0.03168	-0.07699	1	0.00540	0.03864	0.56376
-0.00033	1	-0.01830	0.02538	0.00540	1	-0.00145	-0.03092
0.03168	-0.01830	1	-0.01291	0.03864	-0.00145	1	0.01521
-0.07699	0.02538	-0.01291	1	0.56376	-0.03092	0.01521	1
Model 3							
(i) MAC values with no additional input noise				(ii) MAC values with additional input noise			
1	-0.00046	0.03033	-0.08559	1	0.00665	-0.04751	0.61479
-0.00046	1	-0.01742	0.02397	0.00665	1	-0.00125	-0.03172
0.03033	-0.01742	1	-0.01114	-0.04751	-0.00125	1	-0.01300
-0.08559	0.02397	-0.01114	1	0.61479	-0.03172	-0.01300	1
Model 4							
(i) MAC values with no additional input noise				(ii) MAC values with additional input noise			
1	-0.00410	0.05932	-0.08653	1	-0.00542	-0.02975	0.67300
-0.00410	1	-0.02410	0.07351	-0.00542	1	0.00155	0.07484
0.05932	-0.02410	1	-0.05024	-0.02975	0.00155	1	0.04016
-0.08653	0.07351	-0.05024	1	0.67300	0.07484	0.04016	1
Model 5							
(i) MAC values with no additional input noise				(ii) MAC values with additional input noise			
1	-0.00377	0.05340	-0.06603	1	-0.00698	-0.04005	0.74209
-0.00377	1	-0.02439	0.07692	-0.00698	1	-0.00357	0.031328
0.05340	-0.02439	1	-0.04934	-0.04005	-0.00357	1	8.86E-05
-0.06603	0.07692	-0.04934	1	0.74209	0.031328	8.86E-05	1
Model 6							
(i) MAC values with no additional input noise				(ii) MAC values with additional input noise			
1	-0.0050	0.0615	-0.1141	1	-0.0081	0.0460	0.8236
-0.0050	1	-0.0261	0.0806	-0.0081	1	-0.0004	0.0120
0.0615	-0.0261	1	-0.0559	0.0460	-0.0004	1	0.0146
-0.1141	0.0806	-0.0559	1	0.8236	0.0120	0.0146	1

From the results presented in Table 2.3, we can observe, for the six models simulated, that the off-diagonals of the MAC matrix are affected by introducing additional noise to the input excitation signal. However, the off-diagonals values, which are ideally zero when the exact

modes are utilized, increase in some cases and decrease in some other cases when we add noise to the excitation. We, therefore, used both of the mode sets to identify the stiffness values in order to determine the effect of imposing input noise. The RMS values of the stiffness identification error, at 10% measurement noise, are presented in Table 2.4.

Table 2.4 RMS of stiffness identification error for the six simulated models

	model 1	model 2	model 3	model 4	model 5	model 6
no noise added to i/p	0.0015	0.0039	0.0044	0.0015	0.0045	0.0027
noise is added to i/p	0.0014	0.0013	0.0013	0.0013	0.0011	0.0146

We can also observe, from the identification error values presented in Table 2.4, that the effect of adding input excitation measurement noise does not significantly affect the identification accuracy. The RMS of identification error increases from some cases and decreases for some other cases. Therefore, introducing additional measurement noise in the excitation signal does seem to cause any problem in the stiffness identification.

2.1. Statistical analysis to identify the robustness of the Eigen equation approach

In this chapter, we have investigated the stiffness identification of the frame structures using the Eigen equation. However, only few structure configurations have been tested. Therefore, in order to examine the robustness of this identification approach, we run it for a large number of different structure configurations. These structure configurations are generated with random damage levels occurring in randomly selected elements in a 1-Bay×2-Stories frame structure. For this small frame, we have tested 30,000 randomly selected configurations.

This structure model includes six elements, each is subject to a stiffness reduction that ranges between 0% and 20%. A uniform distribution for both the damage level and the damaged element set is assumed. This distribution is assumed in order to let every element get an equal probability to be damaged, and to let all damage levels equally possible to occur. Otherwise, if any other distribution is applied, some elements will be expected to be damaged more than the others, and some damage levels will be more probable than others. The stiffness identification error in each element is calculated for every structure

configuration, the statistics of this identification error are presented in the box plot shown in Figure 2.14.

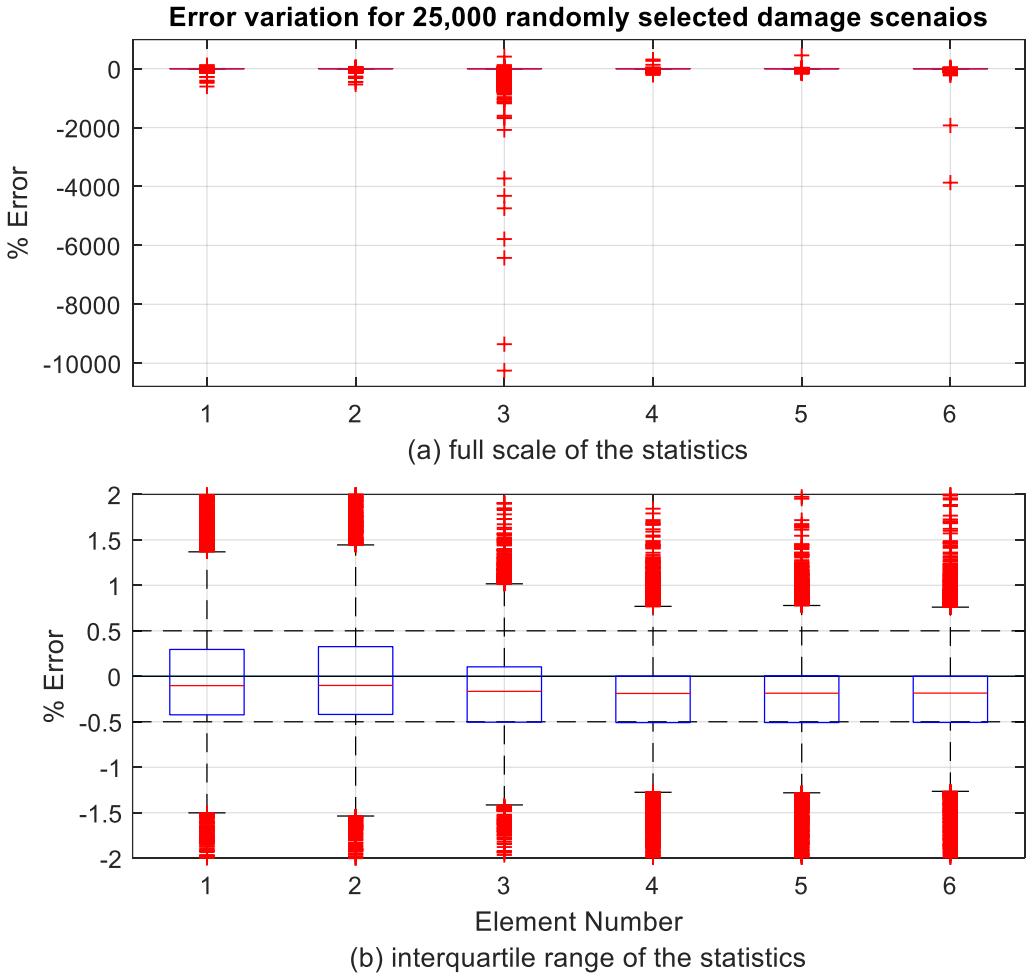

Figure 2.14 Statistics of element stiffness identification error for 30,000 different 1-bay 2-stories structure configurations

Figure 2.14.a provides a full scale representation for the data statistics including the outliers indicated with the red marker (+), while Figure 2.14.b excludes these outliers and zooms in to the interquartile range. The error statistics presented in Figure 2.14.b show that more than 50% of the stiffness identification error lies below the 0.5% absolute error bound.

In order to investigate the outliers that appear in Figure 2.14.a, we would first determine the proportions of both the accurate identification results (the interquartile-range data) and the outliers. Table 2.5 provides these proportions.

Table 2.5 Proportions of the interquartile-range results and the outliers of the stiffness identifictaion error statistics presented in Figure 2.14 for 30,000 randomly selected structure configurations

Element	Interquartile-Range data	Outliers
element 1	92.73%	7.84%
element 2	92.12%	8.56%
element 3	93.65%	6.78%
element 4	99.13%	0.87%
element 5	99.15%	0.85%
element 6	99.56%	0.44%

The results presented in Table 2.5 show the proportions of the outliers that take several values; as little as less than 1% and as high as 6~8%. However, the forthcoming analysis illustrates that these values are insignificant. We first present a sample of the frame configurations that output the outlier solutions we mentioned. The sample, presented in Table 2.6, show two examples for a very high error model (models 1 & 2), two examples for

Table 2.6 Examples for models with outlier solutions

	Large error outliers		Moderate error outliers		Low error outliers	
	model 1	model 2	model 3	model 4	model 5	model 6
Element Reference	37548000	37548000	37548000	37548000	30956093	30144544
	32681981	31785045	32287456	35050281	32068765	37548000
	35873106	37548000	37505326	37548000	33500998	32254285
	36790319	37548000	37548000	32472542	37548000	33560066
	32955353	30227500	36733987	31412661	35267897	37548000
	37548000	34660553	30524270	33416319	37548000	37548000
Element Identified	30527936	37767766	38019662	36320302	31202704	29462481
	51012061	36388898	34329912	34193853	32282755	36811329
	-3.6E+09	-3.5E+09	-5.7E+07	-5.7E+07	29551423	35374863
	32317810	35455574	36822284	33379564	37501616	33587183
	28906491	28533207	36084704	32153075	35343443	37375753
	32957990	32541455	30096825	34212291	37423729	37439727
Element Stiffness	-0.187	0.006	0.013	-0.033	0.0080	-0.0226
	0.561	0.145	0.063	-0.024	0.0067	-0.0196
	-102.506	-93.539	-2.525	-2.525	-0.1179	0.0967
	-0.122	-0.056	-0.019	0.028	-0.0012	0.0008
	-0.123	-0.056	-0.018	0.024	0.0021	-0.0046
	-0.122	-0.061	-0.014	0.024	-0.0033	-0.0029
RMS	**41.849**	**38.187**	**1.031**	**1.031**	**0.0483**	**0.0414**

a moderate error models (models 3 & 4), and two examples for low error (models 5 & 6). For each model, we present the reference (exact) stiffness, followed by the identified stiffness, followed the identification error, and then followed by the RMS of the identification error.

Our primary concern regarding these outliers is the ability to identifying them. In the study we presented, we have been able to identify the outliers based on the statistics of the large population we simulated. In practice, this requires a long history of model testing to be recorded. However, there are two categories of outliers that can be easily identified, the large and the moderate error outliers. That is because they provide a huge error – due to the unreasonable values of the identified stiffness – that can be confidently recognized incorrect. The outliers with the large error look unbounded (they also provide an error level of 10,000%), however, they are more clear and easy to identify than the low-error ones. In addition, it does not matter whether it is a large or a low error level because a following iterative procedure, that we will discuss shortly, has to be applied in order to identify the correct solution. On the other hand, the low-error outliers are not easily identifiable since they provide a reasonable identified stiffness, which could be accepted by the user. Therefore, the same iterative procedure should also be applied. To illustrate this approach, it is required to investigate the possible reasons for the outliers errors discussed earlier.

It is familiar that the system identification algorithms do basically obtain the correlation functions between the measured dynamic response signals, famously known as the 'Markov Parameters', and then they are arranged in a matrix form 'Hankel Matrix' (Juang 1985 and Ljung 1987). Further analysis of this Hankel Matrix - involving Singular Value Decomposition (SVD) – is affected by the singularity of this matrix. On the other hand, the randomly selected structure configurations can possibly possess a certain level of symmetry that provides either very highly correlated or uncorrelated response signals. These situations can create singularities in the aforementioned Hankel matrix. This rough description for the system identification explains how these algorithms could be sensitive to the assumed structure configuration.

Therefore, in order to identify and address the outliers in our study, we have specified all the structure configurations that provided these outliers, and then we have repeated the

identification process with little signal adjustments. These adjustments are applied to both the excitation and response signals by cutting a portion of each of them. Such little adjustment provides a signal that is slightly different from the original one that caused the outlier solution. The Markov Parameters obtained from the adjusted signals are also different from the ones that provide the singularities discussed earlier. This adjustment turned out sufficient to remove the singularities in the system identification process for most of the structure configurations. Some remaining structure configurations required one or two more iterations until they provided an accurate solution that belongs to the same interquartile range of the initially results obtained. Figure 2.15 shows the statistics after addressing the outliers.

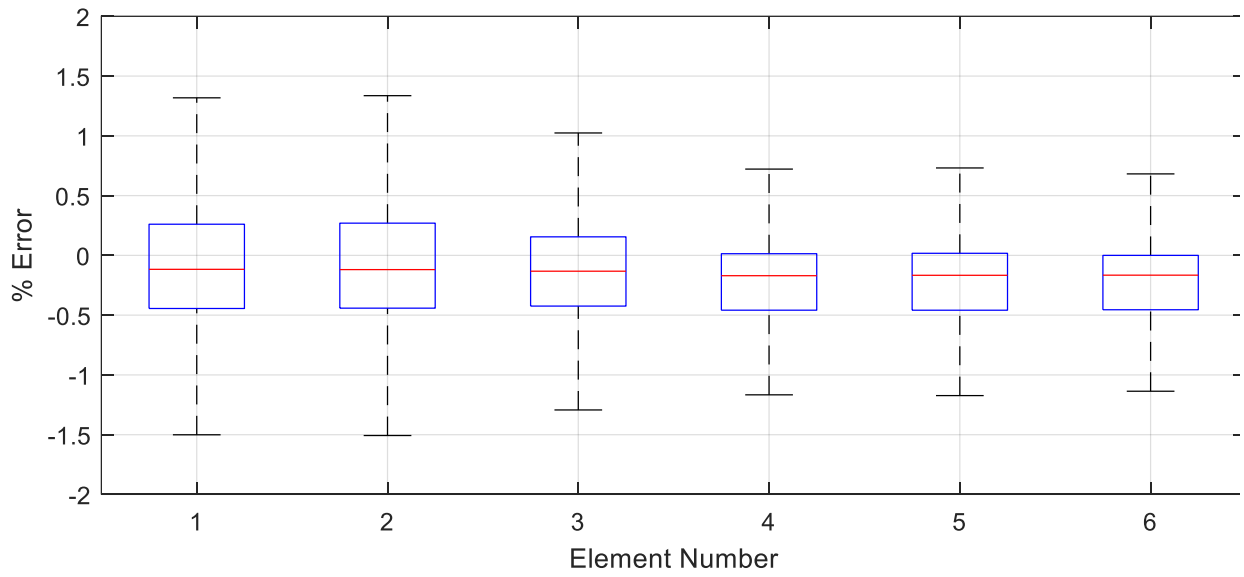

Figure 2.15 Statistics of the element stiffness identification error with the outliers settled.

In practice, we may not be aware of this inter-quartile range, which we consider as a reference in this analysis. Therefore, we will have to apply the previously mentioned iterative procedure for each model, whether or not we observe unreasonable results. That is, we iteratively adjust the input and the output signals associated with every model in order to obtain several identified solutions for this model using the same set of measurements. The obtained set of solutions are utilized to recognize any inconsistent results.

2.2. Conclusion

The paper presents a modal response-based stiffness and damage identification approach for health monitoring of structural frames used in building and other structures. In this study, the main focus is on the utilization of the dynamic flexural strain responses measured at several locations on the structure. The strain responses are considered primarily because they provide more complete and useful information needed for damage identification in structures like structural frames. The dynamic strain responses are first utilized to extract strain mode shapes using the well-known methods such as Stochastic System Identification (SSI) or NXeT-ERA algorithms. The extracted strain mode shapes are then utilized in two step approach involving the pseudo-inversions to first calculate the mean square estimates of the systems mode shapes corresponding to the degrees of freedom needed to describe the system, followed by the estimation of element stiffness values also involving a pseudo inversion. Since pseudo inversions do not provide unique values, but rather provide a version of the mean square estimate for a system of linear equations, the impact of these on the estimates of the system mode shapes, the element stiffness values and damage identification is numerically examined for different examples of multi-story multi-bay frames. The numerical study indicates that for general structural systems it may be necessary to extract and use more than one system modes for accurate estimation of stiffness values and identification of the element damage severities as well as their locations. A method is suggested to calculate the best values of the modal contribution coefficients need for their combination in the proposed damage identification approach. The effectiveness of the proposed approach to identify the damage locations and severities is demonstrated by its successful application to the example problems of two multi-story multi-bay frames in which several structural elements are considered damaged.

This method has been tested for robustness by running a randomly generated set of frame structure configurations. This testing has provided a set of outliers with an error due to some singularities in the modal system identification. Since these outliers are not necessarily recognizable, we may apply an iterative procedure – that identifies the inconsistent results – for every model configuration. Each iteration utilizes a new set of measurements that are

synthesized form the original measured signals. It is observed that a few number of iterations is sufficient to obtain the accurate results.

3. Chapter 3: Damage Identification of 3D Frame Structures

3.1. Introduction

In this section, we apply the stiffness identification approach described earlier to a popular three-dimensional model of a multistory building. The building structure consists of rigid floors supported on building columns. Figure 3.1 shows a representation of this model with two floor slabs supported on columns. This model is, similar to the two-dimensional one described earlier, excited by an earthquake-induced base motions applied in the two orthogonal directions. Since the floor slabs are assumed rigid and supported by inextensible columns, they can only move in their own planes. Depending on the stiffness and mass symmetry of the story columns and floor slabs, we can describe the motion of such a vibrating system in terms of three degrees of freedom per each floor, consisting of the two linear motions (associated with the two horizontal directions) and a rotation in the plane of the slab. The response that will be measured for stiffness identification is assumed to consist of the flexural strains, measured at the ends of the columns. We will use this measured strain response to identify the system stiffness using the approach described earlier. This model is similar to the one used in the benchmark problem (Caicedo et. al.). We could, however, not utilize the benchmark problem model as the experimental results generated for that model did not include any strain measurements. In this section, we examine the applicability of the strain mode shape based approach that we have developed earlier to this model.

3.2. Finite element model of a 3D frame structure

We have to first define the kinematic and kinetic relations of the 3D frame structure in order to develop its mathematical model. The developed equations are primarily related to the horizontal slabs in the frame (floors) since the columns are assumed with negligible linear and rotational inertia.

The motion of the mass center of a rigid horizontal slab in the 3D frame shown in Figure 3.1 is defined by the three plane degrees of freedom, two orthogonal translational movements (u, v) in the x- and y-directions respectively, and one in-plane rotational motion represented by angle θ. Figure 3.2 below shows the movement of a point (p) located at coordinates (x, y)

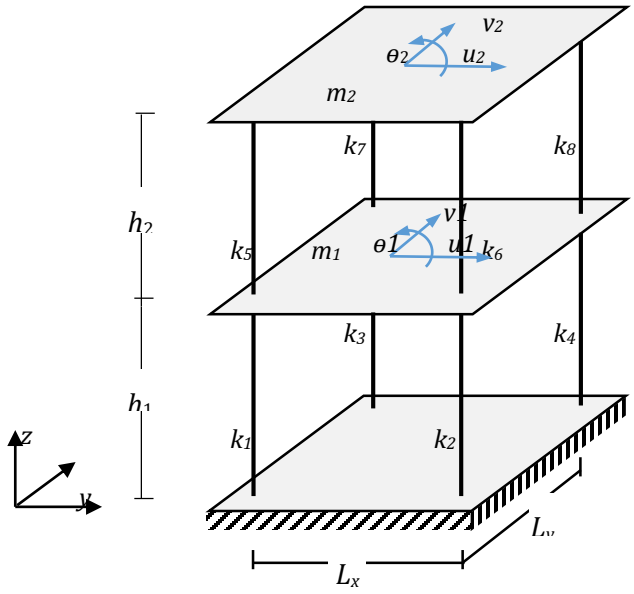

Figure 3.1 A schematic of a 1-Bay × 1-Bay × 2-Stories frame structure

where a column may be connected to the slab in terms of these three mass center motions $(u, v,)$ and θ.

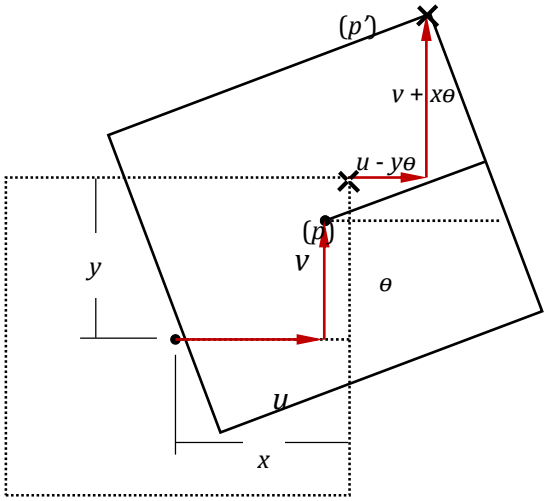

Figure 3.2 Linear and rotational motions of a horizontal slab of the 3D structure

This motion of a general point $p(x, y)$ on the slab can be defined as:

$$pp' = (u, v) + (-y\theta, x\theta) \quad (1.a)$$

$$= (\Delta x, \Delta y) \quad (1.b)$$

Considering all the deformation dependent forces applied by the columns in the story below and above the slab, and assuming that column masses are relatively small compared to the mass of the floor slab, it is straightforward to show that the equations of motion of the j^{th} floor slab mass in the x-, y- and θ-directions can be written as:

$$m_j(\ddot{u}_j + \ddot{x}_g) = -\sum_{e=1}^{n_e} \left\{ \begin{pmatrix} -k_{x_j}^{(e)} \\ k_{x_j}^{(e)} + k_{x_{j+1}}^{(e)} \\ -k_{x_{j+1}}^{(e)} \end{pmatrix} \begin{pmatrix} u_{j-1} \\ u_j \\ u_{j+1} \end{pmatrix} - y^{(e)} \begin{pmatrix} -k_{x_j}^{(e)} \\ k_{x_j}^{(e)} + k_{x_{j+1}}^{(e)} \\ -k_{x_{j+1}}^{(e)} \end{pmatrix} \begin{pmatrix} \theta_{j-1} \\ \theta_j \\ \theta_{j+1} \end{pmatrix} \right\} \quad (2.a)$$

$$m_j(\ddot{v}_j + \ddot{y}_g) = -\sum_{e=1}^{n_e} \left\{ \begin{pmatrix} -k_{y_j}^{(e)} \\ k_{y_j}^{(e)} + k_{y_{j+1}}^{(e)} \\ -k_{y_{j+1}}^{(e)} \end{pmatrix} \begin{pmatrix} v_{j-1} \\ v_j \\ v_{j+1} \end{pmatrix} + x^{(e)} \begin{pmatrix} -k_{y_j}^{(e)} \\ k_{y_j}^{(e)} + k_{y_{j+1}}^{(e)} \\ -k_{y_{j+1}}^{(e)} \end{pmatrix} \begin{pmatrix} \theta_{j-1} \\ \theta_j \\ \theta_{j+1} \end{pmatrix} \right\} \quad (2.b)$$

$$I_j\ddot{\theta}_j = -\sum_{e=1}^{n_e} \left\{ \begin{matrix} -y^{(e)} \begin{pmatrix} -k_{x_j}^{(e)} \\ k_{x_j}^{(e)} + k_{x_{j+1}}^{(e)} \\ -k_{x_{j+1}}^{(e)} \end{pmatrix} \begin{pmatrix} u_{j-1} \\ u_j \\ u_{j+1} \end{pmatrix} + {x^{(e)}}^2 \begin{pmatrix} -k_{y_j}^{(e)} \\ k_{y_j}^{(e)} + k_{y_{j+1}}^{(e)} \\ -k_{y_{j+1}}^{(e)} \end{pmatrix} \begin{pmatrix} \theta_{j-1} \\ \theta_j \\ \theta_{j+1} \end{pmatrix} \\ x^{(e)} \begin{pmatrix} -k_{y_j}^{(e)} \\ k_{y_j}^{(e)} + k_{y_{j+1}}^{(e)} \\ -k_{y_{j+1}}^{(e)} \end{pmatrix} \begin{pmatrix} v_{j-1} \\ v_j \\ v_{j+1} \end{pmatrix} + {y^{(e)}}^2 \begin{pmatrix} -k_{x_j}^{(e)} \\ k_{x_j}^{(e)} + k_{x_{j+1}}^{(e)} \\ -k_{x_{j+1}}^{(e)} \end{pmatrix} \begin{pmatrix} \theta_{j-1} \\ \theta_j \\ \theta_{j+1} \end{pmatrix} \end{matrix} \right\} \quad (2.c)$$

where:

- m_j and I_j are the j^{th} floor mass and inertia respectively,
- $\ddot{u}_j, \ddot{v}_j,$ and $\ddot{\theta}_j$ are the translational and rotational accelerations of the j^{th} floor,
- $\ddot{x}_g$ and $\ddot{y}_g$ are the ground seismic accelerations in x- and y-directions,
- $k_{x_j}^{(e)}$ and $k_{y_j}^{(e)}$ are the stiffness values in x- and y-directions respectively for the element (e) connected to the bottom of story j,
- $k_{x_{j+1}}^{(e)}$ and $k_{y_{j+1}}^{(e)}$ are the stiffness values in x- and y-directions respectively for the element (e) connected to the top of story j, and
- $x^{(e)}$ and $y^{(e)}$ are the coordinates of element (e) w.r.t. the mass center of the slab.

Since the primary objective of this study is to identify the change in the stiffness of individual columns connected to the slabs, it is of interest to express these equations in terms of the individual column stiffness values $k^{(e)}$ that are connected to the slabs. For this we need to express the system stiffness matrix K in terms of both the x- and y-stiffness $k_x^{(e)}$ and $k_y^{(e)}$ as $K = \left[\sum k_x^{(e)} S_x^{(e)} + k_y^{(e)} S_y^{(e)}\right]$ where the matrices $S_x^{(e)}$ and $S_y^{(e)}$ are the allocation matrices. The allocation matrices are independent of the stiffness values; they only depend on the structural geometry. For this we re-write the equation of motion in the x-direction for the j^{th} slab with n attached columns as:

$$m_j \ddot{u}_j + \begin{bmatrix} k_{x_j}^{(1)}(\ldots \quad 0 \quad (\delta-1) \quad 1 \quad \delta \quad 0 \quad \ldots)_{1\times n}\left(I_{n\times n} \mid O_{n\times n} \mid -y^{(e)} I_{n\times n}\right)_{n\times 3n} + \\ \vdots \\ k_{x_{j+1}}^{(n)}(\ldots \quad 0 \quad (\delta-1) \quad 1 \quad -\delta \quad 0 \quad \ldots)_{1\times n}\left(I_{n\times n} \mid O_{n\times n} \mid -y^{(e)} I_{n\times n}\right)_{n\times 3n} \end{bmatrix} \begin{pmatrix} u_1 \\ \vdots \\ u_n \\ v_1 \\ \vdots \\ v_n \\ \theta_1 \\ \vdots \\ \theta_n \end{pmatrix}_{3n\times 1} = -m_j \ddot{x}_g \qquad (3)$$

where $\delta = \begin{cases} 0 \text{ for bottom columns} \\ 1 \text{ for top columns} \end{cases}$

The vectors containing the parameter δ in Eq. 3 above have only three non-zero entries, the index of which depends on the story number. For instance, for a story j, the three non-zero entries $\left((\delta-1),\ 1,\ \pm\delta\right)$ are located at the three indices j-1, j, j+1 respectively, i.e,

for the 1st story, the vector is $(\mathbf{1} \quad -\delta \quad 0 \quad \ldots)_{1\times n}$,

for the 2nd story, the vector is $((\delta-1) \quad \mathbf{1} \quad -\delta \quad 0 \quad \ldots)_{1\times n}$,

for the 3rd story, the vector is $(0 \quad (\delta-1) \quad \mathbf{1} \quad -\delta \quad 0 \quad \ldots)_{1\times n}$,

$\vdots$

for the penultimate story, the vector is $(\ldots \quad 0 \quad (\delta-1) \quad \mathbf{1} \quad -\delta)_{1\times n}$, and

for the last story, the vector is $(\ldots \quad 0 \quad (\delta-1) \quad \mathbf{1})_{1\times n}$.

Eq. 3 can be re-written in the following form in Eq. (4.a),

$$m_j\ddot{u}_j + \left[\sum_{e=1}^{n_e} k_{(e)x} S_{(e)x}\right]^{(j)} \begin{pmatrix} u_1 \\ \vdots \\ u_n \\ v_1 \\ \vdots \\ v_n \\ \theta_1 \\ \vdots \\ \theta_n \end{pmatrix} = -m_j\ddot{x}_g \tag{4.a}$$

where $S_{(e)x}$ is the allocation matrix for the element (e) in the x-direction. For every element (e) in the 3D frame, its x-allocation matrix is

$$\{S_{(e)x}\}_{1\times 3n} = (\ldots \quad 0 \quad (\delta - 1) \quad 1 \quad -\delta \quad 0 \quad \ldots)_{1\times n}\left(I_{n\times n} \mid O_{n\times n} \mid -y^{(e)} I_{n\times n}\right)_{n\times 3n} \tag{4.b}$$

Similarly, the equations of motion in the y- and the θ-direction are,

$$m_j\ddot{v}_j + \left[\sum_{e=1}^{n_e} k_{(e)y} S_{(e)y}\right]^{(j)} \begin{pmatrix} u_1 \\ \vdots \\ u_n \\ v_1 \\ \vdots \\ v_n \\ \theta_1 \\ \vdots \\ \theta_n \end{pmatrix} = -m_j\ddot{y}_g \tag{5.a}$$

$$\{S_{(e)y}\}_{1\times 3n} = (\ldots \quad 0 \quad (\delta - 1) \quad 1 \quad -\delta \quad 0 \quad \ldots)_{1\times n}\left(O_{n\times n} \mid I_{n\times n} \mid x^{(e)} I_{n\times n}\right)_{n\times 3n} \tag{5.b}$$

$$I_j\ddot{\theta}_j + \left[\sum_{e=1}^{n_e} k_{(e)x}\left[S_{(e)x} + S_{(e)\theta x}\right] + \right]^{(j)} \begin{pmatrix} u_1 \\ \vdots \\ u_n \\ v_1 \\ \vdots \\ v_n \\ \theta_1 \\ \vdots \\ \theta_n \end{pmatrix} = 0 \tag{6}$$

The three equations of motion, Eq. 4, 5, and 6, combine together in a single equation in the form:

$$[M]\{\ddot{X}\} + \sum_{e=1}^{n_k} \left(k_{(e)x} S_{(e)\theta x} + k_{(e)y} S_{(e)\theta y}\right) \{X\} = -[M]\{\ddot{u}_g\} \tag{7}$$

where M is the mass matrix, the state and input vectors are defined as,

$$\{X\} = \begin{Bmatrix} u \\ v \\ \theta \end{Bmatrix}; \qquad \{\ddot{u}_g\} = \begin{Bmatrix} \ddot{x}_g \\ \ddot{y}_g \\ 0 \end{Bmatrix} \tag{8}$$

Considering all equations associated with each floor mass, the equations of motion for the combined system can be stated as follows:

$$M\ddot{x} + \left[[S]\{k\}^T\right]x = -M\ddot{u}_g \tag{9}$$

where $\{k\}$ is the vector of column stiffness values (which contains stiffness values of all elements such as $k_{(e)x}$ and $k_{(e)y}$), S is the allocation tensor (which contains the set of allocation matrices, $S_{(e)x}, S_{(e)y}, S_{(e)\theta x}, S_{(e)\theta y}$), and $\ddot{u}_g$ is the ground acceleration vector.

3.3. Stiffness identification using the strain measurements

For model-based vibration response analysis, this system can be characterized by its frequencies and system modes shapes represented by the following eigenvalue problem:

$$K\varphi_j = \omega_j^2 M\varphi_j, \qquad j = 1, \dots, n_k \tag{10}$$

In the proposed strain measurement based identification approach, we measure the flexural strain responses associated with the system vibrations in the x- and y-directions. These responses are the utilized in the SSI or NeXT-ERA algorithms to obtain the system frequencies and the mode shapes associated with the measured responses. These identified response mode shapes are related to the system mode shapes, associated with the system degrees of freedom, by the following simple relationship:

$$\rho_j = T\varphi_j \tag{11}$$

where T is the matrix which translates the system modes to the mode shapes associated with measured response (strain response). Since the SSI and NeXT-ERA provide ρ_j the mode shapes associated with the measured response, we can use Eq. 11 to get the mean square estimate of the system mode shapes by pseudo inversion as

$$\varphi_j = T^+\rho_j, \qquad j = 1, \dots, n_k \tag{12}$$

where $T^+$is the pseudo-inverse of the transformation matrix T that maps the system DOFs, into the flexural strains measured at selected locations on each column. As described earlier, this pseudo-inverse can be symbolically expressed in terms of the transformation matrix T and it transpose as follows,

$$T^+ = [T^T T]^{-1} T^T \tag{13}$$

In numerical calculations, this pseudo-inverse is not necessarily calculated by matrix inversions indicated in Eq. 13 but rather by effectively utilizing singularly value decomposition of matrix T. Having calculated the system modes, we utilize the system eigenvalue problem associated with the equation of motion now stated in terms of the vector of column stiffness values $\{k\}$ as follows:

$$S\varphi_j\{k\} = \omega_j^2 M\varphi_j, \qquad j = 1, \dots, n_k \tag{14}$$

where ω_j and φ_j are the system j^{th} natural frequency and mode shape, respectively. To solve Eq. 14 for the stiffness values $\{k\}$, a similar procedure as discussed in Chapter 2 is used. The term $S\varphi_j$ in Eq. 14 is the product of a three-dimensional tensor with a one-dimensional vector, giving a two-dimensional rectangular matrix, herein again referred to as matrix C_j. Each column of this matrix C_j is a product of an allocation matrix $S_{(e)}$ (which is associated with an element e) with the mode shape φ_j expressed as follows:

$$S\varphi_j = C_j = [c_{1j}|c_{2j}| \dots |c_{ej}| \dots |c_{n_k j}] \tag{15}$$

Eq. 14 is thus expressed as

$$C_j\{k\} = \omega_j^2 M\varphi_j \tag{16}$$

The matrix C_j in Eq. 16 is $n\ x\ n_k$ with n rows and n_k columns. Since for model shown in Figure 3.1, n_k will be much larger than the system degrees of freedom n. For example for numerical example under consideration below the system has $n = 6$ degrees of freedom whereas the number of elements for which the stiffness coefficients need to be determined by pseudo inversion is $n_k = 16$. Thus the Eq. 16 for a single mode is highly under determined, and may be unsuitable for pseudo-inversion. The situation can be improved if several equations like, Eq. 16 are collectively used to form a proper pseudo-inverse problem for identification of element stiffness values. As described in Chapter 2, this can be done by stacking Eq. 16 for different modes to form the following equation appropriate for pseudo inversion:

$$[C]\{k\} = \begin{bmatrix} \alpha_1 C_1 \\ \alpha_2 C_2 \\ \\ \\ \alpha_m C_m \end{bmatrix} \{k\} = \begin{Bmatrix} \alpha_1 v_1 \\ \alpha_2 v_2 \\ \\ \\ \alpha_m v_m \end{Bmatrix} = \{v\} \tag{17}$$

Where α_i is a weighting factor representing the contribution of the i^{th} mode equation to the combined equation, and m is the number of mode considered to form this combination. The weighting factor can be optimally selected as explained in Chapter 2.

The least mean square estimate of the stiffness vector $\{k\}$ can now be obtained by pseudo-inversion of matrix C as follows,

$$\{k\} = [C]^+ \{v\} \tag{18}$$

where $[C]^+$ is the Moore-Penrose pseudoinverse of the matrix C can be symbolically expressed as follows:

$$[C]^+ = [C^T C]^{-1} C^T \tag{19}$$

3.4. Numerical Study

To examine the effectiveness of the proposed approach, we utilize the models of two 2-story 3-D frame structures. Each structure has one bay in the x- and y-direction. The slab is supported by 4 columns placed at each corner of the slab. As mentioned earlier, the floor slab is assumed to be rigid. The columns are assumed to be rigidly connected to the floor slab such that no column end rotations are possible. The geometric properties, mass of the floor slabs and stiffness properties of the supporting columns are defined as follows:

Table 3.1 Geometric properties for the two frame models 1 and 2, both are 1-Bay×1-Bay×2-Stories frames.

	model 1	model 2
Floor mass	10e3 kg	10e3 kg
Floor Inertia	4e5 kg.m^2	4e5 kg.m^2
x-width	4 m	4 m
y-width	5 m	5 m
Height of each story	3 m	3 m
x-Flexural Rigidity of Columns	[10 10 10 8 7.5 10 10 9.7] e6N.m^2	[16 20 20 20 18.2 20 18.6 20] e6N.m^2
y-Flexural Rigidity of Columns	[10 10 10 7.5 7.5 10 10 9.2] e6N.m^2	[16 20 20 20 17.4 20 18 20] e6N.m^2

Table 3.2 Modal parameters for the two frame models 1 and 2, both are 1-Bay×1-Bay×2-Stories frames.

	mode 1	**mode 2**	**mode 3**	**mode 4**	**mode 5**	**mode 6**
			model 1			
Frequencies	**3.61171**	**6.04027**	**8.5884**	**9.45848**	**15.7552**	**22.538**
Mode Shapes	-1.376E-04	5.212E-03	-8.591E-06	-3.322E-04	-8.527E-03	-1.132E-06
	-7.135E-05	8.526E-03	-4.355E-06	-2.156E-04	5.221E-03	1.504E-06
	-1.053E-04	3.912E-06	5.276E-03	4.386E-05	-4.062E-06	8.494E-03
	-1.588E-04	-3.862E-06	8.491E-03	-2.541E-04	2.246E-06	-5.274E-03
	8.303E-04	-3.707E-05	-1.011E-05	-1.345E-03	1.634E-05	2.354E-05
	1.345E-03	4.752E-05	4.161E-05	8.284E-04	-2.497E-05	-1.348E-05
			model 2			
Frequencies	**3.59433**	**6.00058**	**8.56705**	**9.39252**	**15.6485**	**22.3904**
Mode Shapes	-1.819E-04	5.212E-03	-4.547E-06	-2.649E-04	-8.528E-03	-6.045E-07
	-1.415E-04	8.524E-03	-9.510E-06	-2.619E-04	5.221E-03	1.435E-06
	-1.065E-04	1.248E-06	-5.239E-03	2.712E-04	-3.201E-06	8.513E-03
	-1.821E-04	-1.198E-05	-8.514E-03	1.140E-05	1.123E-06	-5.243E-03
	8.275E-04	-3.092E-05	-3.788E-05	-1.346E-03	5.293E-06	2.992E-05
	1.346E-03	5.895E-05	-1.590E-05	8.263E-04	-1.835E-05	-1.929E-05

It is observed that the stiffness values of the two above-mentioned models, in both of the directions, are not uniform. This is purposed in order to avoid symmetry in the 3D frame model. The reason for this concern is that a symmetric 3D structure creates a singularity in

the analysis. Symmetry decouples the two perpendicular motions in *x*- and *y*-directions, which prevents the third degree of freedom, rotation. Consequently, the resulting mode shapes are pure. Every mode describes a pure motion along one of the three degrees of freedom as shown in Table 3.4 below for a symmetric structure.

Table 3.3 Geometric properties for a 1-Bay×1-Bay×2-Stories symmetric frame.

Floor mass	10e3 kg
Floor Inertia	4e5 kg.m^2
x-width	4 m
y-width	5 m
Height of each story	3 m
x-Flexural Rigidity of Columns	[10 10 10 10 10 10 10 10]e6N.m^2
y-Flexural Rigidity of Columns	[20 20 20 20 20 20 20 20] e6N.m^2

Table 3.4 Modal parameters for the 1-Bay×1-Bay×2-Stories symmetric frame of Table 3.3

	mode 1	**mode 2**	**mode 3**	**mode 4**	**mode 5**	**mode 6**
Frequencies	3.7131	6.2210	8.7979	9.7211	16.2869	23.0331
Mode Shapes	0	-0.00526	0	0	-0.00851	0
	0	-0.00851	0	0	0.005257	0
	0	0	-0.00526	0	0	-0.00851
	0	0	-0.00851	0	0	0.005257
	-0.00083	0	0	-0.00134	0	0
	-0.00134	0	0	0.000831	0	0

Therefore, we have introduced some asymmetry to the frame. This can be achieved either by introducing irregularity to the frame geometry, or by introducing irregularity to the stiffness properties of the columns as we have done in this study.

The assumed models are excited by earthquake induced ground accelerations in the two perpendicular directions *x* and *y*. In the x-direction, the recorded El-Centro CA (1940) and in the y-direction the recorded Chi-Chi earthquake (Taiwan, 1990) time histories are used as the inputs at the base of these structural models to induce motions which are measured in terms of the flexural strains to define the measured signals. Both recorded acceleration signals were modified in terms of their signal strength, signal duration and sampling time to make them compatibly similar.

As mentioned earlier, the output is defined in terms of the measured dynamic strain responses at the column ends. It is assumed that the flexural strains due to column bending

in both x- and y-directions are measured. Also these measurements are made at the both ends of the column near the floor slabs and the base. Since there are 4 columns in each story, with possible bending in both the x-and y-directions, there are a total 32 strain measurements available for system stiffness identification.

In this study, the measured dynamic response data is processed using the system identification algorithms SSI (Stochastic Subspace Identification) to obtain an identified dynamic model of the structure. This identification provides the modal parameters such as system frequencies and mode shapes. Since the responses measured are the flexural strains, the SSI provides the strain response mode shapes. The strain response mode shapes are then used to calculate the system mode shapes associated with the system degrees of freedom of the model. The system mode shapes are then used in Eq. 17 to identify the element stiffness values. In the following we present some results of this system identification for the assumed models.

The identified stiffness values of the two models are shown below in Figure 3.5a and b, in addition to the average identification error defined as $Err_{avg} = \frac{1}{n_k}\sum_{e=1}^{n_k}\left|\frac{k_e^{identified}}{k_e^{exact}} - 1\right|$. Table 3.5 shows the element-by-element identification error percentage defined as $\%Error = 100 \times \left(\frac{k_e^{identified}}{k_e^{exact}} - 1\right)$. The results in Figure 3.3 and Table 3.5 are obtained using three different mode sets,

- The exact mode shapes of the model
- The mode shapes identified from a 0% polluted signal
- The mode shapes identified from a 10% polluted signal

The reason for using the exact mode shapes is to assess the strength of the proposed algorithm regardless of the errors induced by noise in the measurements. The modes identified from a 0% and a 10% noise response are utilized to identify the effect of the measurement noise on the proposed identification algorithm.

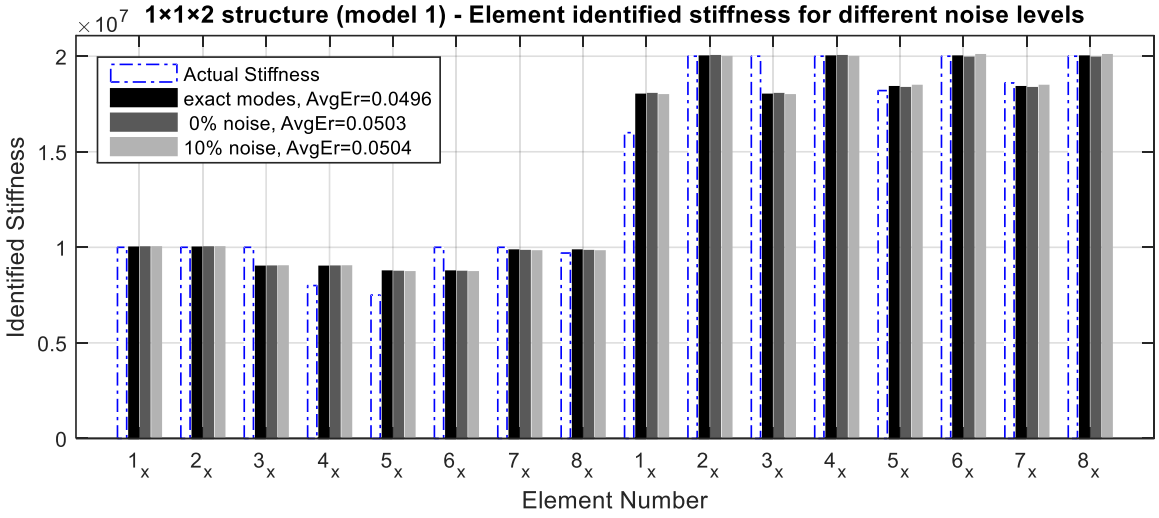

(a) model 1

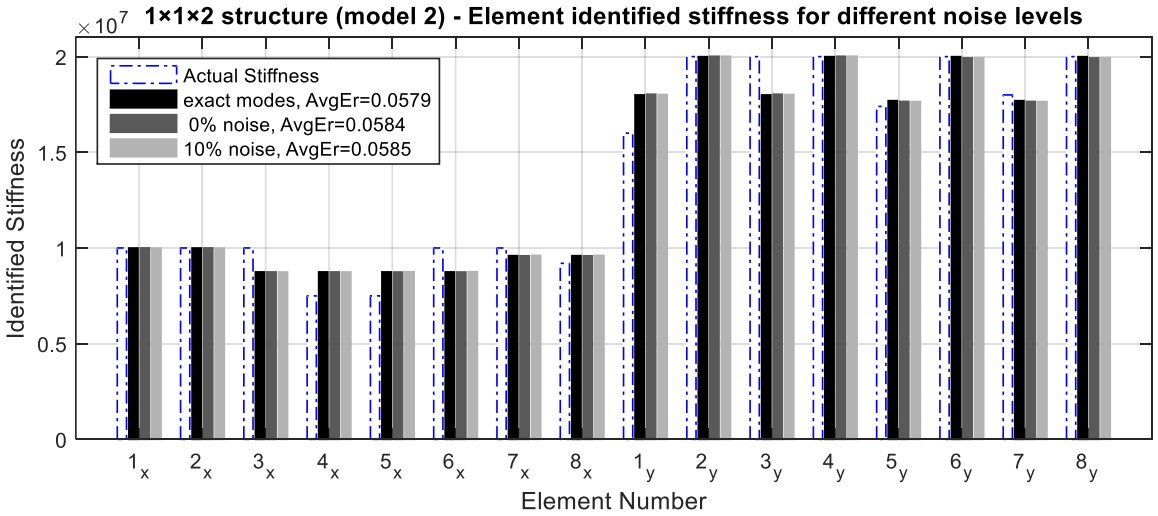

(b) model 2

Figure 3.3 Column stiffness values identified by the proposed approach: (a) for model 1 and (b) for model 2. The first 8 values are for the element stiffness in x-direction and the last eight are for the element stiffness in y-direction

Although the identification errors in some elements are large, they seem to be independent of the level of the measurement noise as the identification error level is about same even when the modes extracted from the noisy measurements are used. This indicates that the system modes are quite accurately extracted from the noisy measurements.

The identification errors shown in Table 3.5 as well the discrepancy in the stiffness comparisons shown in Figure 3.3 seem to have a pattern that is related to the geometric

Table 3.5 Identification errors in the element stiffness values identified by the proposed approach for Models 1 and 2.

				% Error					
Model				**Model I**			**Model II**		
signal noise level				**Exact modes**	**0%**	**10%**	**Exact modes**	**0%**	**10%**
Element No.	X-Stiffness	1st Story	**1**	0.00	0.11	0.17	0.00	0.04	-0.05
			2	0.00	0.11	0.17	0.00	0.04	-0.05
			3	-10.00	-9.91	-9.83	-12.50	-12.50	-12.55
			4	12.50	12.61	12.72	16.67	16.67	16.60
		2nd Story	**5**	16.67	16.42	16.18	16.67	16.61	16.84
			6	-12.50	-12.68	-12.86	-12.50	-12.54	-12.37
			7	-1.50	-1.76	-1.94	-4.00	-4.08	-3.89
			8	1.55	1.27	1.09	4.35	4.26	4.47
	Y-Stiffness	1st Story	**1**	12.50	12.74	12.34	12.50	12.74	12.64
			2	0.00	0.11	-0.13	0.00	0.09	0.11
			3	-10.00	-9.81	-10.13	-10.00	-9.81	-9.88
			4	0.00	0.11	-0.13	0.00	0.09	0.11
		2nd Story	**5**	1.10	0.82	1.45	1.72	1.50	1.46
			6	0.00	-0.32	0.37	0.00	-0.33	-0.30
			7	-1.08	-1.35	-0.73	-1.67	-1.89	-1.93
			8	0.00	-0.32	0.37	0.00	-0.33	-0.30

layout of the columns and their assumed stiffness values. Since the identification errors for the exact modes as well as modes extracted from noisy measurements have very similar values and similar patterns, to understand this pattern we examine the element stiffness error results obtained with the exact modes as they do not have any issues related to the measurement noise. First we look at the values in Table 3.5 just for Model 1. We note that the stiffness values of element 1 and 2 in the x-direction have zero identification errors whereas those of elements 3 and 4 are very large errors but of the opposite signs. Similarly, in the second story the errors in elements 5 and 6 are very large whereas the errors in elements 7 and 8 are relatively much smaller. The common feature of the elements with zero errors is that these elements are aligned parallel to the x-axis and that they have equal stiffness values in the assumed model. The elements with large identification errors are also aligned parallel to the x-axis but their stiffness values differ by: 20% for elements 3 and 4, 2.5% for element 5, and 6 and 3% for elements 7 and 8, as shown in Table 3.5. We note that we have larger identification errors in the aligned elements if their model stiffness values have a large deference. This error is also the same as the percent difference between the

actual element stiffness value and the average of the two element stiffness values. That is, this identification approach cannot identify the difference between the stiffness of the elements in a row parallel to an axis even if they had different stiffness values. Rather, the mean square Euclidean length minimization approach used in the pseudo inversion algorithm assigns them a value which is equal to the average of all aligned element stiffness values (Udwadia et. Al, 1996). The same observation can be made about the errors in y-direction, as well as for structural model 2.

Indeed, if a model with equal element stiffness values in all columns in row parallel to an axis is used the element stiffness values are accurately identified. To verify this, we used a model, called Model 3, with element stiffness values shown in as follows Table 3.6:

Table 3.6 Geometric properties for model 3, a 1-Bay×1-Bay×2-Stories frame.

Floor mass	10e3 kg
Floor Inertia	4e5 kg.m^2
x-width	4 m
y-width	5 m
Height of each story	3 m
x-Flexural Rigidity of Columns	[7.5 7.5 10 10 10 10 9.2 9.2]e6N.m^2
y-Flexural Rigidity of Columns	[20 16 20 16 18 20 18 20] e6N.m^2

Table 3.7 Modal parameters for the two frame models 3, a 1-Bay×1-Bay×2-Stories frame.

	mode 1	**mode 2**	**mode 3**	**mode 4**	**mode 5**	**mode 6**
Frequencies	**3.5071**	**5.88376**	**8.3526**	**9.46626**	**15.7648**	**22.2881**
Mode Shapes	4.224E-04	-5.386E-03	-9.298E-05	-2.573E-04	-8.410E-03	-8.185E-07
	4.270E-04	-8.387E-03	-1.479E-04	-4.578E-04	5.408E-03	5.158E-07
	2.161E-04	-1.508E-05	5.206E-03	-1.206E-03	6.730E-07	-8.450E-03
	1.775E-04	-3.741E-05	8.246E-03	-1.838E-03	-2.578E-06	5.347E-03
	8.529E-04	-2.301E-05	2.705E-04	1.303E-03	1.471E-05	2.458E-06
	1.327E-03	1.253E-04	-2.206E-04	-8.207E-04	1.398E-05	1.494E-05

For this Model 3, the results are shown in Figure 3.4 and in Table 3.8. Figure 3.4 compares the exact and identified stiffness values of the elements. Also provided in the figure legend is the average identification error as defined in the previous example. Table 3.8 shows the % identification error in all the elements. Clearly in Figure 3.4 and Table 3.8, the average error is very little even at the high noise level. Individual element error is low as well with one maximum value of 1.15%.

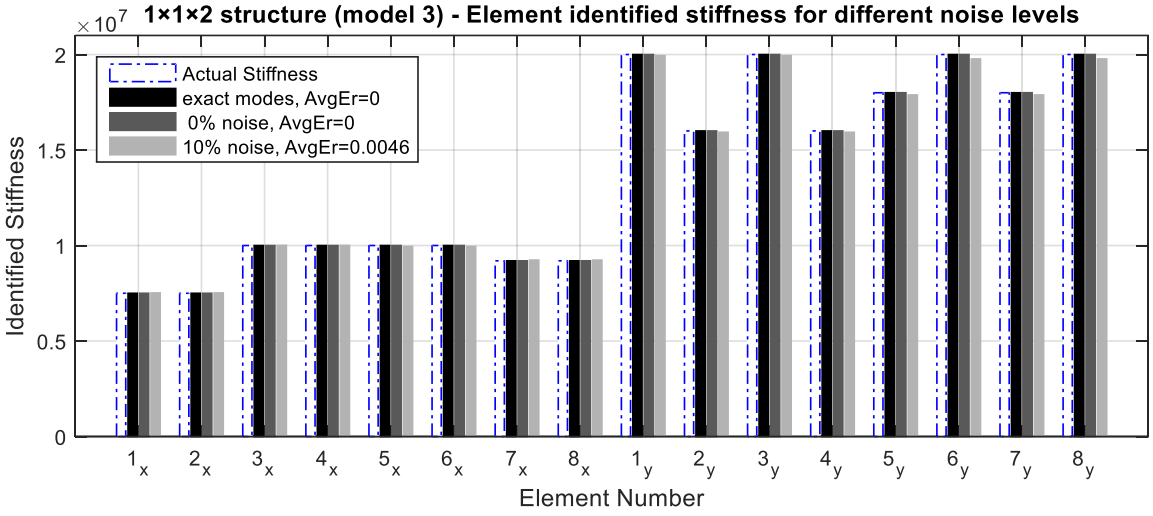

Figure 3.4 Stiffness identified for a 1-Bay×1-Bay×2-Stories frame structure. The stiffness of the frame columns is selected to be equally distributed in each direction.

Table 3.8 Element stiffness identification error for the 1×1×2 frame presented in Figure 3.4.

Model				% Error		
signal noise level				Exact modes	0%	10%
Element No.	X-Stiffness	1st Story	**1**	1.3E-13	8.3E-12	0.24
			2	2.7E-13	8.1E-12	0.24
			3	0.0E+00	-9.8E-12	0.08
			4	0.0E+00	-9.8E-12	0.08
		2nd Story	**5**	-8.9E-14	-9.9E-12	-0.46
			6	0.0E+00	-9.1E-12	-0.46
			7	-2.2E-13	7.8E-12	0.40
			8	-3.2E-13	7.8E-12	0.40
	Y-Stiffness	1st Story	**1**	0.0E+00	-2.8E-11	-0.29
			2	0.0E+00	-1.1E-11	-0.44
			3	0.0E+00	-2.8E-11	-0.29
			4	0.0E+00	-1.1E-11	-0.44
		2nd Story	**5**	0.0E+00	-4.2E-11	-0.64
			6	0.0E+00	-4.5E-11	-1.15
			7	0.0E+00	-4.2E-11	-0.64
			8	0.0E+00	-4.5E-11	-1.15

The element stiffness values identified for a system with unequal stiffness in the columns aligned along an axis can, of course, be used to estimate accurately the total stiffness of the columns in a row parallel to an axis. To confirm this observation, we use the identified

stiffness values of each column, shown earlier in Figure 3.3 for Models 1 and 2, to obtain the combined stiffness of columns in a row along the *x*-, and *y*-directions as follows:

Elements in *x*-direction in story 1 and 2

$$k_{12_x} = k_{1_x} + k_{2_x}; k_{34_x} = k_{3_x} + k_{4_x};$$
$$k_{56_x} = k_{5_x} + k_{6_x}; k_{78_x} = k_{7_x} + k_{8_x}; \quad (20.a)$$

Elements in *y*-direction in story 1 and 2

$$k_{13_y} = k_{1_y} + k_{3_y}; k_{24_y} = k_{2_y} + k_{4_y};$$
$$k_{57_y} = k_{5_y} + k_{7_y}; k_{68_y} = k_{6_y} + k_{8_y}; \quad (20.b)$$

These combined identified values along the x- and y-directions are now compared with the exact values in the models, and the difference between these two values expressed as % identification error is shown in Table 3.9 and Table 3.10. These error values are nearly equal to zero for the exact modes and very small for the modes extracted from the noisy data. Thus, the identified stiffness values can be used to get a good estimate of the combined stiffness values.

The reason for a reduced identification error in the combined stiffness of the aligned elements can be explained as follows. All elements aligned parallel to an axis will have the same allocation matrices associated with their element stiffness values. That is, some of the vectors c_{ij} appearing in Eq. 15 will be identical for the elements that are aligned parallel to an axis. For example, in the numerical example of Model 1 and 2 under consideration, the vectors c_{1j} and c_{2j} associated with elements 1-x and 2-x (as well as other vectors associated with elements parallel to an axis) will be identical. The stiffness coefficients of these aligned elements can be combined into a single coefficient as they all post multiply the same allocation matrices. This will reduce the number of stiffness coefficients to be determined and, of course, the size of matrix C_j. For example, for the structural model under consideration, this will reduce the size of matrix C_j to 6 x 8 from its earlier size of 6 x16. This reduces the "highly under determined" nature of the pseudo inverse problem associated with Eq. 16. If only a single mode is considered, the problem is still "under determined" as

there are more variables (that is, 8) than the number of equations (which is 6). However, as explained earlier in the development of Eq. 17 we can again combine the equations for several modes before pseudo-inversion is used to estimate the element stiffness values. The pseudo inverse will again provide the least mean square solution for the combined stiffness values of the aligned columns.

This approach with a reduced size matrix C_j was utilized to identify the row-wise combined stiffness values of the column elements which are aligned parallel to an axis. For example, the pair of elements (1-x and 2-x), and (3-x and 4-x) in the first story and pairs (5-x and 6-x) and (7-x and 8-x) in the second story are aligned parallel to the x-direction. Similarly, the pairs (1-y and 3-y) and (2-y and 4-y) in the first story and pairs (5-y and 7-y) and (6-y and 8-y) in the second story are aligned parallel to the y-direction. Since the paired elements have the same allocation matrices each pair can be replaced by a single element with its stiffness equal the sum of their stiffness values. Thus as mentioned earlier, the reduced size of the matrix C_j is 6 x 8, and the vector $\{k\}$ will only have 8 elements. These modal Eq. 16 for all modes were used to form Eq. 17. The identification error of the optimal pseudo-inverse solution of this set are given in Table 3.10. The identification error values are slightly different from those in Table 3.9 because of slight variation caused by optimization with different C matrix than what was used to generate the results shown in Table 3.9.

Table 3.9 Identification errors in the row stiffness values calculated directly calculated with reduced size C_j matrix

		% Error					
Model		**Model I**			**Model II**		
Stiffness direction	Row of column	signal noise level			signal noise level		
		Exact modes	**0%**	**10%**	**Exact modes**	**0%**	**10%**
X-Stiffness	k_{12_x}	0	0.169	0.112	0	-0.052	0.047
	k_{34_x}	-4.4E-14	0.193	0.100	-1.67E-13	-0.055	0.016
	k_{56_x}	0	-0.413	-0.210	4.44E-14	0.148	-0.046
	k_{78_x}	-3.3E-14	-0.446	-0.268	4.44E-14	0.115	-0.061
Y-Stiffness	k_{13_y}	0	-0.142	0.210	0	0.128	0.217
	k_{24_y}	0	-0.131	0.113	0	0.112	0.096
	k_{57_y}	0	0.352	-0.275	0	-0.263	-0.208
	k_{68_y}	0	0.365	-0.322	0	-0.302	-0.319

Table 3.10 Story-wise identification % errors in the combined stiffness values for models 1 and 2

		% Error					
Model		**Model I**			**Model II**		
Stiffness direction	Row of column	signal noise level			signal noise level		
		Exact modes	**0%**	**10%**	**Exact modes**	**0%**	**10%**
X-Stiffness	k_{1234_x}	-2.2E-14	-1.565	-0.942	-8E-14	0.993	1.529
	k_{5678_x}	-2.2E-14	0.535	0.360	4E-14	-0.365	-0.560
Y-Stiffness	k_{1234_y}	0	-0.194	0.083	0	0.214	0.214
	k_{5678_y}	0	0.455	-0.217	0	-0.400	-0.414

Next we examine the possibility of estimating the stiffness values for the whole story utilizing the element stiffness values or utilizing the row stiffness values of aligned elements identified by pseudo inversion of Eq. 17. To examine this, we define the stiffness coefficients for the whole story as follows:

$$k_{x^{(story)}} = \sum_{e=1}^{4} k_{x^{(e)}} \tag{21.a}$$

$$k_{y^{(story)}} = \sum_{e=1}^{4} k_{y^{(e)}} \tag{21.b}$$

$$k_{\theta^{(story)}} = \sum_{e=1}^{4} y_{(e)}^2 k_{x^{(e)}} + x_{(e)}^2 k_{y^{(e)}} \tag{21.c}$$

The first two equations provide the total story stiffness in the *x*- and *y*-directions. The last equation provides the torsional stiffness of the story. When the combined stiffness of the paired columns are used, the number of the summation terms will be half of what is shown in the above equation. The identified values of these story stiffness coefficients were calculated by the using the k_i values calculated from the pseudo inverse solution of Eq. 17. The identified story stiffness values were then compared with the corresponding exact values of the models. The difference between the exact and identified values expressed as the % identification error is now shown in Table 3.11. The table again provides the errors both for exact modes and modes extracted from the noisy measurements. The errors of identification are seen to be low in all cases, even for the modes extracted from the data with 10% added noise.

Table 3.11 The % identification errors in the total story stiffness coefficients obtained using the identified element stiffness values for the two models. The identified element stiffness values used to calculate these story stiffness values are the same as those shown in Figure 3.3

		% Error					
Model		**Model I**			**Model II**		
Stiffness direction	Story no.	signal noise level					
		Exact modes	**0%**	**10%**	**Exact modes**	**0%**	**10%**
X-Stiffness	1st Story	0.00	-0.01	0.01	0.00	0.03	-0.05
	2nd Story	0.00	0.00	0.02	0.00	-0.07	0.13
Y-Stiffness	1st Story	0.00	-0.02	0.02	0.00	0.15	0.12
	2nd Story	0.00	-0.06	0.01	0.00	-0.28	-0.28
Θ-Stiffness	1st Story	0.00	-0.02	0.03	0.00	-0.04	0.03
	2nd Story	0.00	-0.06	-0.04	0.00	-0.12	-0.09

Large 3D frames

In this section, we test the application of the approach for a larger frame a 3-story shear beam model consisting of two bays in in the x- and y- direction and 4 stories. Figure 3.5 shows the layout of the building frame. The slabs in the frame are supported by 3 rows of 3 columns with total of 9 columns in each story and a total of 36 columns in all four stories. To test the applicability of the basic identification methodology to a larger problem with multiple rows of supporting columns, we will present the numerical validation results only using the exact modes. If a larger supercomputing system were easily available, we could also have used the noisy strain response measurements to extract the system modes. Since it would have taken a long time to obtain the similar results with the easily available computing resources with the writer, it was considered appropriate to use the exact system modes (calculated by a straightforward eigenvalue analysis) to demonstrate the application of the approach for the element and story stiffness identification. In the results presented earlier for smaller models it was observed that exact modes results were similar to those obtained with the identified modes. We, thus, consider the results obtained from these exact modes as an indication of the effectiveness of the proposed approach to large structural systems. The chosen properties and parameters of the frame are given in Table 3.12.

Table 3.12 Mass, stiffness and geometric properties for model 3, a 4-Stories shear beam frame with three rows of columns in the x- and y-directions.

Floor mass	40e3 kg	
Floor Inertia	1.6e6 kg.m^2	
x-width of each bay	4 m	
y-width of each bay	5 m	
Height of each story	3 m	
x-Flexural Rigidity of Columns	$story_1$ [10 10 10 8 7.5 10 10 9 9] $story_2$ [10 10 9 10 10 10 10 10 10] $story_3$ [10 8 10 10 9 10 10 8.4 10] $story_4$ [10 9.7 8.1 10 8.9 10 10 10 9.5]	e6N.m^2
y-Flexural Rigidity of Columns	$story_1$ [16 20 20 20 18 20 18 20 20] $story_2$ [20 16.2 20 20 20 20 20 20 20] $story_3$ [20 20 20 18 20 16 20 20 14] $story_4$ [19 20 20 19.6 20 20 20 17 20]	e6N.m^2

The identified stiffness values both for *x*- and *y*-directions are shown in Figure 3.5. The pattern of error observed in the identified stiffness for this large frame model is similar to the pattern observed in Figure 3.3 for the previous smaller models. That is, there are element with large stiffness identification errors. However, next we show that these estimated element stiffness values can be effectively utilized to obtain accurate estimates of the collective stiffness of the column rows in the x- and y- directions. The identified values can

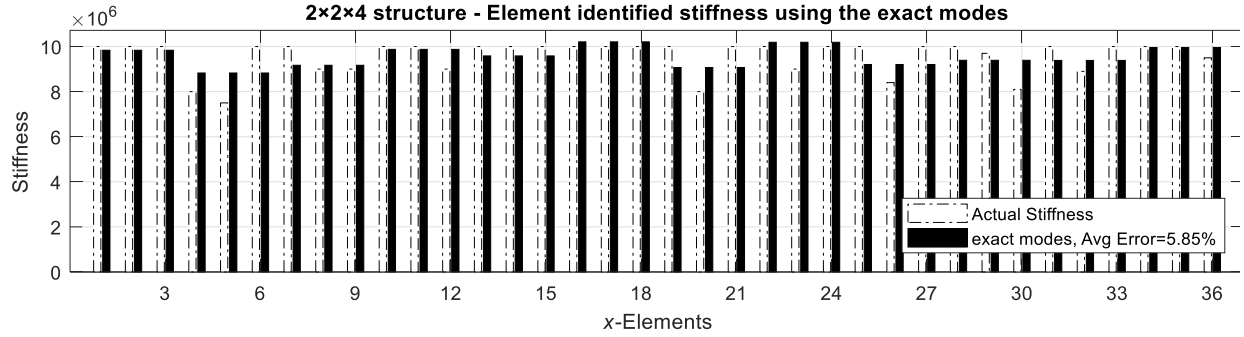

(a) Stiffness identified in *x*-direction

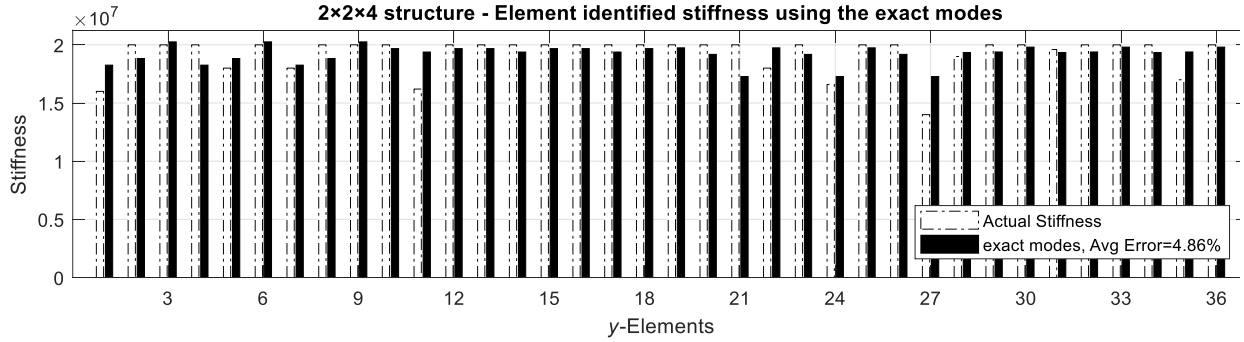

(b) Stiffness identified in *y*-direction

Figure 3.5 Stiffness identified in y-direction for a 2-Bay×2-Bay×4-Stories frame structure.

also be used to estimate the total story stiffness values including the torsional stiffness values of each story. In this frame, each story has 9 columns. That is, it has three rows of columns, and each row containes three columns with one similar coordinate. Therefore, We will consider each row of columns for identifictaion as a single element. The results, as presented in Figure 3.6, are considerably more accurate than the element-by-element identifictaion shown in Figure 3.5.

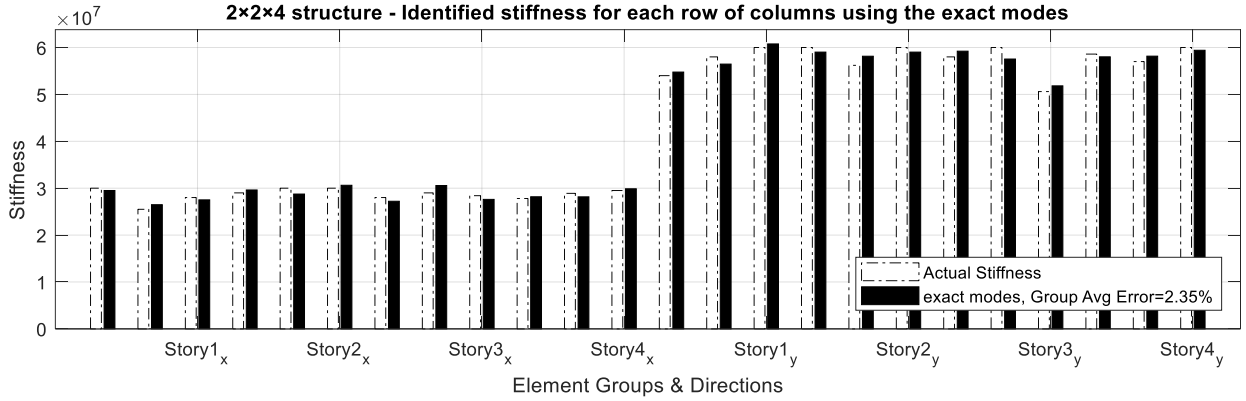

Figure 3.6 Stiffness identified for a 2-Bay×2-Bay×4-Stories frame structure for the combined sets of elements in each story in each direction. There are three combined sets for each story and each combined set includes 3 elements having the same allocation matrix

The identifictaion errors for different rows of columns are given in Table 3.13. The errors for the middle rows, both in the x- and y- directions, have higher identification errros. These rows are also near the mas center. There is another trend associated with these rows. All midlle row errors are opposite of the errors in the outer rows, indicating that the the combined errors of the all paraellel rows are much small and thus suggesting that this approach will more identify the total story stiffness values more accurately. Thus in Figure 3.7 we compare the exact and identified story stiffness values, and in Table 11 we provide the identification

Table 3.13 Stiffness identification error on a row-by-row basis for a 2-Bay×2-Bay×4-Stories structure. Each story has three rows and each row includes three elements which have the same allocation matrix.

		% Error	
Model		***x*-Stiffness**	***y*-Stiffness**
Stiffness direction	Story no.	**Exact modes**	**Exact modes**
1st Story	1st Row	-1.63451	1.418842
	2nd Row	3.845897	-2.64198
	3rd Row	-1.75126	1.276958
2nd Story	1st Row	2.150117	-1.62379
	2nd Row	-4.15689	3.467159
	3rd Row	2.078446	-1.62379
3rd Story	1st Row	-2.80417	2.115217
	2nd Row	5.414954	-4.08942
	3rd Row	-2.76468	2.424556
4th Story	1st Row	1.339224	-0.99271
	2nd Row	-2.5765	2.041141
	3rd Row	1.262048	-0.96954

error for these story stiffness parameters. An excellent comparison in Figure 3.7 and the low estimation values shown in

Table 3.14 confirm that this approach should be able to identify these total story parameters very accurately. Although we utilized the exact system modes in the just presented results, the identified modes are also expected to provide a similar low levels of error if the system modes can be accurately extracted from the measured data.

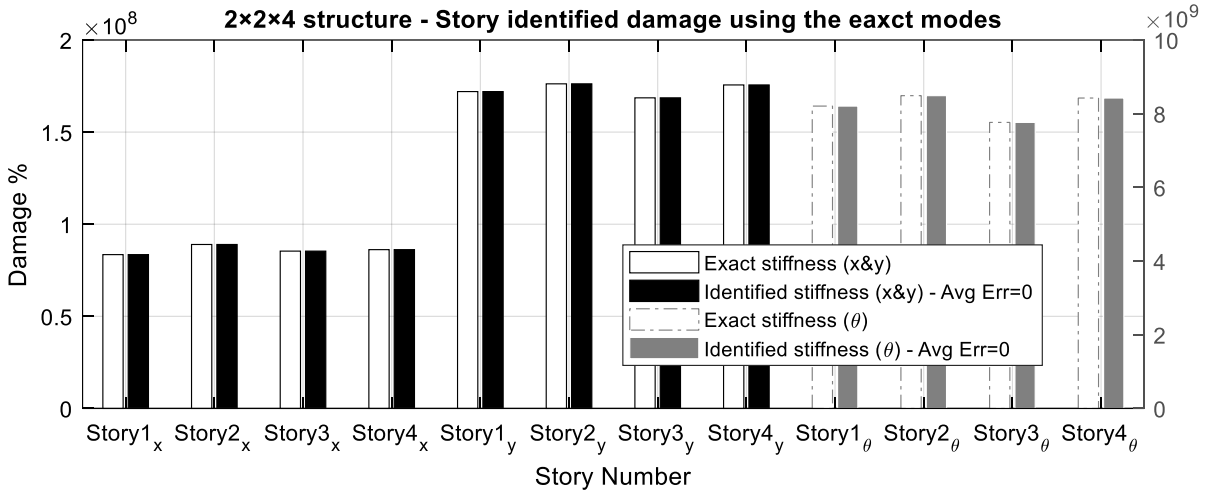

Figure 3.7 Total story stiffness values identified for a 2-Bay×2-Bay×4-Stories structure.

Table 3.14 Stiffness identification error on a story-by-story basis for a 2-Bay×2-Bay×4-Stories structure. Each story has three rows and each row includes three elements which have the same allocation matrix.

	% Error	
Model	***x*-Stiffness**	***y*-Stiffness**
Stiffness direction	**Exact modes**	**Exact modes**
1st Story	-3.33067E-14	-5.55112E-14
2nd Story	3.10862E-13	-5.55112E-14
3rd Story	-1.77636E-13	1.77636E-13
4th Story	0	3.10862E-13

Damage Identification

In order to obtain the damage in a certain structure, we need to first obtain its identified stiffness parameters at two different states, an initial undamaged state and a final damaged state. The damage is defined as the reduction in stiffness from the initial state to the final state. The stiffness parameters in both states are identified using the identification approach illustrated earlier in this chapter. In this study, we consider one of the models described in the previous section (model 1) as the initial undamaged state of the structure, and then we define two new model to be considered for the final damaged state. The two damage

scenarios are designed so that one of them has a relatively low damage (about 5% to 15%), while the other has a relatively high damage (about 15% to 30%). The two models, we call them model 4 and model 5, have the following stiffness parameters:

Model 4

- *x*-Flexural Rigidity = [10 10 10 7 7 10 10 8.2]e6N.m^2
- *y*-Flexural Rigidity = [14 20 20 20 17.2 20 15.6 20]e6N.m^2

Model 5

- *x*-Flexural Rigidity = [10 10 10 7 7 10 10 8.2]e6N.m^2
- *y*-Flexural Rigidity = [14 20 20 20 17.2 20 15.6 20]e6N.m^2

The identified damage occurring in models 4 and 5 is obtained using the exact modes shapes of the structure, the mode shapes identified at 0% polluted measurement, and the mode shapes identified at 10% polluted measurement. The results, presented in Figure 3.8, show the actual and identified levels of damage in various elements. It is clearly noted that some of the damaged elements have been completely missed as well as damage is indicated where none exists. Thus the approach cannot be used to identify the element-by-element level or location of the damage. This inability of identify the damage is very much related to the identification problem observed when the results in Figure 3.3 were being examined. However, since the approach was found to be effective in identifying the combined stiffness values of the column elements aligned parallel to the coordinate axes or story stiffness values, the approach can thus be used to identify the change in these combined stiffness values representing the damage in a row of columns or in stories.

To show this we present Figure 3.9 and Figure 3.10. Also,

and Table 3.16 provide the identification errors in the damage identifications. In Figure 3.9 we now show the identified change in the stiffness values in the two rows of columns aligned along the *x*- and *y*-directions in the first and second stories of the models. In

we give the damage identification errors representing the difference between the estimated and exact damage values if any in these *x*- and *y*-rows of the column. In Figure 3.10 we show the level of story wide damage and compare with the actual damage assumed in the model. The corresponding identification errors are shown in Table 13.

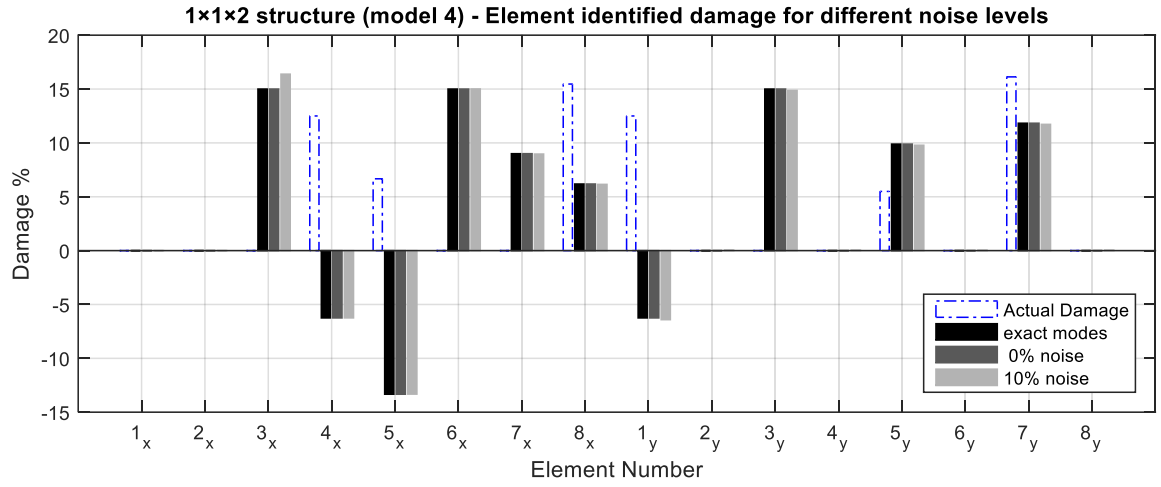

(a) model 4.

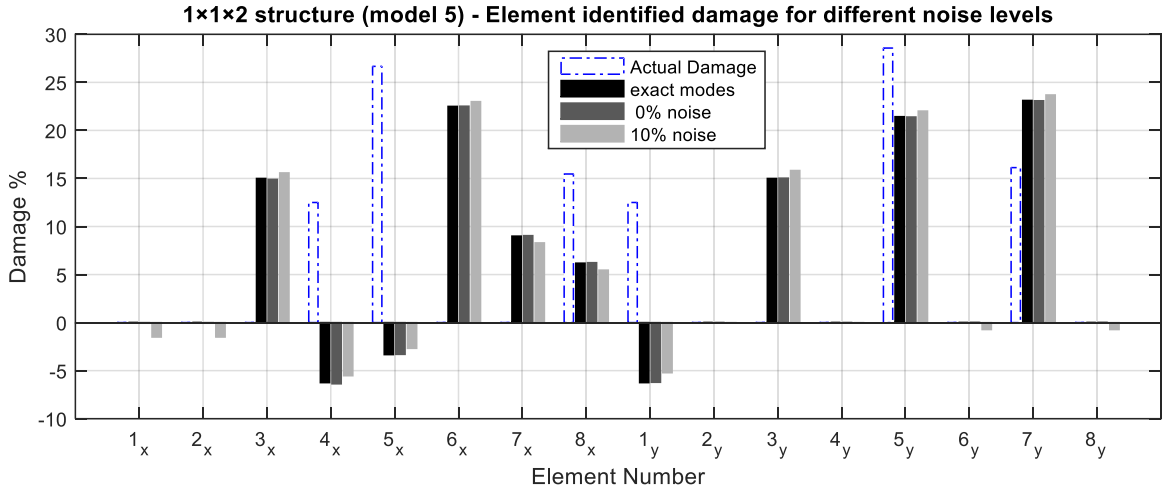

(b) model 5.

Figure 3.8 Damage identified for a 1-Bay×1-Bay×2-Stories frame structure, models (4) and (5)

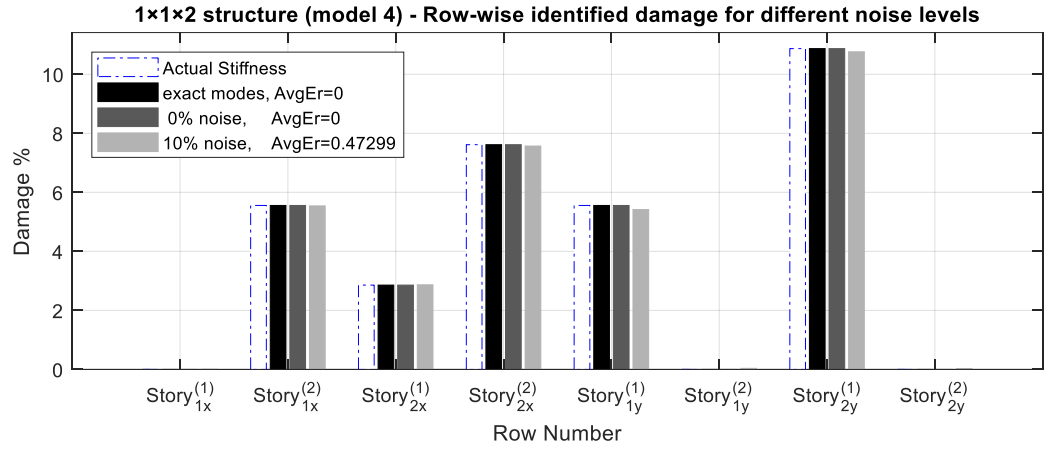

(a) model 4

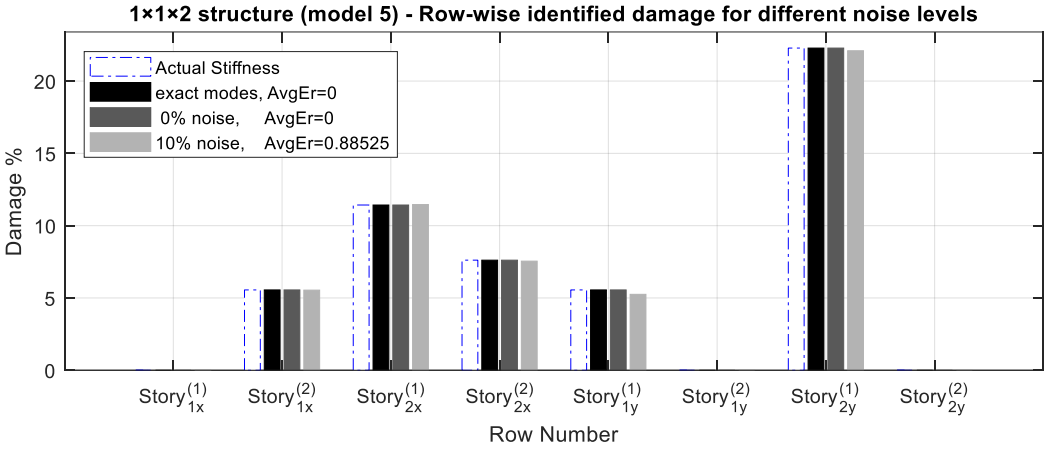

(b) model 5

Figure 3.9 Row-wise identified damage in both x- and y-directions for high damage levels.

Table 3.15 Damage identification errors in different column rows for model (4) and model (5).

		% Error					
Model		**Model IV**			**Model V**		
Stiffness direction	Story no.	signal noise level			signal noise level		
		Exact modes	**0% noise**	**10% noise**	**Exact modes**	**0% noise**	**10% noise**
1st story X	Row 1	0.00	0.00	0.00	0.00	0.00	0.00
	Row 2	0.00	0.00	-0.28	0.00	0.00	-0.24
2nd story X	Row 1	0.00	0.00	0.33	0.00	0.00	0.26
	Row 2	0.00	0.00	-0.61	0.00	0.00	-0.89
1st story Y	Row 1	0.00	0.00	-2.54	0.00	0.00	**-5.48**
	Row 2	0.00	0.00	0.00	0.00	0.00	0.00
2nd story Y	Row 1	0.00	0.00	0.00	0.00	0.00	0.00
	Row 2	0.00	0.00	0.03	0.00	0.00	-0.20

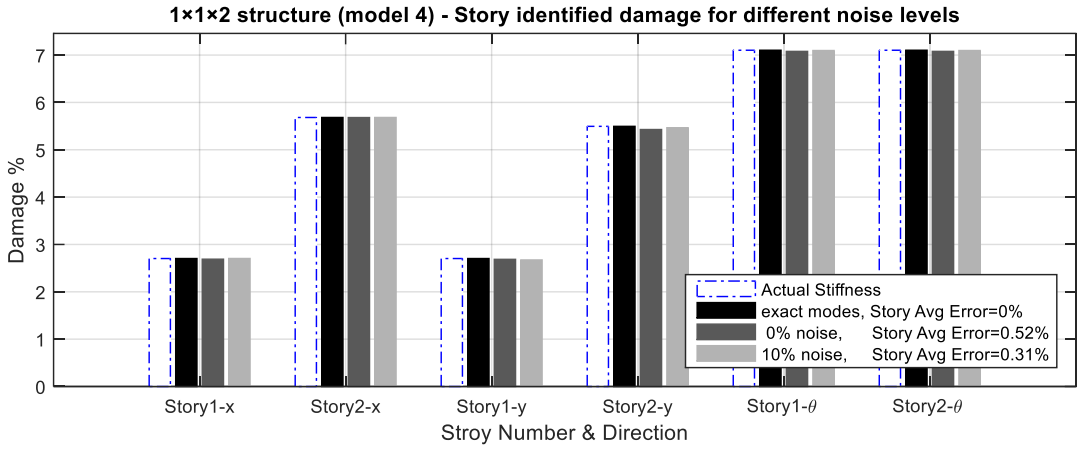

(a) model 4

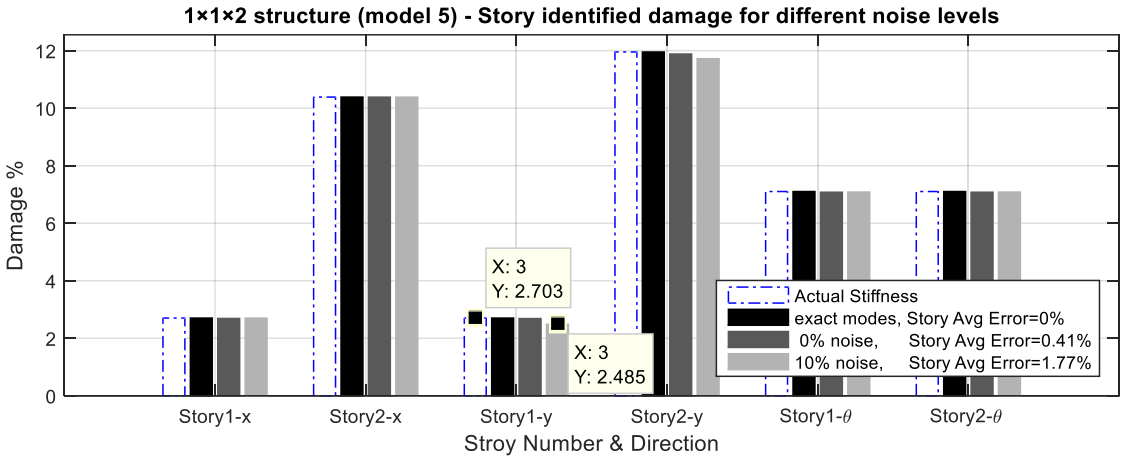

(b) model 5

Figure 3.10 Row-wise identified damage in both x- and y-directions for low damage levels.

Table 3.16 Story damage identification errors in the x- and y- directions for model (4) and model (5).

		% Error					
Model		**Model IV**			**Model V**		
Stiffness direction	Story no.	signal noise level			signal noise level		
		Exact modes	**0% noise**	**10% noise**	**Exact modes**	**0% noise**	**10% noise**
X-Stiffness	1st Story	0.00	-0.52	0.03	0.00	-0.52	-0.07
	2nd Story	0.00	-0.03	0.00	0.00	-0.02	-0.03
Y-Stiffness	1st Story	0.00	-0.64	-1.11	0.00	-0.64	**-8.06**
	2nd Story	0.00	-1.22	-0.54	0.00	-0.60	-1.94
θ-Stiffness	1st Story	0.00	-0.35	-0.09	0.00	-0.35	-0.26
	2nd Story	0.00	-0.35	-0.09	0.00	-0.35	-0.26

The story and column row damage identification errors are observed to be very small compared to the element-by-element damage identification. Moreover, in Tables 11 and 12, the error values are in general very low as well. We do observe one relatively high error

value (in the y-stiffness of the 1st story in model 5). This row damage also affects the damage in the same story, as shown in Table 12. However, the reason for this high error value is that the identified damage value is relatively low. A slight variation in the identified value can, thus, result in a high error. For this value in specific, the actual damage, as shown in Figure 3.10.b, is 2.703% while the identified damage is 2.485%. For all practical purposes, the identified value seems quite near the actual value but their percent difference is large.

3.5. Concluding Remarks

This chapter has focused on the application of the identification approach developed in Chapter 2 to 3-D shear beam models to examine its applicability and its limitations. A simplified model is used where the floor slabs are assumed to be rigid and supported by several columns. A similar model was used in the well-known ASCE Benchmark Problem study. An experimental study was also conducted with this model at the University of British Columbia in Canada for the purpose of generating data for structural health monitoring study. However, this data did not include any data for flexural strain which could be utilized for structural identification. In this study, thus, a simple but similar model has been used for which the flexural strain data providing time histories of strain at several locations on the structural elements was numerically generated. This numerically generated data with or without noise pollution has been used to identify the strain mode shapes and then system mode shapes. This modal information generated for several variations of the structural model has been used for system stiffness identifications by the proposed approach.

The numerical results generated for the stiffness identification of the supporting columns indicate that the approach can be effectively used to accurately identify the total story stiffness and the collective stiffness of a row of columns, even from highly polluted strain measurements (10% measurement noise). This stiffness identification is, of course, needed to identify damage or any change (reduction) in the stiffness that might have occurred from any earlier state of the structural system. Indeed, this approach was applied to identify the damage in the rows of columns and the whole story, and was found to be very successful. The approach was, however, not quite successful in identifying the individual column

element stiffness values and thus it will not be effective in the finer localization of the damage an individual column element.

4. Chapter4: Damage Identification using the Strain Flexibility

4.1. Introduction

The previous two chapters focused on the application of mode-based system identification and damage detection approach described in Chapter 2 to the frames and 3-D shear beam structures. In this Chapter we formulate a different strain flexibility based approach and test its applicability and limitations for the system and damage identification in the frame structures. The modal strain energy method has initially been proposed by Stubbs and his associates (1996)

The flexibility-based approach is also a global mode-based approach where we utilize the response and system mode shapes which are extracted from the measured response data. Among the global methods, there are basically two approaches. In the first approach, the measured response is directly used to estimate the damping and stiffness matrices of the system. For this, a norm of the difference between the calculated response (which depends upon the system matrices) and the measured response is minimized to estimate the elements of the system matrices. The least square estimation-based methods are most commonly used for this purpose. The second approach consists of extracting modal properties from the measured response, which are then used to estimate the changes in the system stiffness matrix. The use of the modal properties directly to obtain stiffness matrix is, however, very difficult as it needs the higher modes which are very difficult to extract from the measured response. On the other hand, the calculation of the flexibility matrix using only a first few modes is quite accurate as the contribution of the higher modes diminishes in inverse proportion to their frequency-squared values. In such methods therefore the flexibility matrix is commonly used for damage identification. A significant change in the flexibility signals indicates the presence of the damage (Bernal 2006; Duan et al. 2005; Gao & Spencer 2002; Pandey et al. 1991).

The localization of damage as well as its quantification can be facilitated if some localized measure of the flexibility of different structural elements is used. A significant change in this localized flexibility measure of a structural element then identifies the damage location. Duan et al. (2004) proposed the concept of rotational flexibility for better localization of the damage. This approach consists of applying a couple with equal and opposite forces at the ends of an element, and it thus measures the rotational tendency of the element on which the couple applied. It is not quite clear

how a couple is applied to a structural system, but this approach has been claimed to have helped in localization of the damage in the stories of a shear beam model of the structure (Duan, 2004).

A more element specific flexibility measure can be defined in terms of the element curvature flexibility. Since the damage in the structural elements is usually associated with the flexural deformations and the internal moments, localized curvature of the element can be a good measure of these quantities. Herein, therefore, we introduce the concept of curvature flexibility for damage localization as well as its quantification. Again we are focusing on the strain response measurement based approach. As mentioned earlier, the flexural strain response captures the effect of the member end rotations more directly than the commonly measured acceleration response. Also, since the measured flexural strain directly defines the localized curvature where the strain is measured the utilization of this measurement is expected to provide better information for damage identification which is primarily caused by excessive bending of structural elements.

4.2. Curvature Flexibility

For a structural member applied with a bending moment, the flexural strain e_x at a distance y from the neutral axis is directly related to its curvature ρ as $\epsilon_x = \rho y$. Since the strain is directly proportional to the curvature, herein the terms strain flexibility or curvature flexibility are interchangeably used. The strain flexibility with respect to a force applied at a point on the structure is thus defined as the level of strain caused by a unit force. For a structural system subjected to several forces, the measured strains at several different locations are related to the levels of deformation that are experienced by the structural members or structural elements. In a linear system, the strains ρ or curvatures at several locations of a structure can be simply defined in terms of the generalized system displacements u by the following equation:

$$\rho = Tu \tag{1}$$

In which T is a transformation matrix which relates the strain vector ρ to the generalized displacement vector at the system degrees of freedom u. Thus the flexibility matrix for strain or curvature, herein denoted as F_ρ, can be simply defined in terms of the flexibility matrix of the generalized displacement degrees of freedom, herein denoted as F_c, as follows:

$$F_\rho = TF_c \tag{2}$$

To define the strain flexibility associated with the measured strain response, we first extract the strain mode shapes and the system frequencies using the SSI algorithm. For the frame models in which the inertia-less rotation degrees of freedom are condensed out and only the linear degrees of freedom are kept, there are only as many significant modes as the kept degrees of freedom. Thus if the number of the kept degrees of freedom associated with the system's inertial masses is n_k, the number of extracted system frequencies and the strain modes will also be n_k. These strain mode shapes are used to obtain the structural system's mode shapes associated with the generalized degrees of the freedom using the following relationship:

$$\varphi_{\rho j} = T\varphi_{j,} \qquad j = 1, \dots, n_k \tag{3}$$

Where $\varphi_{\rho j}$ is the extracted j^{th} strain mode shape vector, φ_j is the j^{th} system mode shape vector and as mentioned earlier n_k is the number of the kept degrees of freedom associated with the system's inertial masses. The system mode shape vector φ_j is obtained by the mean square pseudo inversion of Eq. 3 as follows:

$$\varphi_j = T^+\varphi_{\rho j}, \qquad j = 1, \dots, n_k \tag{4}$$

wherein the pseudo inverse matrix is symbolically defined as:

$$T^+ = [T^T T]^{-1} T^T \tag{5}$$

In numerical calculations, this pseudo-inverse is not necessarily calculated by matrix inversions indicated in Eq. 5 but rather by effectively utilizing singular value decomposition of matrix T.

These extracted strain mode shapes as well calculated system mode shapes are utilized in the flexibility matrix calculations described below. However, before these modes are used in the flexibility matrix calculations, it is necessary that they both be normalized with respect to the system mass matrix. The factors calculated for the normalization of the system mode

shapes φ_j can also be used to normalize of the strain mode shapes which are directly extracted from the data by the SSI algorithm.

It is noted that the system eigen vector φ_j has all values associated with the kept as well as the reduced degrees of freedom. It is simple to show that the flexibility matrix associated with the force applications along the kept degrees of freedom can be obtained using the mass normalized modes associated as follows:

$$F_{kk} = \sum_{j=1}^{n_k} \frac{1}{\omega_j^2} \varphi_j^k \varphi_j^{k^T} \tag{6}$$

Where in φ_j^k is the upper part of the system mode shape φ_j associated only with the kept degrees of freedom. The flexibility matrix associated with the reduced degrees of freedom then can be defined in terms of F_{kk} as:

$$F_{rk} = -K_{rr}^{-1} K_{rk} F_{kk} \tag{7}$$

Using Eq. 6 and 7, the complete flexibility matrix associated with all generalized degrees of freedom is thus defined as:

$$[F_c] = \begin{bmatrix} F_{kk} \\ F_{rk} \end{bmatrix}, = \begin{bmatrix} F_{kk} \\ -K_{rr}^{-1} K_{rk} F_{kk} \end{bmatrix} = \begin{bmatrix} I \\ -K_{rr}^{-1} K_{rk} \end{bmatrix} F_{kk} \tag{8}$$

The complete flexibility F_c can also be expressed in terms of the full system mode shapes and the mode shapes associated with the kept degrees of freedom as:

$$F_c = \sum_{j=1}^{n_k} \frac{1}{\omega_j^2} \varphi_j \, \varphi_j^{k^T} \tag{9}$$

The strain flexibility can then be defined using Eq. 2 in terms of the strain and system mode shapes as follows:

$$F_\rho = T \sum_{j=1}^{n_k} \frac{1}{\omega_j^2} \varphi_j \, \varphi_j^{k^T} = \sum_{j=1}^{n_k} \frac{1}{\omega_j^2} \varphi_{\rho j} \, \varphi_j^{k^T} \tag{10}$$

The equation 10 now defines the strain flexibility matrix using the system frequencies, the strain mode shapes and the system mode shapes associated with the kept degrees of freedom. Both, the strain as well as system mode shapes are mass normalized.

For m number of strain measurements, the flexibility matrix F_ρ is of size $m \times n_k$. We will use this flexibility matrix to identify the stiffness coefficient values of the frame elements. If some of the extracted modes are suspected to be not very accurate, then it is quite acceptable to utilize only the contribution of those mode to this flexibility matrix. In the following we describe this identification approach.

Stiffness Identification

The system flexibility is a direct function of the stiffness values of the structural elements of the system. It is desired to obtain these system stiffness values such that the flexibilities associated with the strain response at the points of measurements are the same as the flexibility defined by Eq. 10. These flexibilities are a part of the total flexibility matrix defined as the inverse of the full stiffness matrix of the systems. To identify this relationship, consider a frame structure under a static loading scenario as:

$$K\,u = \mathrm{F} \tag{11}$$

The inverse of the stiffness matrix K defines the complete flexibility matrix of the system. However, considering the partitioning of the system degrees of freedom into the kept and the reduced degrees of freedom, and realizing that in a dynamic environment the force F will not have any component applied along the reduced degrees of freedom, we re-write this equation as:

$$\begin{bmatrix} K_{kk} & K_{kr} \\ K_{rk} & K_{rr} \end{bmatrix} \begin{Bmatrix} u_k \\ u_r \end{Bmatrix} = \begin{Bmatrix} f \\ 0 \end{Bmatrix} \tag{12}$$

where K_{kk}, K_{kr}, K_{rk} and K_{rr} are the sub stiffness matrices of the system stiffness matrix. To calculate the kept coordinates, this equation can be reduced to:

$$K^* u_k = f \tag{13}$$

where K^*, the condensed stiffness matrix, defined as

$$K^* = (K_{kk} - k_{kr}K_{rr}^{-1}K_{rk}) \tag{14}$$

The solution of Eq. 12 can also be expressed in terms of whole system flexibility $\mathcal{F}$ as:

$$\begin{Bmatrix} u_k \\ u_r \end{Bmatrix} = K^{-1}\begin{Bmatrix} f \\ 0 \end{Bmatrix} = \mathcal{F}\begin{Bmatrix} f \\ 0 \end{Bmatrix} = \begin{bmatrix} F_{kk} & F_{kr} \\ F_{rk} & F_{rr} \end{bmatrix}\begin{Bmatrix} f \\ 0 \end{Bmatrix} \tag{15}$$

where F_{kk}, F_{kr}, F_{rk}, and F_{rr} are submatrices of the full flexibility matrix $\mathcal{F}$. Eq. 15, thus, defines the flexibility sub matrices for both the kept and reduced degrees of freedom as follows:

$$u_k = F_{kk}f = [K^*]^{-1}f \tag{16}$$

$$u_r = F_{rk}f = -K_{rr}^{-1}K_{rk}[K^*]^{-1}f \tag{17}$$

For a unit force, Eqs. 16 and 17 can be used to define the combined flexibility matrix for the frame in terms of the element stiffness values as follows:

$$[F_c] = \begin{bmatrix} F_{kk} \\ F_{rk} \end{bmatrix} = \begin{bmatrix} K^{*-1} \\ -K_{rr}^{-1}K_{rk}[K^*]^{-1} \end{bmatrix} \tag{18}$$

Utilizing Eq. 2, we then define the strain flexibility matrix in terms of the system submatrices, and thus the element stiffness coefficients as below:

$$F_\rho = T\begin{bmatrix} I \\ -K_{rr}^{-1}K_{rk} \end{bmatrix}K^{*-1} \tag{19}$$

The objective of the identification approach is to choose the element stiffness coefficients such that strain flexibility matrix defined by Eq. 19 is as close to the flexibility matrix defined by Eq. 10 which is obtained from the measurement driven information on the system frequencies and the strain and system modes.

To achieve this objective, we expand the flexibility matrix defined by Eq. 10 in a Taylor series about a flexibility matrix which is close to this matrix as follows:

$$\left[F_\rho(k)\right] = \left[F_\rho(k^o)\right] + \left[\frac{\partial F_\rho}{\partial k_m}\right]\{\Delta k\}_k + \frac{1}{2}\{\Delta k\}_n^T\left[\frac{\partial^2 F_\rho}{\partial k_m \partial k_n}\right]\{\Delta k\}_m + \text{higher order terms} \tag{20}$$
$$(\Delta k = k - k^o)$$

where the $F_\rho(k)$ refer to the current flexibility matrix at the element stiffness values of k (which need to be determined), $F_\rho(k^o)$ is the flexibility matrix at the assumed element stiffness values of k^o, and Δk is the differential change in element stiffness. This expansion is done for each element of the flexibility matrix F_ρ. The 1st order and the 2nd order derivative matrices in Eq. 12 represent the gradient and Hessian of the curvature flexibility matrices. These derivative matrices are obtained by differentiating Eq. 12 with respect to an element stiffness coefficient. It can be shown that they are defined by the following two equations:

$$\frac{\partial F_\rho}{\partial k_m} = -T\mathcal{F}\frac{\partial K}{\partial k_m}F_c \tag{21}$$

$$\frac{\partial^2 F_\rho}{\partial k_m \partial k_n} = T\,\mathcal{F}\left(\frac{\partial K}{\partial k_n}\mathcal{F}\frac{\partial K}{\partial k_m} + \frac{\partial K}{\partial k_m}\mathcal{F}\frac{\partial K}{\partial k_n}\right)F_c \tag{22}$$

Eq. 20 is solved iteratively. It is first solved by omitting the second order term. The stiffness values obtained at this step are then used to calculate the second order term which is then used back in Eq. 20 to refine the previously calculated stiffness values. The process is repeated till a desired level of convergence is reached.

Eq. 20 with only the first order terms is:

$$\left[F_\rho(k)\right] = \left[F_\rho(k^o)\right] + \left[\frac{\partial F_\rho}{\partial k_m}\right]\{\Delta k\}_k \tag{23}$$

If the strain measurement are made at m location, the the flexibility $F_\rho(k)$ is (m by n_k) where n_k is the number of the kept degrees of freedom. To solve this equation, this flexibility matrix is reshaped in a vector form (of size $mn_k \times 1$). This also reshapes the 3rd order derivative tensor $\frac{\partial F_\rho}{\partial k}$ into a matrix of ($mn_k \times n_e$) where n_e is the number of element in the system whose stiffness values are to be identified. The reshaped first order equation is re-written as follows:

$$\left\{F_\rho\right\}_{\mathrm{m}n_k\times 1} = \left\{F_\rho^o\right\}_{\mathrm{m}n_k\times 1} + \left[\frac{\partial F_\rho}{\partial k}\right]_{\mathrm{m}n_k\times n_e}\{\Delta k\}_{n_e\times 1} \tag{24}$$

The change in stiffness Δk can be calculated using the pseudo-inversion as:

$$\{\Delta k\}_{n_e\times 1} = \left[\frac{\partial F_\rho}{\partial k}\right]^{+}_{\mathrm{m}n_k\times n_e} \left\{F_\rho - F_\rho^o\right\}_{\mathrm{m}n_k\times 1} \tag{25}$$

Note that the derivative matrix $\frac{\partial F_\rho}{\partial k}$ is defined at the assumed k^o values which are changed at each subsequent iterative step.

The improved stiffness values k from the first order equation are used to estimate the second order term which is then used in Eq. 20 to solve the revised first order equation as follows:

$$\{\Delta k\}_{n_e\times 1} = \left[\frac{\partial F_\rho}{\partial k}\right]^{+}_{n_e\times \mathrm{m}n_k} \left\{\left\{F_\rho - F_\rho^o\right\}_{\mathrm{m}n_k\times 1} - \frac{1}{2}\Delta k_i H_{\epsilon mij}\Delta k_j\right\}_{\mathrm{m}n_k\times 1} \tag{26}$$

The steps in Eqs. 25 and 26 are repeated till a desired level of convergence is reached.

The initial starting stiffness values k^o can be assumed to be equal to the nominal values used in the frame design. However, it may happen that in pseudo inversing process, some of these values may be higher than the initial assumed values. To avoid estimating overly high values, a starting upper bounding values can be established. Any stiffness value higher than this upper bounding value can be trimmed before a new pseudo inversing step is attempted. This upper bounding was seen to improve the identification and damage estimation in the results reported in Chapter 2, and thus it was also applied in this approach. The following equation shows this adjustment.

$$K_e^{identified} = \begin{cases} K_e^{intial}, & if\ K_e^{identified} > K_e^{intial} \\ K_e^{identified}, & otherwise \end{cases}$$

4.3. Numerical Study

We have tested the algorithm illustrated earlier on two moment resistant frame structures, a 1–bay × 4–stories structure (Figure 4.1a) and a 2–bay × 4–stories structure (Figure 4.2b). The first structure has 12 elements and 12 DOFs (4 translational and 8 rotational), while the second structure has 20 elements and 16 DOFs (4 translational and 12 rotational). Both of the structures are first tested for stiffness realization using the exact modal parameters of

the structure, then using the modal parameters identified from the measured dynamic response.

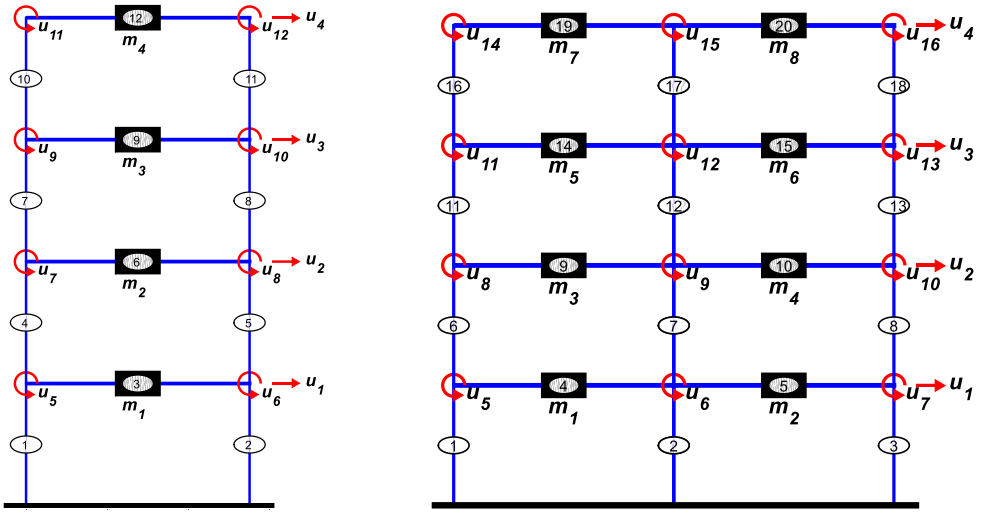

Figure 4.1 moment resistant frame structures (a) 1–bay × 4–stories, (b) 2–bays × 4–stories

We have these two test models for the 1–bay frame:

Model 1: Undamaged

Model 2: Damaged

However, for the 2–bays frame, we have the following six test models:

Model 1: Symmetric Undamaged

Model 2: Symmetric Damaged (Damage Scenario I)

Model 3: Symmetric Damaged (Damage Scenario II)

Model 4: Asymmetric Undamaged

Model 5: Asymmetric Damaged (Damage Scenario I)

Model 6: Asymmetric Damaged (Damage Scenario II)

Table 4.1 below presents the average error in the identified stiffness for all the 1-bay and 2-bays frames listed above, all using the exact modal parameters. The average error is defined as $Err_{avg} = \frac{1}{N_{elements}} \sum_{e=1}^{N_{elements}} \left| \frac{identified\ stiffness^{(e)}}{exact\ stiffness^{(e)}} - 1 \right|$

Table 4.1 Average error in identified stiffness using the exact modal parameters

Model	1-Bay Frame		2-Bays Frame					
	model 1	model 2	model 1	model 2	model 3	model 4	model 5	model 6
Avg Error	9.53E-16	4.39E-03	7.33E-16	4.85E-14	1.03E-13	9.69E-14	4.69E-15	1.02E-14

The almost-zero values shown in Table 4.1 demonstrate the accuracy of the curvature flexibility method. We then apply the same procedure for the same set of frames, however, using the identified modal parameters. These identified modal parameters are extracted from the measured dynamic response that, practically, may be polluted. Therefore, we have the measured dynamic response simulated at two levels of noise, 0% and 10%. Table 4.2 shows the average error in addition to the individual element error in stiffness identification.

Table 4.2 Average error and element-by-element error in identified stiffness using all of the identified modal parameters at 0% and 10% measurement noise

Element no.		1-Bay Frame				2-Bays Frame											
		model 1		model 2		model 1		model 2		model 3		model 4		model 5		model 6	
	noise	0%	10%	0%	10%	0%	10%	0%	10%	0%	10%	0%	10%	0%	10%	0%	10%
	Avg. Error	0.0072	0.0007	0.0043	0.0091	0.0093	**0.3527**	**0.2122**	0.0361	0.0466	0.0210	0.0364	**0.1810**	**0.1029**	**0.0526**	**0.0705**	0.0074
1	Element Stiffness Error	0.000	0.000	-0.001	-0.006	0.000	0.000	**-0.503**	**-0.085**	**-0.080**	0.017	**-0.088**	0.000	0.000	**-0.136**	**0.111**	-0.028
2		0.000	0.000	-0.003	-0.013	0.000	-0.026	0.011	-0.019	-0.007	-0.022	-0.005	-0.032	-0.016	-0.015	0.000	-0.025
3		-0.003	-0.002	-0.003	0.000	0.000	**-0.887**	0.000	0.000	**0.079**	**-0.049**	0.000	**-0.498**	**-0.174**	0.000	**-0.136**	-0.020
4		0.000	-0.002	-0.020	-0.006	-0.003	0.000	**-0.504**	**-0.066**	**-0.083**	0.037	**-0.097**	0.000	**0.176**	**-0.114**	**0.053**	0.003
5		0.000	-0.001	0.000	0.000	-0.003	**-0.869**	0.000	0.000	0.000	-0.029	0.000	**-0.447**	**-0.181**	0.000	**-0.133**	0.000
6		-0.002	0.000	-0.006	-0.002	-0.004	0.000	**-0.485**	**-0.052**	**-0.069**	0.000	**-0.076**	0.000	**0.053**	**-0.096**	0.000	0.000
7		0.000	-0.001	0.000	-0.019	-0.013	0.000	0.000	0.000	0.000	0.000	0.000	0.000	0.000	0.000	-0.006	0.000
8		0.000	-0.002	-0.012	-0.033	-0.004	**-0.854**	**0.111**	**0.083**	0.000	-0.014	0.000	**-0.421**	**-0.181**	**0.111**	**-0.143**	0.000
9		0.000	0.000	-0.006	-0.005	0.000	0.000	**-0.492**	**-0.064**	**-0.082**	0.039	**-0.094**	0.000	0.000	**-0.104**	**0.111**	0.009
10		-0.037	0.000	0.000	0.000	0.000	**-0.873**	0.000	0.000	0.000	-0.026	0.000	**-0.439**	**-0.190**	0.000	**-0.122**	0.000
11		-0.037	0.000	0.000	0.000	0.000	0.000	**-0.518**	**-0.073**	**-0.092**	0.026	**-0.101**	0.000	0.000	**-0.100**	**0.064**	0.003
12		-0.008	0.000	0.002	0.025	0.000	-0.021	-0.037	-0.013	-0.009	-0.015	-0.013	-0.012	0.018	-0.003	-0.004	-0.013
13						0.000	**-0.890**	0.031	0.031	0.000	-0.036	0.000	**-0.443**	**-0.195**	0.031	**-0.127**	0.000
14						0.000	0.000	**-0.504**	**-0.078**	**-0.079**	0.000	**-0.087**	0.000	0.000	**-0.112**	0.000	-0.008
15						0.000	**-0.890**	0.000	0.000	0.031	-0.039	0.000	**-0.455**	**-0.195**	0.000	**-0.129**	-0.009
16						-0.051	0.000	**-0.493**	**-0.064**	**-0.082**	0.000	**-0.084**	0.000	0.000	**-0.101**	0.000	0.000
17						**-0.040**	0.000	0.030	0.005	-0.004	0.000	0.000	0.000	-0.037	0.000	0.000	0.000
18						**-0.051**	**-0.873**	0.020	0.020	**0.076**	-0.025	0.000	**-0.435**	**-0.246**	0.020	**-0.116**	0.013
19						-0.009	0.000	**-0.505**	**-0.067**	**-0.076**	0.020	**-0.082**	0.000	**0.176**	**-0.108**	0.020	0.004
20						-0.009	**-0.871**	0.000	0.000	**0.083**	-0.024	0.000	**-0.437**	**-0.220**	0.000	**-0.135**	0.012

In Table 4.2, the single-bay frames have relatively low average error as well as the element-by-element error. However, for the multi-bays ones, the error is higher both on the average and for individual elements (elements with error > 4% are bolded). One explanation for this observation is the system rank indeterminacy. For the multi-bay frames, the number of unknown elements is greater than the number of measured DOFs. On contrary, a single bay

structure has a number of elements equal to the number of its DOFs. This would affect the pseudo-inverse process of the derivative matrix $\frac{\partial F_\rho}{\partial k}$ in Eqs. 25 and 26.

On the other hand, the first identified mode is predominantly the most accurate compared to the higher modes. In addition, the flexibility matrix can be constructed using one single mode. Therefore, we attempt to use the first mode alone to construct the flexibility matrix, which seems to be sensitive to the inaccuracies in the identified higher modes. Table 4.3 below shows the average error as well as the individual element error in stiffness identification using only the first identified mode.

Table 4.3 Average error and element-by-element error in identified stiffness using only the first identified mode at 0% and 10% measurement noise

Element no.		1-Bay Frame				2-Bays Frame											
		model 1		model 2		model 1		model 2		model 3		model 4		model 5		model 6	
	noise	0%	10%	0%	10%	0%	10%	0%	10%	0%	10%	0%	10%	0%	10%	0%	10%
	Avg. Error	0.014	0.000	0.005	0.004	0.019	0.002	0.018	0.011	0.022	0.022	0.003	0.001	0.027	0.011	0.022	0.021
1	Element Stiffness Error	0.000	0.000	-0.002	0.000	-0.010	-0.002	0.000	0.000	**-0.044**	-0.038	0.000	-0.001	0.000	0.000	-0.023	-0.030
2		0.000	0.000	-0.001	-0.006	0.000	-0.003	**-0.041**	-0.013	0.000	0.000	-0.007	-0.002	-0.002	-0.012	0.000	0.000
3		-0.003	0.000	-0.003	0.000	-0.010	-0.002	0.000	-0.022	-0.015	-0.008	0.000	-0.002	-0.026	-0.025	-0.002	-0.012
4		0.000	0.000	-0.017	-0.025	-0.003	-0.002	-0.008	-0.003	0.007	0.006	-0.004	-0.001	0.000	0.002	0.008	0.007
5		0.000	0.000	0.000	0.000	-0.003	-0.002	-0.015	-0.016	-0.004	-0.006	0.000	-0.001	-0.018	-0.016	-0.007	-0.005
6		-0.003	0.000	-0.006	-0.002	0.000	-0.002	0.014	0.004	0.000	0.000	0.000	-0.001	0.017	0.004	0.000	0.000
7		0.000	0.000	0.000	0.000	-0.022	-0.002	0.000	0.000	0.000	-0.002	0.000	-0.001	-0.006	0.000	0.000	-0.001
8		0.000	0.000	-0.010	-0.007	0.000	-0.002	-0.009	-0.026	-0.007	-0.029	0.000	-0.002	-0.006	-0.022	**-0.054**	-0.027
9		0.000	0.000	-0.011	0.000	0.000	-0.002	0.000	0.000	0.023	0.019	-0.002	-0.001	-0.001	0.000	0.018	0.023
10		-0.073	0.000	0.000	0.000	0.000	-0.002	0.000	-0.001	-0.022	-0.026	0.000	-0.001	-0.001	0.000	-0.020	-0.024
11		-0.073	0.000	0.000	0.000	0.000	-0.002	**-0.051**	-0.013	0.005	0.019	-0.016	-0.001	-0.010	-0.009	0.031	0.018
12		-0.021	0.000	0.010	-0.003	0.000	-0.002	**-0.055**	-0.006	-0.006	-0.001	-0.016	-0.001	0.032	-0.005	-0.013	0.000
13						0.000	-0.002	-0.028	0.011	-0.032	-0.022	-0.011	-0.001	0.008	0.010	-0.010	-0.018
14						0.000	-0.002	-0.018	-0.005	0.000	0.000	0.000	-0.001	0.000	-0.004	0.000	0.000
15						0.000	-0.002	-0.008	0.000	-0.010	-0.009	-0.009	-0.001	0.000	0.000	-0.015	-0.010
16						**-0.108**	-0.001	0.000	0.000	**-0.078**	**-0.066**	0.000	-0.001	**-0.069**	0.000	0.000	**-0.063**
17						**-0.070**	-0.002	**0.045**	-0.015	-0.006	-0.001	0.000	-0.001	**-0.104**	-0.014	0.000	0.000
18						**-0.108**	-0.001	0.020	-0.038	**0.055**	**0.068**	0.000	-0.001	**-0.169**	-0.037	**0.111**	**0.060**
19						-0.022	-0.002	0.035	0.018	**-0.074**	**-0.069**	0.000	-0.001	-0.002	0.025	**-0.052**	**-0.067**
20						-0.022	-0.002	-0.012	-0.036	**0.055**	**0.059**	0.000	-0.001	**-0.075**	-0.035	**0.072**	**0.051**

Comparing the error results in Table 4.2 and Table 4.3, we can consider that using the first mode alone to identify the stiffness is more accurate than using all of the modes together.

However, we should note that the flexibility matrix constructed using a single mode is rank deficient if the system is indeterminate, (the number of DOFs is less than the number of elements, which is the multi-bay problem). For instance, the flexibility matrix derivative of a 2–bays × 4–stories frame has the size 20×160. However, using one mode to construct it; it

will have a rank 16 rather than 20 when using all of the modes. Therefore, we attempted to balance the number of elements to the number of DOFs for the multi-bays frames to get a full rank matrix. We assume knowledge of the stiffness of a few number of elements (4 in our example) so that the remaining number of elements is equal to the number of DOF (16 in our example). We did randomly select a set of the undamaged elements in a sense that the remaining elements provide a full-rank flexibility derivative matrix $\frac{\partial F_\epsilon}{\partial k}$. The stiffness identification error in this new attempt is presented in Table 4.4 (note that the 1-Bay frame results are the same since they have no rank deficiency problem).

Table 4.4 Average error and element-by-element error in identified stiffness using only the first identified mode at 0% and 10% measurement noise – with reduced number of unknown elements

Element no.		1-Bay Frame				2-Bays Frame											
		model 1		model 2		model 1		model 2		model 3		model 4		model 5		model 6	
	noise	0%	10%	0%	10%	0%	10%	0%	10%	0%	10%	0%	10%	0%	10%	0%	10%
	Avg. Error	0.014	0.000	0.005	0.004	0.012	0.002	0.024	0.016	0.031	0.030	0.003	0.001	0.025	0.016	0.028	0.029
1	Element Stiffness Error	0.000	0.000	-0.002	0.000	-0.008	-0.002	0.000	0.000	-0.028	-0.025	0.000	-0.001	0.000	0.000	-0.012	-0.018
2		0.000	0.000	-0.001	-0.006	0.000	-0.003	**-0.048**	-0.013	-0.003	0.000	-0.007	-0.002	-0.005	-0.012	-0.003	0.000
3		-0.003	0.000	-0.003	0.000	0.000	0.000	0.000	0.000	**0.176**	**0.176**	0.000	0.000	0.000	0.000	**0.176**	**0.176**
4		0.000	0.000	-0.017	-0.025	-0.003	-0.002	0.004	0.010	0.009	0.009	-0.004	-0.001	0.012	0.014	0.011	0.011
5		0.000	0.000	0.000	0.000	-0.003	-0.002	-0.009	-0.012	-0.007	-0.009	0.000	-0.001	-0.013	-0.012	-0.010	-0.008
6		-0.003	0.000	-0.006	-0.002	0.000	-0.002	0.016	0.009	0.000	0.000	0.000	-0.001	0.020	0.008	0.000	0.000
7		0.000	0.000	0.000	0.000	-0.020	-0.002	0.000	-0.001	0.000	-0.006	0.000	-0.001	-0.006	0.000	-0.003	-0.005
8		0.000	0.000	-0.010	-0.007	0.000	0.000	**0.111**	**0.111**	0.000	0.000	0.000	0.000	**0.111**	**0.111**	0.000	0.000
9		0.000	0.000	-0.011	0.000	0.000	-0.002	0.000	0.000	0.024	0.022	-0.002	-0.001	0.000	0.000	0.021	0.025
10		-0.073	0.000	0.000	0.000	0.000	-0.002	-0.005	-0.006	-0.019	-0.023	0.000	-0.001	-0.003	-0.005	-0.018	-0.021
11		-0.073	0.000	0.000	0.000	0.000	-0.002	**-0.051**	-0.015	0.006	0.020	-0.016	-0.001	-0.009	-0.011	0.030	0.018
12		-0.021	0.000	0.010	-0.003	0.000	-0.002	**-0.046**	-0.001	-0.009	-0.003	-0.016	-0.001	0.032	-0.001	-0.015	-0.002
13						0.000	0.000	0.031	0.031	0.000	0.000	0.000	0.000	0.031	0.031	0.000	0.000
14						0.000	-0.002	-0.026	-0.016	0.000	0.000	0.000	-0.001	-0.009	-0.015	0.000	0.000
15						0.000	-0.002	-0.014	-0.008	-0.011	-0.010	-0.009	-0.001	0.000	-0.007	-0.015	-0.011
16						**-0.096**	-0.001	0.000	0.000	**-0.079**	**-0.067**	0.000	-0.001	**-0.062**	0.000	-0.004	**-0.065**
17						**-0.064**	-0.002	**0.050**	-0.001	-0.006	-0.001	0.000	-0.001	**-0.064**	0.000	0.000	0.000
18						0.000	0.000	0.020	0.020	**0.111**	**0.111**	0.000	0.000	0.020	0.020	0.111	**0.111**
19						-0.020	-0.002	**0.042**	0.033	**-0.064**	**-0.060**	0.000	-0.001	0.030	0.038	**-0.044**	**-0.057**
20						-0.020	-0.002	-0.005	-0.032	**0.065**	**0.067**	0.000	-0.001	**-0.067**	-0.031	**0.078**	**0.060**

The results shown in Table 4.4 provide an unnoticeable improvement to the accuracy. For a comprehensive look at the results, Table 4.5 presents the average errors only, collected from Table 4.2, Table 4.3, and Table 4.4.

To conclude the tabulated results in Table 4.1-Table 4.5 above, it is observed that stiffness identification using the 1st mode alone is more accurate for the multi-bay structures. However, for the single-bay ones, both solutions using all modes or the first mode alone are comparable. Therefore, in the following section, we run damage identification for the single

Table 4.5 Average error in identified stiffness From Tables 2, 3, and 4

		1-Bay Frame				2-Bays Frame											
		model 1		model 2		model 1		model 2		model 3		model 4		model 5		model 6	
noise		0%	10%	0%	10%	0%	10%	0%	10%	0%	10%	0%	10%	0%	10%	0%	10%
Avg Error	All modes	0.007	0.001	0.004	0.009	0.009	0.353	0.212	0.036	0.047	0.021	0.036	0.181	0.103	0.053	0.070	0.007
	Mode 1/20E	0.014	0.000	0.005	0.004	0.019	0.002	0.018	0.011	0.022	0.022	0.003	0.001	0.027	0.011	0.022	0.021
	Mode 1/16E					0.012	0.002	0.024	0.016	0.031	0.030	0.003	0.001	0.025	0.016	0.028	0.029

bay structures using both the first mode and all-modes while, for the multi-bay structures, using the first mode only.

Damage Identification

The previously discussed results show the identified stiffness of the structure at a specific state. However, health monitoring requires damage identification which, in turn, requires the awareness of multiple states in order to monitor the deterioration of the structure. Therfore, in this section, we identify the damage in the structure by considering the identified stiffness at two states, an intial undamaged state and a final damaged one. The

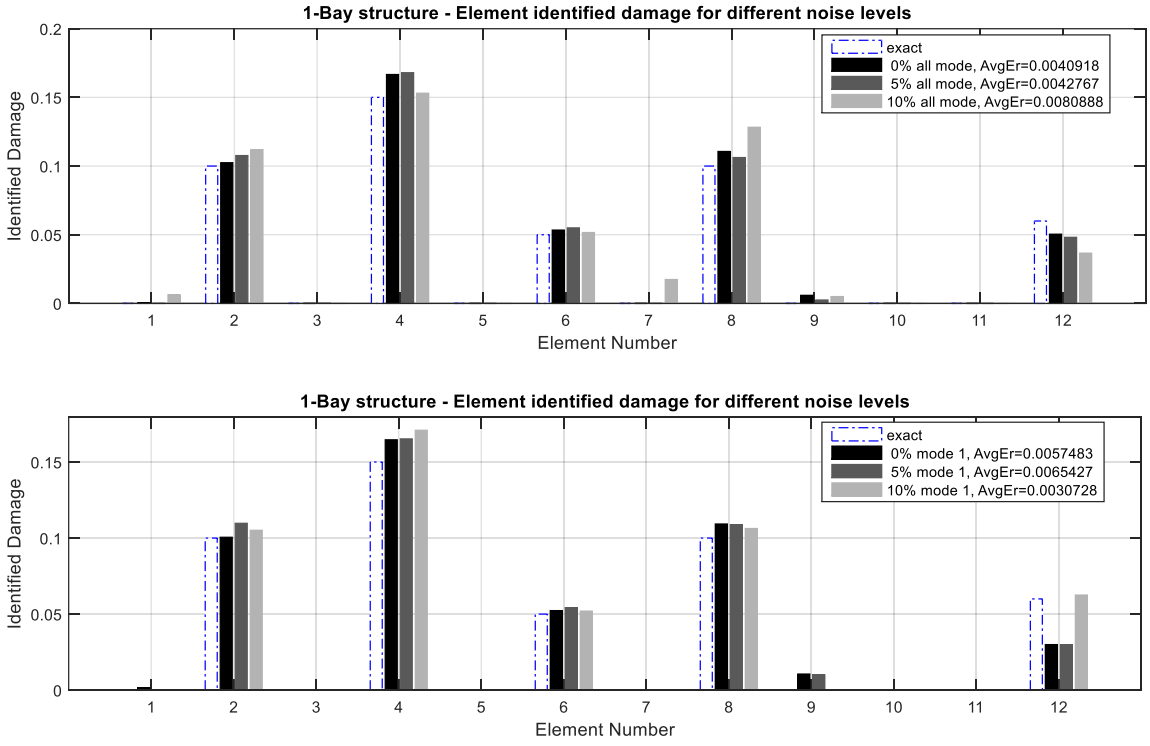

Figure 4.2 Identified damage at 3 different mesurement noise levels (0%, 5%, and 10%) for a 1-Bay × 4-Story frame structure using (a) all modes, and (b) the first mode only

damage is claculated as the difference in stiffness between both of the states. The bar plots in Figure 4.2a, b and Figure 4.3a-d below show the identified damage for three different noise levels (0%, 5%, and 10%) in comparison to the exact damage. Figure 4.2 present the damage identifictaion results for the 1-Bay frame using, (a) all identified mode shapes and frequencies, and (b) only the first identified mode shape, to identify the damage. Figure 4.3 show the damage identifictaion results for the 2-Bay frame with its 4 models (Models 2, 3, 5, and 6), however, using only the first identified frequency and mode shape.

The results in Figure 4.2 for the 1-Bay×4-Stories structure show a relatively low error compared to the multi-bay structures presented in Figure 4.3. The stiffness identification error rises with increasing the mesurement nosie. An average error of 0.41% for the 0% noise is the lowest, then 0.43% for 5% noise and 0.81% for 10% noise. Next, we identify the damage for the multi-bay frame structures, which is a little different form the one-bay ones in terms of the identifocation error.

The damage of four multi-bay models is identified and presented in Figure 4.3. For these models, the average identification error is generally higher than the single-bay ones. However, the error in stiffness identifictaion appears to be indpendent of the meansurement noise level. For instance, the identifictaion error in models 2 and 5 (Figure 4.3a and c) slightly decreases with increasing the measurement noise. However, for models 3 and 6 (Figure 4.3b and d) fluctuates up then down with increasing the measurement noise level. In addition, we can observe that the identifictaion error increases at the upper stories. The last five elements (the 4th story) have the largest errors compared to the previous elements for all models, followed by the 3rd story, and so on. This could be encouraging since the lower elements are the most critical and susciptible to damage.

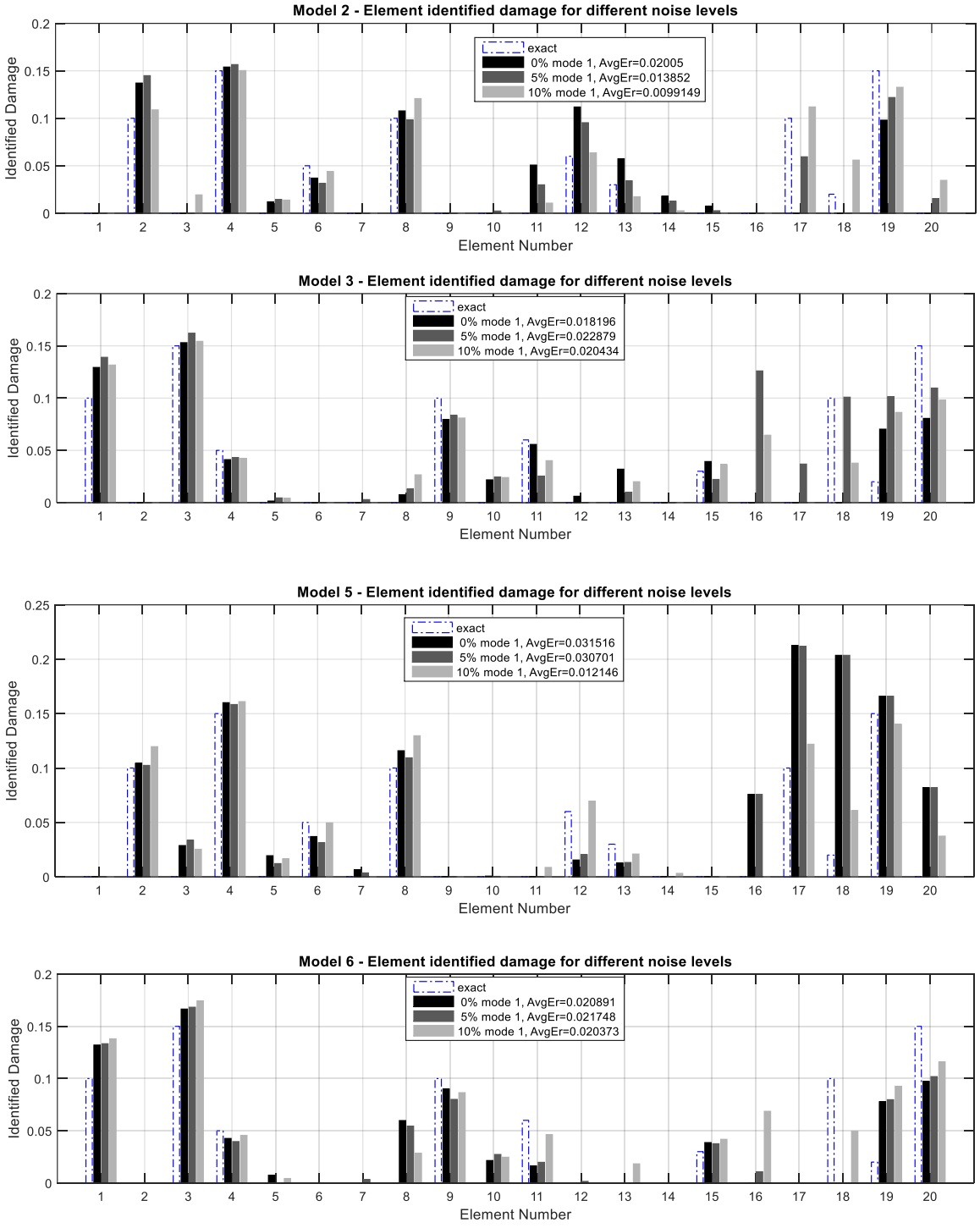

Figure 4.3 Identified damage at 3 different noise levels (0%, 5%, and 10%) using the first identified mode for: (a) model 2, (b) model 3, (c) model 5, and (d) model 6.

4.4. Conclusion

In this study, we use a flexibility-based approach to identify damage in frame structures. The main advantage of using this approach is its ability to identify the stiffness of the structure using limited number of frequencies and mode shapes. It can work using as little as one single mode and frequency. This advantage is effective in situations where the higher modes are not easily identifiable or are highly polluted by the noise that affect the measured dynamic response. However, it is observed that this stiffness identification approach is very sensitive to the inaccuracies collateral to the identification of the structure modal parameters, and that it provides lower stiffness identification accuracy compared to the earlier approach that utilizes the Eigen equation. Therefore, we recommend applying it in the above-mentioned situations where only limited number of lower modes are available.

In order to examine the effectiveness of this approach, we first applied it using the exact mode shapes and frequencies of the structure. This provided an exact solution. However, when using the modes and frequencies identified from the measured dynamic response of the structure, error has obviously risen. The level of this error varies depending on the configuration of the structure itself. For instance, the average error in damage identification in the elements of a single-bay frame structures does not exceed 0.0091 (0.91%). Such structures have a number of elements that are equal to the number of degrees of freedom of the structure. Other structure configurations, like the multi-bays frame structures in our numerical studies, have the number of unknown elements greater than the number of degrees of freedom. Such configurations provide higher error levels in stiffness identification. The average identification error in the structure element stiffness may reach as high as 0.35 (35%). However, the aforementioned results are obtained while including the full number of identified modes into the analysis, which include the higher order polluted modes. Utilizing only the first identified mode, which is the most accurate, in the stiffness identification has provided a significant enhancement to the accuracy of the results. With the first mode alone utilized in identification, the average error in the structure elements' stiffness drops to considerably lower levels. The average error level in this case does not exceed 0.027 (2.7%) for multi-bay structures and 0.014 (1.4%) for single-bay structures.

In other words, the identification error depends primarily on two factors, the structure configuration and the mode selection. Structures where the number of unknown elements is greater than the degrees of freedom contained in this structure, this structure is expected to provide higher error levels than those with balanced number of elements and degrees of freedom. In addition, especially for the structures with number of elements greater than the number of degrees of freedom, including several identified modes together augment the identification inaccuracies. However, the accuracy level remains acceptable for the other balanced structure configuration.

5. Chapter5: Sensitivity Analysis-Based Optimal Sensor Placement

5.1. Introduction

For a precise application of Structural Health Monitoring (SHM), there is a crucial demand for a careful and optimized placement of sensors around the structure. The optimum placement aims to both minimize the number of sensors, which reduces the sensor installation cost as well as the data processing effort, and maximize the accuracy of damage identification. This optimization accounts for several constraints whether they are particular to the structure or generally related to the model. The structure-specific constraints are field related, and will not be considered in our study. Examples of such parameters are the cost of installing and running the sensing system and the cost of unnecessary inspections caused due to miss-diagnosing the problem. Such a high-level of consequence assessment impacted by the optimal sensor installation and damage identification is beyond the scope of this research. In this research, we are concerned about the common parameters that are common and globally fit to all problem configurations.

The objective of the current study is to optimally place the sensors such that they provide data that is sufficiently accurate for damage identification. In the context of this research, we will identify the locations where a given number of sensors should be placed for best damage identification. For an optimal placement for a chosen set of sensors, we propose an approach that evaluates the sensitivity of each sensor w.r.t. the change in stiffness occurring in every element in the structure. Following this approach, we can favor the sensor selection based on their sensitivity to damage.

In this study, we determine the derivative of the strain response w.r.t. the change in the stiffness of the structural elements. We then use the mean square values of this derivative as a measure for its sensitivity to damage.

5.2. Problem Formulation

Consider the dynamics of a structural system,

$$M\ddot{x} + C\dot{x} + Kx = -Mr\ddot{x}_g(t) \quad (1)$$

where the matrices *M, C, K* are the mass, damping, and stiffness matrices respectively. The system expressed by Eq. 1 is a 2D frame structure that is described in details in Chapter 2. This frame structure is composed of interconnected 1D elements, aligned vertically and horizontally as columns and beams, through rigid joint. The frame elements are assumed massless, while the structure mass is concentrated in the structure floors and, hence, attached to the horizontal elements (beams) in the frame. The variable *x* in Eq. 1 represents the degrees of freedom of the system, which are the displacements of the floors and the rotations of the joints that connect the columns.

Assuming that we are capable of obtaining the measurements of a few quantities at several locations in the system, the question is: which one of them is the most sensitive to the change in the strength of this structure as represented in the stiffness of its elements. In practice, we are able to measure quantities like acceleration, displacement, and strain in limited locations around the structure. In order to favor one of these measures to the others, we need to understand how each of them responds to any change in the structure's stiffness. In other words, obtaining the rate of change of a measured quantity w.r.t. the stiffness of the structural elements, this reflects the sensitivity of this quantity to any damage happening in those structural elements. This provides a criterion to optimally position the measuring sensors around the structure. One approach to obtain the rate of change of these quantities is explained in this section.

We first set a dynamical system that describes the derivatives of the measured quantities. Differentiating the physical system described by Eq. 1 w.r.t. the element stiffness values $\left(\frac{d}{dk_e}\right)$ (under the assumption that the mass and damping properties are independent of the element stiffness values), this provides the following dynamical system,

$$M\ddot{x}' + C\dot{x}' + Kx' = -\frac{\partial K}{\partial k_e}x \quad (2)$$

Eq. 2 describes a new dynamical system, its unknown is the derivative of the measuring quantity (x'). This means that this equation applies for the acceleration derivative, the displacement derivative, and the strain derivative.

Our objective is to evaluate the sensitivity of the three measuring quantity mentioned earlier, applied in the measuring locations of concern around the structure, w.r.t. the change in stiffness in every element in the frame. For this objective, we will use the mean square values of the response derivatives to assess the strength of the response of each sensor. These mean square values can be provided using the autocorrelation function at zero time-shift $\left(R_{\ddot{x}'\ddot{x}'}(0), R_{x'x'}(0), R_{\varepsilon'\varepsilon'}(0)\right)$. However, a sort of normalization is required so that the derivatives of the three measures are consistent. Therefore, we normalize the derivatives of the quantities w.r.t. the mean square values of the physical quantities themselves, i.e.,

$$\text{Normalized Sensitivity of acceleration} = \frac{R_{\ddot{x}'\ddot{x}'}(0)}{R_{\ddot{x}\ddot{x}}(0)} \tag{3.a}$$

$$\text{Normalized Sensitivity of displacement} = \frac{R_{x'x'}(0)}{R_{xx}(0)} \tag{3.b}$$

$$\text{Normalized Sensitivity of strain} = \frac{R_{\varepsilon'\varepsilon'}(0)}{R_{\varepsilon\varepsilon}(0)} \tag{3.c}$$

Each of the three terms obtained in Eq. 3 represents the normalized sensitivity of one of the three measures; acceleration, displacement, and strain.

5.3. Mean square values of the measured response quantities of the structure

In this section, we will obtain the mean square values of the measures and their derivatives. We first map the dynamic systems in Eq. 1 and Eq. 2 using the new modal coordinates (q, p) defined as:

$$x = \Phi q \tag{4.a}$$

$$x' = \Phi p \tag{4.b}$$

With this coordinate transformation, we can express the dynamic system in Eq. 1 as:

$$\ddot{q}_j + 2\beta_j\omega_j\dot{q}_j + \omega_j^2 q_j = -\gamma\ddot{x}_g \tag{5.a}$$

while the dynamic system of the derivatives described in Eq. 2 can be expressed as:

$$\ddot{p}_j + 2\beta_j\omega_j\dot{p}_j + \omega_j^2 p_j = G_j^T q \tag{5.b}$$

where,

$$\gamma = \phi_j^T M r \tag{5.c}$$

$$G_j^T = \phi_j^T (K_{kr}K_{rr}^{-1}A_L - A_U)\Phi \tag{5.d}$$

$$A^{(e)} = \begin{Bmatrix} A_U \\ A_L \end{Bmatrix} = \frac{\partial K}{\partial k_e} J \tag{5.f}$$

$$J = \begin{bmatrix} I \\ -K_{rr}^{-1}K_{rk} \end{bmatrix} \tag{5.g}$$

In order to obtain the mean square values of the three quantities (acceleration, displacement, and strain) and their derivatives, we need to obtain their correlation functions. The correlation functions for the three quantities in terms of the modal coordinates (q) are:

$$R_{\ddot{x}\ddot{x}}(\tau) = \Phi R_{\ddot{q}\ddot{q}}(\tau)\Phi^T \tag{6.a}$$

$$R_{xx}(\tau) = \Phi R_{qq}(\tau)\Phi^T \tag{6.b}$$

$$R_{\varepsilon\varepsilon}(\tau) = [T_E J] R_{xx}(\tau)[T_E J]^T \tag{6.c}$$

The correlation functions for the quantities' derivatives; the rate of change of: the acceleration $\ddot{x}'$, the displacement x', and the strain ε' in terms of the modal coordinates 'p' are,

$$R_{\ddot{x}'\ddot{x}'}(\tau) = \Phi R_{\ddot{p}\ddot{p}}(\tau)\Phi^T \tag{7.a}$$

$$R_{x'x'}(\tau) = \Phi R_{pp}(\tau)\Phi^T \tag{7.b}$$

$$R_{\varepsilon'\varepsilon'}(\tau) = D_p R_{pp}(\tau)D_P^T + D_p R_{pq}(\tau)D_q^T + D_q R_{qp}(\tau)D_P^T + D_q R_{qq}(\tau)D_q^T \tag{7.c}$$

where,

$$D_p = T_{strain} J \Phi \tag{7.d}$$

$$D_q = T_{strain}\begin{bmatrix} O \\ -K_{rr}^{-1}A_L \end{bmatrix}\Phi \tag{7.e}$$

Obtaining the mean square values of the measures and their derivatives, represented in their zero-shift correlation functions, requires obtaining the mean square values of the corresponding modal coordinates as described in Eq. 6 and 7. In order to obtain these quantities, we first consider the random process of the exciting seismic acceleration (ground excitation) $\ddot{x}_g$, which we can obtain its autocorrelation function $R_{\ddot{x}_g\ddot{x}_g}(\tau)$. This autocorrelation function is related to the autocorrelations of the modal coordinates $R_{qq}(\tau)$ and $R_{pp}(\tau)$ through Eq. 5.a and Eq. 5.b. With further analysis, the autocorrelation functions of these modal quantities, which provide their mean square values, and their derivatives can be obtained as follows,

$$R_{\ddot{p}_j\ddot{p}_k}(\tau) = \sum_m \sum_n G_{jm}G_{kn} \int_{-\infty}^{\infty} \gamma_m\gamma_n\omega^4 e^{i\omega\tau}\Phi_g(\omega)H_j(\omega)H_k^*(\omega)H_m(\omega)H_n^*(\omega)d\omega \tag{8.a}$$

$$R_{p_jp_k}(\tau) = \sum_m \sum_n G_{jm}G_{kn} \int_{-\infty}^{\infty} \gamma_m\gamma_n e^{i\omega\tau}\Phi_g(\omega)H_j(\omega)H_k^*(\omega)H_m(\omega)H_n^*(\omega)d\omega \tag{8.b}$$

$$R_{p_jq_k}(\tau) = \sum_m G_{jm} \int_{-\infty}^{\infty} \gamma_m\gamma_k e^{i\omega\tau}\Phi_g(\omega)H_j(\omega)H_k^*(\omega)H_m(\omega)d\omega \tag{8.c}$$

$$R_{q_j p_k}(\tau) = \sum_m G_{km} \int_{-\infty}^{\infty} \gamma_j \gamma_m e^{i\omega\tau} \Phi_g(\omega) H_j(\omega) H_k^*(\omega) H_m^*(\omega) d\omega \tag{8.d}$$

$$R_{q_j q_k}(\tau) = \int_{-\infty}^{\infty} \gamma_j \gamma_k e^{i\omega\tau} \Phi_g(\omega) H_j(\omega) H_k^*(\omega) d\omega \tag{8.e}$$

$$R_{A\ddot{q}_j \ddot{q}_k}(\tau) = \int_{-\infty}^{\infty} \gamma_j \gamma_k e^{i\omega\tau} \Phi_g\left(\omega_j^2 + 2i\beta_j\omega_j\omega\right)\left(\omega_k^2 - 2i\beta_k\omega_k\omega\right)(\omega) H_j(\omega) H_k^*(\omega) d\omega \tag{8.f}$$

$$R_{\ddot{q}_j \ddot{q}_k}(\tau) = \int_{-\infty}^{\infty} \gamma_j \gamma_k \omega^4 e^{i\omega\tau} \Phi_g(\omega) H_j(\omega) H_k^*(\omega) d\omega \tag{8.g}$$

where:

$$H_j(\omega) = \frac{1}{\left(\omega_j^2 - \omega^2\right) + 2i\beta_j\omega_j} \tag{9.a}$$

$$\Phi_g(\omega) = \frac{\Phi_g^{(N)}}{\Phi_g^{(D)} \Phi_g^{(D)*}} \tag{9.b}$$

$$\Phi_g^{(N)} = S^2\left(4\beta_g^2\omega_g^2\omega^2 + \omega_g^4\right) \tag{9.c}$$

$$\Phi_g^{(D)} = -\omega^2 + 2i\beta_g\omega_g\omega + \omega_g^2 \tag{9.d}$$

$$\Phi_g^{(D)*} = -\omega^2 - 2i\beta_g\omega_g\omega + \omega_g^2 \tag{9.e}$$

where $\Phi_g(\omega)$ in Eq. 9.b is the spectral density function of the exciting seismic acceleration. The site dominant frequency ω_g, damping β_g, and power spectral intensity S^2 are taken according to the Kanai-Tajimi model to be 18.85 rad/s, 0.65 and 38.3 $\times$ 10^{-4} $m^2/s^3/rad$, respectively (Lin and Yong 1986).

The complex integrands in Eq. 8 consist of conjugates of poles and zeros. They can be obtained using the method of residues. Consider, for example, $R_{\ddot{p}_j\ddot{p}_k}(0)$ in Eq. 8.a which we can present in the form,

$$R_{\ddot{p}_j\ddot{p}_k}(0) = \sum_m \sum_n G_{jm} G_{kn} \gamma_m \gamma_n f(j,k,m,n) \tag{10.a}$$

where,

$$f(j,k,m,n) = \int_{-\infty}^{\infty} \omega^4 \Phi_g(\omega) H_j(\omega) H_k^*(\omega) H_m(\omega) H_n^*(\omega) d\omega \tag{10.b}$$

$$= \int_{-\infty}^{\infty} \frac{\Phi_g^{(N)}}{\Phi_g^{(D)} \Phi_g^{(D)*}} \omega^4 H_j(\omega) H_k^*(\omega) H_m(\omega) H_n^*(\omega) d\omega \tag{10.c}$$

Substituting the frequency response functions defined in Eq. 9 into Eq. 10.c, the conjugate pairs in the integrand can be emphasized as shown in Eq. 11.a,

$$f(j,k,m,n) = \int_{-\infty}^{\infty} \left(\frac{S^2 \times 4\beta_g^2 \omega_g^2 (\omega - z_1)(\omega - z_2)\omega^4}{(\omega - p_{g1})(\omega - p_{g2})(\omega - p_{g3})(\omega - p_{g4})} \frac{1}{(\omega - p_{j1})(\omega - p_{j2})} \right. \\ \left. \frac{1}{(\omega - p_{k1})(\omega - p_{k2})} \frac{1}{(\omega - p_{m1})(\omega - p_{m2})} \frac{1}{(\omega - p_{n1})(\omega - p_{n2})} d\omega \right) \tag{11.a}$$

The poles and zeros in the above equation are defined as,

$$p_{g1} = \left(i\beta_g + \sqrt{1 - \beta_g^2} \right) \omega_g, \qquad p_{j1} = \left(i\beta_j - \sqrt{1 - \beta_j^2} \right) \omega_j$$

$$p_{g2} = \left(i\beta_g - \sqrt{1 - \beta_g^2} \right) \omega_g, \qquad p_{j2} = \left(i\beta_j + \sqrt{1 - \beta_j^2} \right) \omega_j \tag{11.b}$$

$$p_{g3} = \left(-i\beta_g + \sqrt{1 - \beta_g^2} \right) \omega_g, \qquad p_{k1} = \left(-i\beta_k - \sqrt{1 - \beta_k^2} \right) \omega_k$$

$$p_{g4} = \left(-i\beta_g - \sqrt{1-\beta_g^2}\right)\omega_g, \qquad p_{k2} = \left(-i\beta_k + \sqrt{1-\beta_k^2}\right)\omega_k$$

$$p_{m1} = \left(i\beta_m - \sqrt{1-\beta_m^2}\right)\omega_m, \qquad p_{n1} = \left(-i\beta_n - \sqrt{1-\beta_n^2}\right)\omega_n$$

$$p_{m2} = \left(i\beta_m + \sqrt{1-\beta_m^2}\right)\omega_m, \qquad p_{n2} = \left(-i\beta_n + \sqrt{1-\beta_n^2}\right)\omega_n$$

$$z_1 = \frac{i\omega_g}{2\beta_g}, \qquad z_2 = -\frac{i\omega_g}{2\beta_g}, \qquad z_0 = 0$$

For all of the conjugate pairs displayed in Eq. 11, we can use the method of residues to evaluate it. If the integrand in the function $f(j,k,m,n)$ has N poles, then:

$$f(j,k,m,n) = \int_{-\infty}^{\infty} \frac{g(\omega)}{h(\omega)} d\omega = 2\pi i \sum_{j=1}^{N} Residue\left(\frac{g(\omega)}{h(\omega)}, p_j\right) \tag{12}$$

and the mean square value is,

$$R_{\ddot{p}_j\ddot{p}_k}(0) = \sum_{m=1}^{N_{DOF}} \sum_{n=1}^{N_{DOF}} G_{jm}G_{kn}\gamma_m\gamma_n 2\pi i \sum_{j=1}^{N} Residue\left(\frac{g(\omega)}{h(\omega)}, p_j\right) \tag{13}$$

Similarly, we calculate the integrations of the other mean square quantities as indicated in Eq. 8. Performing the integrals described in Eq. 8 allows us to obtain the mean square values of the measuring quantities and their derivatives and, therefore, obtaining the sensitivity of each quantity at each measuring location to the damage occurring in the elements of the structure. We will utilize such sensitivity to optimally place the sensors in their measuring locations around the structure.

5.4. Numerical Study

We tested four different models to investigate the effectiveness of optimizing the number of sensors, based on their sensitivity to damage, on the stiffness identification. Three of the four models are 1-Bay×2-Stories as shown in Figure 5.1, and the fourth model is a 2-Bays×4-

Stories frame. These models follow the same assumptions of the earlier 2D frame model discussed in Chapter 2. The structure, in these models, are assumed to consist of columns that are massless, while the masses are concentrated in the floors, i.e., attached to the horizontal beams. The joints connecting the frame columns are moment resistant. The frame contains six elements, each of which has two strain sensors attached to its ends. Positioning the strain sensors at the ends of each element follows the fact that the strain, which is proportional to the curvature, increases with increasing the bending moment. Therefore, the strain will reach a maximum value at the ends of the columns of the frame structure where the bending moment is a maximum value as well.

The three models are selected so that; the first model is uniform both in stiffness and in geometry, the second model is non-uniform in stiffness but uniform in geometry, while the third model is non-uniform both in stiffness and in geometry.

Model 1

The first model (model 1) is a 1-Bay×2-Stories model, as shown in Figure 5.1. This model follows the same assumptions of the earlier 2D frame model discussed in Chapter 2. The structure columns are massless, the masses are concentrated in the floors (attached to the

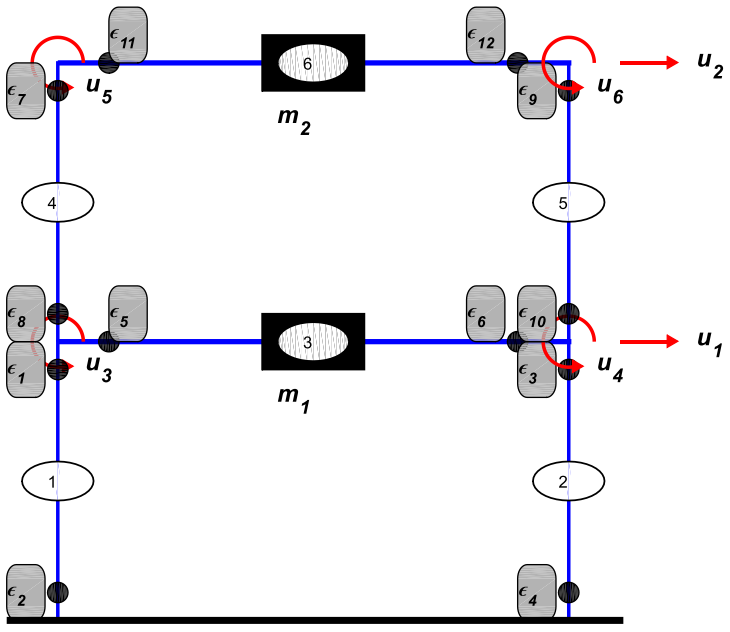

Figure 5.1 A 1-Bay×2-Stories frame with strain sensors indicated

horizontal beams), and the joints are moment resistant. It contains six elements, each of which contains two strain sensors attached to it. This model has the following properties:

- Columns' stiffness = [37.54 37.54 37.54 37.54 37.54 37.54] N/mm^2
- Floor mass = 18.75 tons
- Length = 5.5 m
- $Height_{story1} = Height_{story2} = 3$ m
- Fundamental Frequency = 2.588 Hz

For this model, we have calculated the sensitivities of different sensors to the change in damage in every element. The sensitivities are calculated based on the mean square values illustrated earlier. Table 5.1 below shows the normalized sensitivities of the three measures (acceleration, displacement, and strain). Each column in Table 5.1 contains the sensitivities of the measurement quantities w.r.t one of the six elements in the frame structure. Each

Table 5.1 Relative sensitivities of acceleration, displacement, and strain w.r.t. the stiffness change in each element for a 1-Bay×2-Stories frame (model 1). The sensitivities are grey-shaded according to their value. Light shading is for low sensitivity and dark shading is for high sensitivity.

	Elements					
	e1	e2	e3	e4	e5	e6
	Acceleration Relative Sensitivity					
acc1	1.0000	1.0000	1.5647	0.5434	0.5434	0.8323
acc2	1.0029	1.0029	1.8708	0.3813	0.3813	0.8529
	Displacement Relative Sensitivity					
disp1	1.0195	1.0195	1.8895	0.3707	0.3707	0.8532
disp2	1.0065	1.0065	1.8958	0.3706	0.3706	0.8585
	Strain Relative Sensitivity					
str1	1.2284	1.0619	1.8968	0.3876	0.4076	0.8562
str2	1.0483	1.0271	1.8796	0.3722	0.3752	0.8529
str3	1.0619	1.2284	1.8968	0.4076	0.3876	0.8562
str4	1.0271	1.0483	1.8796	0.3752	0.3722	0.8529
str5	1.0041	1.0053	1.9266	0.3699	0.3691	0.8554
str6	1.0053	1.0041	1.9266	0.3691	0.3699	0.8554
str7	1.0050	1.0061	1.8894	0.7302	0.3775	0.8846
str8	1.0092	1.0448	1.9031	0.7993	0.4255	0.8814
str9	1.0061	1.0050	1.8894	0.3775	0.7302	0.8846
str10	1.0448	1.0092	1.9031	0.4255	0.7993	0.8814
str11	1.0050	1.0061	1.8894	0.4013	0.3775	1.0225
str12	1.0061	1.0050	1.8894	0.3775	0.4013	1.0225

Sensors

column includes three groups of sensitivity values, 1) acceleration sensitivities, 2) displacement sensitivities, and 3) strain sensitivities. The values in Table 5.1 are grey shaded according to their magnitude, where the lightest shade (white) corresponds to the lowest sensitivity, and the darkest shade (black) corresponds to the highest sensitivity.

It clearly appears from Table 5.1 that the sensitivity of the strain measurements to damage is the highest compared to both the acceleration and the displacement sensitivities. For example, to accurately estimate the stiffness values for the 1×2 frame structure presented earlier, it is better to use the six strain sensors that are highlighted by a dark shading in Table 5.1. That is, (str1, str3, str5 (or str6), str8, str10, and str11 (or str12)).

This selected set of high-sensitivity sensors is used alone to identify the stiffness of the structural elements. To emphasize the effectiveness of these highly sensitive sensors, another set of sensors is constructed, that is the complement of the highly sensitive set mentioned earlier. All of the experiments we present in this study will apply only to the strain measurements. That is because the two other response measures, acceleration and displacement, are collected at the translational degrees of freedom. These translational degrees of freedom, alone, are incapable of identifying the structure stiffness unless they also represent the rotational degrees of freedom at the joints. However, as pointed earlier in Chapter 2, it is not simple to measure the rotational movements or the rotational

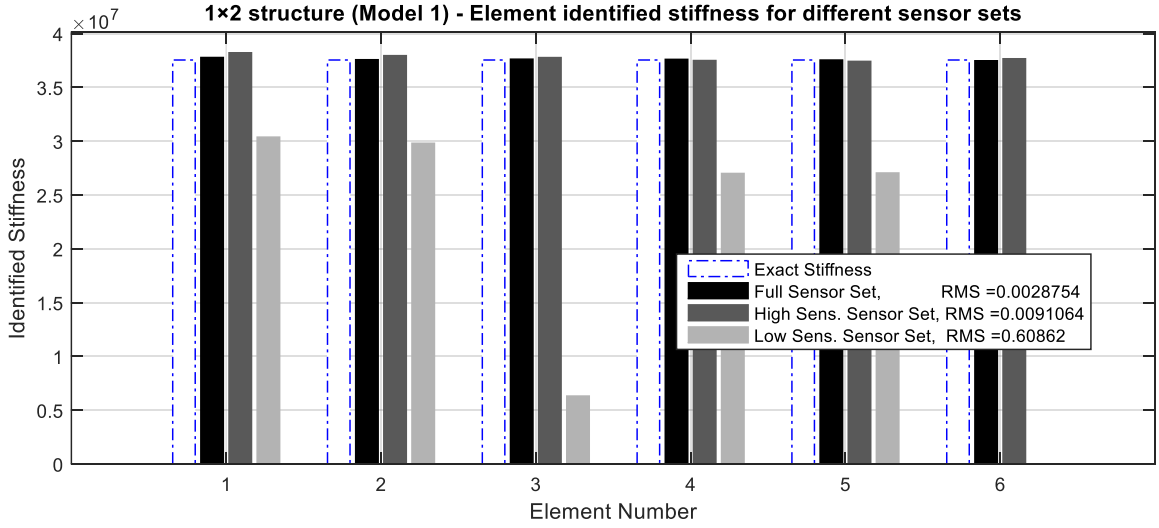

Figure 5.2 Identified stiffness for a 1-Bay×2-Stories frame (model 1) using three sets of sensors; 1) all sensors, 2) highly sensitive sensor set, and 3) less sensitive sensor set

accelerations. This is the primary motive to using the measured strain response in this study. The results of the identified stiffness is presented in Figure 5.2, which includes three sets of results; 1) using all of the sensors, 2) using the sensor set with high sensitivity, and 3) using the set of sensors complement to the highly sensitive set.

It appears, from the results presented in Figure 5.2, the sufficiency of using the highly sensitive sensor set. Reducing the number of sensors to half has a very little effect on the stiffness identification accuracy. The RMS of error has increased from 0.0029 to 0.0091, which is still highly accurate. However, replacing this set of sensors with the complement set of sensors has a remarkable effect on the identification error. The RMS of error jumps from 0.0029 to 0.6086.

Model 2

Another model with a different configuration is tested, model 2. It is a 1×2 frame as well as model 1, but it has non-uniform stiffness values, which removes the symmetry that appears in model 1. The stiffness values for the six elements of model 2 and its other parameters are,

- Columns' stiffness = [37.54 33.79 37.54 31.92 37.54 35.67]N/mm^2
- Floor mass = 18.75 tons
- Length = 5.5 m
- Height$_{story1}$ = Height$_{story2}$ = 3 m
- Fundamental Frequency = 2.540 Hz

Table 5.2 Relative sensitivities of acceleration, displacement, and strain w.r.t. the stiffness change in each element for a 1-Bay×2-Stories frame (model 2). The sensitivities are grey-shaded according to their value. Light shading is for low sensitivity and dark shading is for high sensitivity.

	Elements					
	e1	e2	e3	e4	e5	e6
	Acceleration Relative Sensitivity					
acc1	1.0000	1.0615	1.5197	0.6720	0.5251	0.8469
acc2	1.0206	1.0322	1.8283	0.4664	0.3704	0.8644
	Displacement Relative Sensitivity					
disp1	1.0388	1.0489	1.8477	0.4535	0.3608	0.8650
disp2	1.0256	1.0341	1.8537	0.4528	0.3604	0.8701
	Strain Relative Sensitivity					
Sensors: str1	1.2380	1.0905	1.8587	0.4722	0.3934	0.8676
str2	1.0671	1.0567	1.8385	0.4552	0.3651	0.8649
str3	1.0802	1.2751	1.8500	0.5032	0.3781	0.8695
str4	1.0466	1.0818	1.8376	0.4600	0.3624	0.8650
str5	1.0234	1.0331	1.8852	0.4521	0.3590	0.8669
str6	1.0244	1.0319	1.8854	0.4511	0.3602	0.8671
str7	1.0236	1.0350	1.8465	0.8424	0.3675	0.8942
str8	1.0248	1.0798	1.8545	0.9204	0.4128	0.8916
str9	1.0246	1.0334	1.8467	0.4617	0.7220	0.8998
str10	1.0560	1.0404	1.8614	0.5151	0.7674	0.8907
str11	1.0236	1.0350	1.8465	0.4925	0.3675	1.0483
str12	1.0246	1.0334	1.8467	0.4617	0.3868	1.0350

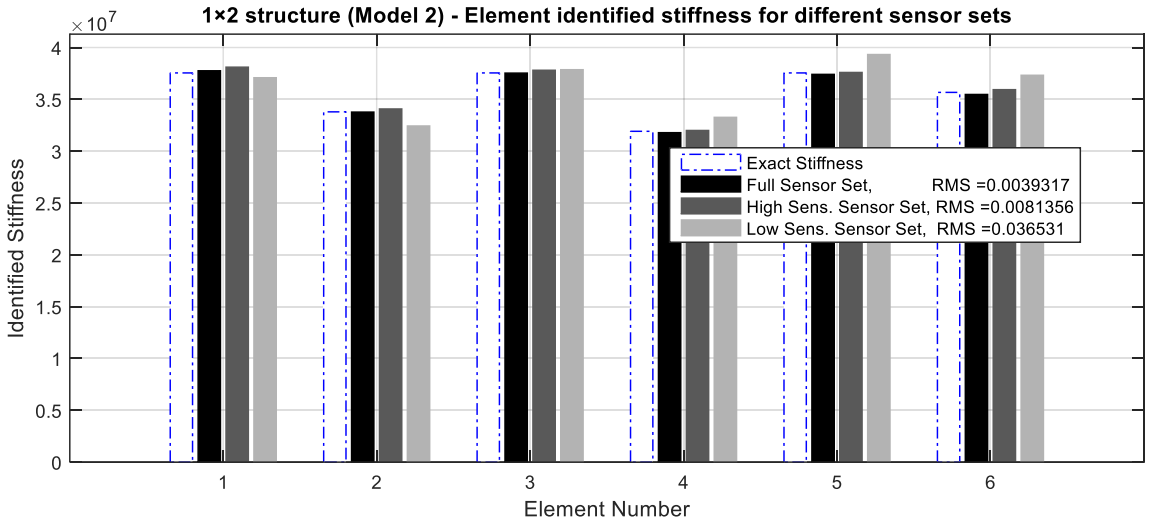

Figure 5.3 Identified stiffness for a 1-Bay×2-Stories frame (model 2) using three sets of sensors; 1) all sensors, 2) highly sensitive sensor set, and 3) less sensitive sensor set

The results presented in Figure 5.3 demonstrates the strength of using the high sensitivity sensors even for several configurations. Moving from the full set of sensors to the reduced set of high sensitivity sensors increases the identification error from 0.0039 to only 0.0081. However, replacing the high sensitivity sensor set with its compliment raises the error ten times, from 0.0039 to 0.0365.

Model 3

A third model that is non-uniform both in stiffness and in geometry is also tested. The parameters of model 3 are,

- Columns' stiffness = [35.67 33.79 31.92 26.28 37.54 35.67]N/mm^2
- Floor mass = 18.75 tons
- Length = 5.5 m
- Height$_{story1}$ = 3.3 m
- Height$_{story2}$ = 3.0 m
- Fundamental Frequency = 2.270 Hz

Table 5.3 and Figure 5.4 below show both sensors' sensitivities and the stiffness identification results for model 3. This third model provides results similar to the ones obtained from the earlier two models. Moving from the full set of sensors to the reduced set of high sensitivity sensors increases the identification error from 0.0060 to only 0.0228. However, replacing the high sensitivity sensors set with its compliment raises the error from 0.0060 to 0.0529.

Table 5.3 Relative sensitivities of acceleration, displacement, and strain w.r.t. the stiffness change in each element for a 1-Bay×2-Stories frame (model 3). The sensitivities are grey-shaded according to their value. Light shading is for low sensitivity and dark shading is for high sensitivity

Sensors	Elements					
	e1	e2	e3	e4	e5	e6
	Acceleration Relative Sensitivity					
acc1	1.0000	1.0471	1.6841	0.7352	0.4547	0.7185
acc2	1.0524	1.0458	1.9373	0.5059	0.2975	0.6868
	Displacement Relative Sensitivity					
disp1	1.0712	1.0614	1.9639	0.4852	0.2826	0.6866
disp2	1.0614	1.0501	1.9680	0.4843	0.2817	0.6890
	Strain Relative Sensitivity					
str1	1.2300	1.0884	1.9906	0.5026	0.3063	0.6927
str2	1.0942	1.0669	1.9578	0.4874	0.2861	0.6873
str3	1.1008	1.2427	1.9753	0.5376	0.3020	0.6974
str4	1.0770	1.0874	1.9567	0.4922	0.2851	0.6877
str5	1.0602	1.0492	1.9990	0.4833	0.2808	0.6869
str6	1.0601	1.0488	1.9976	0.4828	0.2813	0.6871
str7	1.0574	1.0506	1.9584	0.8906	0.2908	0.7084
str8	1.0515	1.0996	1.9672	1.0513	0.3445	0.7180
str9	1.0590	1.0484	1.9588	0.4963	0.6294	0.7202
str10	1.0983	1.0508	1.9789	0.5877	0.7294	0.7221
str11	1.0574	1.0506	1.9584	0.5475	0.2908	0.8887
str12	1.0590	1.0484	1.9588	0.4963	0.3140	0.8595

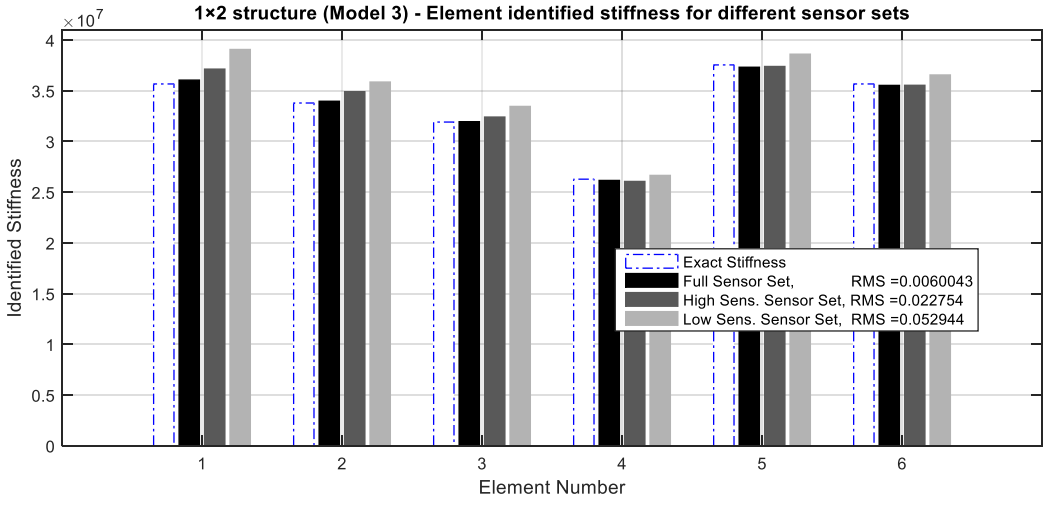

Figure 5.4 Identified stiffness for a 1-Bay×2-Stories frame (model 3) using three sets of sensors; 1) all sensors, 2) highly sensitive sensor set, and 3) less sensitive sensor set

Model 4

This models is a 2x4 frame structures. Its properties and parameters are defined below, and the stiffness identification error for using different sets of sensors is presented in Table 5.4:

- Columns' stiffness = $\begin{bmatrix} 37.54 & 33.79 & 37.54 & 37.92 & 37.54 \\ 35.67 & 37.54 & 33.79 & 37.54 & 37.54 \\ 37.54 & 35.30 & 36.42 & 37.54 & 37.54 \\ 37.54 & 33.79 & 36.80 & 31.92 & 37.54 \end{bmatrix}$ N/mm^2
- Floor mass = 37.50 tons
- Width of all bays = 5.5 m
- Height of all stories = 3.0 m
- Fundamental Frequency = 1.158 Hz

Table 5.4 RMS of identification error for model 4 using three sets of strain sensors, Full set of sensors, high sensitivity set of sensors, and the lower sensitivity set of sensors

Sensors utilized	Full no. of sensors	High sensitivity sensors	Low sensitivity sensors
RMS of Error	**0.254473**	**1.129211**	**1.842925**

In Table 5.4, we present the RMS of error in stiffness identification. It is clear the very high identification error level. Since the identified stiffness values have this very high level of error, its bar plot will look very awkward and uninformative, and, therefore, we will not plot the identified stiffness as we done to the previous examples.

On the other hand, this error is presented and explained in details in Chapter 2. This error is due to the mean square estimate in the pseudo-inversion operations performed to obtain the identified stiffness. To overcome this error, we need to apply the optimization algorithm, which we discussed in detail in Chapter 2 as well, that considers the modal contribution to the system. This optimization algorithm is applied to this model, and the optimized solution is presented in Table 5.5.

Table 5.5 RMS of identification error for model 4 using three sets of strain sensors, Full set of sensors, high sensitivity set of sensors, and the lower sensitivity set of sensors. An optimization algorithm is applied for rectification of the results

Sensors utilized	Full no. of sensors	High sensitivity sensors	Low sensitivity sensors
RMS of Error	**0.003852839**	**0.004758283**	**0.002423587**

Although the results in Table 5.4 have a very error, they provide the same trend that we used to find the earlier three 1-Bay×2-Stories frame models. The high sensitivity sensors provide an error that is less than the lower sensitivity ones, but still larger than the full number of sensors. However, the enhanced solution presented in Table 5.5 provides a different pattern. All the sets of sensors generate the same low level of error. This does not imply that the three sets of sensors have the same equal effect on identification. It rather denotes the effectiveness of the optimization algorithm, which is capable of extracting the stiffness of the frame elements with as little as half the number of sensors. In addition, it implies that this optimization approach, although proven effective for the first three small frames, may need to be combined with other algorithms if the structure model is more complex.

5.5. Conclusion

Optimal Sensor Placement (OSP) is investigated in this study. Our objective is to choose a reduced group of sensors placed in locations that provide the highest accuracy in stiffness identification. The optimality criteria we utilized in the sensor selection is to select the sensors that are highest sensitive w.r.t. the change in the structure stiffness properties. In order to assess the sensitivity of one of the measured quantity to damage, we obtained the mean square value of this quantity as well as its derivative w.r.t. the elements' stiffness in the structure. The mean square values of this derivative is the measure of sensitivity for the quantity being assessed.

In this study, we did first investigate the sensitivity of three quantities, acceleration, displacement, and strain, w.r.t. the change in stiffness properties of the structure. We realized that the strain measure is the most sensitive to the change in the element stiffness compared to the two other quantities.

Then, we applied the same approach to examine the sensitivity of each measuring location to the damage in the structure elements. Our model considers two strain measuring locations at the ends of each element in the frame. For each of these locations, we have obtained the sensitivity to damage w.r.t. each other element in the frame. Our numerical study provided the sensitivity values of the sensors', which allowed us to pick a highly sensitive set of

sensors and to use them for identifying the structure stiffness. The results showed a very high identification accuracy, especially for the smaller frames, when using this reduced set of sensors compared to the identification accuracy when using the full number of sensors. That is, we could reduce the number of sensors and, consequently, the amount of data processed and the processing time, while keeping the identification error at the same low level.

For the frames that are larger in size, the inaccuracy in identification, due to the pseudo-inversion, dominates the enhancement that the sensitivity approach provides. Therefore, we need to incorporate other algorithms to the solution that makes the identification accuracy of all mode sets equal to each other. This sensitivity approach, therefore, might not be effective with structures with complex configuration.

Chapter 6: Summary and Concluding Remarks

Systems Health Assessment (SHA) of infrastructure systems is of utmost importance in the modern societies. From the transportation networks to the internet of things, health assessment is necessary to maintain these systems operating and to reduce the probability of failure that may lead to catastrophic consequences. Health assessment of civil infrastructure components such as buildings, bridges and other structural systems, is one important application to the SHA. It is commonly referred to as structural health monitoring (SHM). Health monitoring of a structural system begins with acquiring response inputs about the structure and is then followed by the analysis of these inputs to come up with useful information that can lead to action and decision taking.

The primary objective of the study is to utilize the measured dynamic strain response of a structure to identify the current damage. For that purpose, we need to develop efficient and accurate structural health monitoring approaches to identify the damage. That is to detect, locate, and quantify the damage in the structural elements, represented by a reduction in the stiffness characteristics of the structure such as the flexural rigidity (EI) of a beam element. The focus of this study is on the damage identification in the frame structural systems that consist of interconnected beam elements by utilizing the measured dynamic response.

In the first part of the study, we developed a modal response-based stiffness and damage identification approach for frame structures. This approach utilized the Eigen equation of the assumed FE model of the structure to identify stiffness values of its elements from the measured dynamic strain response. We have considered the strain response since it provides more complete and useful information for frame-like structures than the commonly measured acceleration response. First step involves the extraction of strain mode shapes from the measured dynamic strain responses using the Stochastic Subspace Identification (SSI) algorithm. The extracted strain mode shapes are then utilized to estimate the mean square estimate of the system mode shapes associated with the generalized degrees of freedom of the assumed model through pseudo inversion operations. For a more accurate estimation of system mode shapes from the strain mode shapes, it is necessary to have a large number of strain measurements at many points on the structure to provide an over

determined system of equations for the mean square estimation by pseudo inversion. In the next step, the estimated system modes are used in the Eigen equation of the model to obtain element stiffness coefficients. This process again involves a pseudo inversion providing the mean square estimates of the stiffness coefficients of the elements. The Eigen equation of a single mode is not likely to be over determined as in highly indeterminate frames there usually will be more elements than the degrees of freedom. To increase the determinacy of the pseudo inversion problem, we can combine the Eigen equation of more modes, but since the higher modes are usually less accurately extracted it might enhance the inaccuracy of pseudo inversion. To deal with this accuracy problem, we have utilized a constraint on the output of this pseudo-inversion operation according to the settings of the problem. This approach seeks an optimal combination of the Eigen equations of different modes to provide a more accurate solution with the constraint such that the identified element stiffness values do not exceed an upper limit. We have demonstrated the effectiveness of the proposed approach and algorithm, in damage identification, through the numerical example problems of two-dimensional multi-story multi-bay frames in which several structural elements are considered damaged.

In addition, in order to generalize the application of this approach, we have extended the two-dimensional model to a three-dimensional shear beam model of a building supported by several beam-columns. In the application of this approach to the 3D models, it is observed that if several elements in the story of the structure are collinear to the coordinate axes of the model, then they have identical contribution to the finite element model and, thus, their stiffness combine together to act as a single element. In such cases, this approach is only able to identify the collective stiffness of the elements and not the stiffness of individual elements. The approach can also identify the combined stiffness of the whole story, including the torsional stiffness provided by the columns. This stiffness identification allows an accurate identification of the damage, represented as a reduction in the stiffness values between two structural stages, for the rows of element as well as the whole story.

In the above Eigen equation-based approach, it is necessary to utilize several structural modes including higher order modes and their frequencies. However, accurate extraction of higher modes is not an easy process with the available algorithms. This provides a good

motivation to consider another approach that may work with a few lower modes which are usually easily identified with a high accuracy. As a first few modes contribute most to the flexibility matrix of a structural system, in Chapter 4 we investigated a curvature or strain flexibility-based system identification approach.

This flexibility-based approach is first tested with the utilization of the exact modal parameters of the frame structures, and it provided the exact solutions, which demonstrates the concepts applied in this approach. However, when using the modes identified form the measured dynamic response, this approach is observed to be very sensitive to the inaccuracies in identified modal parameters of the structure, and that it provides higher stiffness identification error compared to the earlier Eigen equation approach. Despite this sensitivity, this approach provides an acceptable accuracy in stiffness identification in two scenarios. First, when only the first mode shape alone is used, the error resulting from the inclusion of the polluted higher modes is avoided. However, it works much better with structure configurations where the number of unknown stiffness parameters is equal to the number of degrees of freedom represented in the system. Therefore, we recommend applying the flexibility-based approach to structures that have balanced configurations (between elements and degrees of freedom), or for other configurations of structures but using only the lowest modes. It is also suggested to use this flexibility-based approach primarily in situations where the higher modes are not easily or accurately identifiable.

The two mentioned approaches, the Eigen equation and the flexibility-based approaches, demonstrated their effectiveness in identifying the damage in the frame structures. There are, however, situations where insufficiency of information may favor one approach over the other. However, modern engineering problems are also challenged by the abundance of information. In such situations, analyzing a huge volume of measured response data may become difficult. It is, therefore, desirable to use some criteria to select the most effect effective measurements that can provide the same level of accuracy in the identification as a large set of data. In this study, we searched for a criterion to optimally select the measurement locations that provide the most accurate results for the minimum volume of processed data. The optimality criteria utilized in our study for sensor selection is to identify the ones that have highest sensitivities with respect to the change in the stiffness of the

structural elements. Our numerical study in Chapter 5 has shown, first, that the dynamic strain measurements are more sensitive than other quantities such as the acceleration and displacement measurements. Second, that some strain sensors are more sensitive than others. The sensitivity of each strain response sensor is assessed by the magnitude of the mean square value of the response derivative with respect to element stiffness values normalized by the mean square values of the response. The utilization of the half number of sensors with highest sensitivities was observed to provide as accurate identification as with the full number of sensors.

Limitations to real buildings

In this study, we focused on two-dimensional frame structures, built of interconnected one-dimensional beam elements, and three-dimensional shear buildings built of beam elements connected to rigid slabs. However, in practice, it happens that several element configurations could be included in the structures as well, such as the two-dimensional plate elements (e.g. building walls). Although this study is limited to the one-dimensional element structures, it can, however, be further extended in order to include these other types of elements. Plates, for instance, can be modeled as a two-dimensional structural element following the plate theory, but it can also be modeled by a truss (built of interconnected one-dimensional elements) that is equivalent to the plate element in terms of the carried and transmitted loads.

Contribution of this research

It has been common to use the measured acceleration response for damage identification in structures. Associated studies, however, focused on the structure configurations where the acceleration response is sufficient to identify the damage occurring therein. In practice, several situations occur where the rotations at the nodal degrees of freedom of a structure are required in order to identify occurring damage. Moreover, several studies has demonstrated the high sensitivity of the strain response to little changes in the structure stiffness properties as well as this current study. The common approaches applying the strain measurements, in the literature, utilizes the strain modal energy that provides a damage index capable of localization or quantification of the damage. This study, however,

utilizes the strain mode shapes that are sufficient to detect, locate, and quantify the damage in the structure. Two approaches utilizing the strain mode shapes are presented. Each of them is more efficient in different situations based on the abundance and accuracy of the identified strain mode shapes of the structure.

In addition, several approaches have been developed to select the optimal locations for placing the measurement sensors. They primarily place the sensors in locations that maximize the purity of the mode shapes identified from the response measurements. This study, however, proposed a new approach based on statistical analysis of the response measurements. This approach reduces the number of measuring sensors, which are favored based on their sensitivity to the changes in the stiffness properties of the structure. The highly sensitive selected set of sensors provide a stiffness identification error that is as low as the error level provided by the complete set of sensors.

References

Abdel Wahab M. M, DE ROECK G. (1999), Damage Detection in Bridges Using Modal Curvatures: Application to a Real Damage Scenario,

Bernal, D. (2014), Damage Localization and Quantification from the Image of Changes in Flexibility, Journal of Engineering Mechanics, Vol. 140, No. 2 279–286, ©ASCE, ISSN 0733-9399/2014/2-279–286/

Bernal, D. 2006. Flexibility-based damage localization from stochastic realization results. *Journal of Engineering Mechanics* 132(6): 651-658.

Bernal, D., Damage Localization and Quantification from the Image of Changes in Flexibility, Journal of Engineering Mechanics, Vol. 140, No. 2, February 1, 2014. 279–286, ©ASCE, ISSN 0733- 9399/2014/2-279–286/

Bernasconi O., Ewins D. J. (1989), Application of Strain Modal Testing to Real Structures, 7th International Modal Analysis Conference.

Caicedo J M, Dyke S J, and Johnson E A. 2004. "Natural Excitation Technique and Eigensystem Realization Algorithm for Phase I of the IASC-ASCE Benchmark Problem: Simulated Data". *Journal of Engineering Mechanics*. 10.1061/(ASCE)0733-9399(2004)130:1(49)

Campbell, James B.; Wynne, Randolph H., Introduction to Remote Sensing 5th edn. The Guilford Press, 2011.

Cornwell, P., Doebling S. W. and Farrar C. R. (1999) "Application of the strain energy damage detection method to plate like structures", Journal of Sound and Vibration, 224, 2, 359-374

-[582472]. DOI: 10.1155/2012/582472

Duan Z., G. Yan & Ou, J. 2004. Structural Damage Localization Based on Rotational Flexibility Matrix. *Proceedings of The Third International Conference on Earthquake Engineering* 846-850.

Esfandiari A., Sanayei M,, Bhaktiari-Nejad F. and A.-Rahai, Finite Element Model Updating Using Frequency Response Function of Incomplete Strain Data, AIAA Journal, 2010, Vol. 48, No. 7.

Esfandiari A., Structural Model Updating Using Incomplete Transfer Function of Strain Data, Journal of Sound and Vibration, 333 (2014), 3657-3670

Gao Y., & Spencer B. F. 2002 Damage localization under ambient vibration using changes in flexibility. *Journal of Earthquake Engineering and Engineering Vibration* 1(1).

Guan, H. and Karbhari V. M. (2008) “Improved damage detection method based on element modal strain damage index using sparse measurement”, Journal of Sound and Vibration, 309, 465-494.

Hsu, T-Y. and Loh, C-H. (2007) ``Damage diagnosis of frame structures using modified modal strain energy change method'', Journal of Engineering Mechanics, 134, 11, 1000-1012.

Hu, S-L. J., Wang S. and Li H. (2006) “Cross-Modal Strain Energy Method for Estimating Damage Severity”, Journal of Engineering Mechanics, 132, 4, 429-437.

Hu, H. and Wu, C. (2009) “Development of Scanning Damage Index for Damage Detection of Plate Structures Using Modal Strain Energy Method”, Mechanics Systems and Signal Processing, 23, 274-287.

James G.H., Carne T. G. and Lauffer J. P., The natural excitation technique (NExT) for modal parameter extraction from operating structures, *Modal Analysis: the International Journal of Analytical and Experimental Modal Analysis*, **1995**, 10, 260}277.

James Ill , George H.; Carrie, Thomas G.; Lauffer, James P. (1993), The Natural Excitation Technique (NExT) for Modal Parameter Extraction From Operating Wind Turbines. Sandia National Laboratories

Juang, J.-N. and Pappa R. S. "An eigensystem realization algorithm for modal parameter identification and model reduction", Journal of Guidance, Control, and Dynamics, Vol. 8, No. 5 (1985), pp. 620-627.

Juang, Jer-Nan; Applied system identification, Prentice-Hall, 1994

Li, D. B. Zhuge, H. C., and Wang, B "The principles and techniques of experimental strain modal analysis". Proc. 7th International Modal analysis conference, Vol. 2, pp. 1285-1289 (1989)

Li, H., Yang, H. and Hu S-L. J. (2006) "Modal Strain Energy Decomposition Method for Damage Localization in 3D Frame Structures", Journal of Engineering Mechanics, 132, 9, 941-951.

Li, M., Cheng, L., Gong, J. et al. Sci. China Ser. E-Technol. Sci. (2008) "Post-earthquake assessment of building damage degree using LiDAR data and imagery" 51(Suppl 2): 133. doi:10.1007/s11431-008-6014-1

Li Y. Y. (2010), Hypersensitivity of strain-based indicators for structural damage identification: A review, Mechanical Systems and Signal Processing 24 (2010) 653–664

Lin Y. K., ASCE F., and Yong Y. (1987), "Evolutionary Kanai-Tajimi Earthquake Models", Journal of Engineering Mechanics, Vol. 113, No. 8

Liang, RY; Hu, J; Choy, F; (1992), Theoretical study of crack-induced eigenfrequency changes on beam structures. J. Eng. Mech., 118(2): 384-396

LJUNG L., *System Identification: Theory for the User*, Englewood Cliffs, NJ, USA: Prentice- Hall, 1987

Mahmood, S. M. F., Haritos, N, Gad, E. and Zhang, L. A Multi-reference –Based Mode Selection Approach for the Implementation of NExT-ERA in Modal-Based Damage Detection, *Structural Control and Health Monitoring*, 2104; 21: 1137-1153. DOI 10.1002/stc.1638

Engineering Structures, 27, 1762–1773

Ostachowicz, Wieslaw and Güemes J. Alfredo, New Trends in Structural Health Monitoring, Springer, 2013

Overschee, Peter Van; De Moor, Bart (1996), Continuous-time frequency domain subspace system identification, Signal Processing Volume 52, Issue 2, July 1996, Pages 179–194

Pandey, A. K., Biswas, M., & Samman, M. M. 1991 Damage detection from changes in curvature mode shapes. *Journal of Sound and Vibration* 145(2): 321-332.

Pandey, A.K., Biswas, M. (1994), Damage Detection in Structures Using Changes in Flexibility, Journal of Sound and Vibration Volume 169, Issue 1, Pages 3–17

Park, Hyun-Jun; Koo, Ki-Young and Yun, Chung-Bang (2007), Modal Flexibility-based Damage Detection Technique of Steel Beam by Dynamic Strain Measurements Using FBG sensors, *Steel Structures* 7, 11-18

Pedram, Esfandiari A. and Khedmati M. R., Finite Element Model Updating Using Strain-based Power Spectral Density for Damage Detection, Structural Control and Health Monitoring, 2016, 23:1314-1333 DOI:10.1002/stc.1833

Peeters, Bart; De Roeck, Guido (1999), Reference-Based Stochastic Subspace Identification For Output-Only Modal Analysis, Mechanical Systems and Signal Processing 13(6), 855}878

Qiao, Pizhong; Fan, Wei; 2011; Vibration-based Damage Identification Methods: A Review and Comparative Study, Structural Health Monitoring, 10:1;83–29

Reynders, Edwin; De Roeck, Guido; Bakir, Pelin Gundes and Sauvage, Claude (2007), Damage Identification on the Tilff Bridge by Vibration Monitoring Using Optical Fiber Strain Sensors, Journal of Engineering Mechanics, Vol. 133, No. 2

Samali, B., Li, J., Choi, F. C. and Crews, K. (2010) "Application of the Damage Index Method for Plate-Like Structures to Timber Bridges", Structural Control and Health Monitoring, 17, 849-871.

Sanayei M. and Saletnik M. J., Parameter Estimation of Structures from Static Strain Measurements. I: Formulation, *Journal of Structural Engineering*, ASCE, 1996, Vol. 122, No. 5, 555-562

Shi, Z. Y., Law, S. S. and Zhang, L. M. (1998) "Structural Damage Localization from Modal Strain Energy Change", Journal of Sound and Vibration, 218, 5, 825-844.

Shi, Z. Y., Law, S. S. and Zhang, L. M. (2000) "Structural Damage Detection from Modal Strain Energy Change", Journal of Engineering Mechanics, 126, 12, 1216-1223.

Shi, Z. Y., Law, S. S. and Zhang, L. M. (2002) "Improved Damage Quantification from Elemental Modal Strain Energy Change", Journal of Engineering Mechanics, 128, 5, 521-529.

Singh M. P. & S. Bisht 2006. Vibration Data-Based Damage Detection and Quantification. *Proceedings of the 3rd Annul Workshop of the Asian-Pacific Network of Centers for Research in Smart Structure Technology*, Lake Tahoe, USA.

Singh, M. P. and Bisht, S. "Structural damage identification using curvature flexibilities", World Forum on Smart Materials and Smart Structures Technology, Chongqing and Nanjing, China, May, 22-27, 2007

Sipple J. D. and Sanayei M., Finite element model updating using frequency response functions and numerical sensitivities, Structural Control Health Monitoring. 2014; 21:784–802,

Stubbs, Norris; Kim, Jeong-Tae (1996), Damage Localization in Structures without Baseline Modal Parameters, AIAA Journal Vol. 34, No. 8

Tsang, W. F. (1990), Application of Strain Modal Testing to Real Structures, 8th International Modal Analysis Conference.

Udwadia F. E., Structural Identification and Damage Detection from Noisy Modal Data, *Journal of Aerospace Engineering* 2005, Vol. 18, No. 3, ©ASCE, ISSN 0893-1321/2005/3-179–187

Udwadia, Firdaus E. and Kalaba. Robert E. "Analytical dynamics: a new approach", 1996, *Cambridge University Press*

Unger, J. F., Teughels, A. and De Roeck, G. (2005) "Damage Detection of a Prestressed Concrete Beam Using Modal Strains", Journal of Structural Engineering, 131, 9, 1456-1463.

VAN OVERSCHEE P. and B. DE MOOR 1996 *Subspace Identification for Linear Systems*: *Theory*, *Implementation*, *Applications*. Dordrecht, Netherlands: Kluwer Academic Publishers.

Wang S., Iterative Modal Strain Energy Method for Damage Severity Estimation Using Frequency Measurements, *Structural Control and Health Monitoring,* 2013, 20, 230-240

Yao G. C., Chang, K. C. and Lee G. C. (1992), Damage Diagnosis of Steel Frames Using Vibrational Signature Analysis. Journal of Engineering Mechanics, Vol. 118, No. 9